Parametric wave growth in a frequency integrated wave model

by:

Marlies Antoinette VAN DER LUGT
(4156870)

In partial fulfillment of the requirements for the degree

Master of Science
in Hydraulic Engineering
Specialization: Environmental Fluid Dynamics

September 21, 2017

Graduation Committee:

Prof. Dr. Ad RENIERS	Delft University of Technology
Prof. Dr. Dano ROELVINK	IHE Delft Institute for Water Education, Deltares
Prof. Dr. Martin VERLAAN	Delft University of Technology, Deltares
Dr. Ap VAN DONGEREN	Deltares
Johan REYNS MSc.	IHE Delft Institute for Water Education, Deltares

An electronic version of this thesis is available at `http://repository.tudelft.nl`

TU Delft

Deltares
Enabling Delta Life

”Er zijn twee stadia in de opleiding tot wetenschappelijk onderzoeker: een eerste, waarin gepoogd wordt de juiste eenheden aan getallen toe te kennen en een tweede, waarin geprobeerd wordt ze weer weg te halen door invoering van dimensieloze kentallen.”

van der Westhuysen et al. (2015)

Abstract

Waves in coastal waters play a role in forecasting storm conditions, as boundary conditions for the assessment of coastal risk and in coastal structure design. Assessment of their impact can be made through numerical modeling. In a forecasting context, the CPU time of the wave model is decisive in its suitability. Recent years wave model approaches have been to describe both linear and non-linear generation, dissipation and transfer processes in the wave spectrum explicitly. This resulted in computationally demanding tools. Such models are very suitable for research purposes or for design and assessment if time is available, but are rather heavy tools for forecasting applications on larger scales. Parametric models describe the wave spectrum through characteristics in a smaller solution space compared to spectral models, which makes them potentially faster solvers. In this thesis the suitability for forecasting of a spectrally integrated approach to the wave action balance is investigated. The stationary wave drivers from the storm impact assessment model XBeach were taken as a starting point. A second balance equation was identified to model the evolution of the mean period. In estuaries and behind shoals, locally generated waves can be dominant over offshore wave conditions. As part of the project, a wave generation mechanism is developed for the modified wave drivers based on prediction relations for growth of wind-waves under fetch-limited conditions. The two-equation approach was discretized and tested in a 1D Matlab model and the solution was proven to converge towards the literature prescribed growth curves for total wave energy and mean wave period. This approach was then implemented in the unstructured Frequency Integrated wave drivers in D-Flow FM. The implementation has been verified through semi-1D test cases and showed convergence behavior equal to the Matlab model. A hindcast of a 1982 storm in the Haringvliet was performed to compare the model skill of the unstructured frequency integrated model (FIM-FM) to the spectral wave model SWAN. In this hindcast the model skill of FIM-FM is comparable to SWAN for significant wave height and mean wave period for all locations apart from directly behind a shoal. Depth and wave height dependence of bottom friction coefficients should be studied in more validation cases to improve the prediction of wave steepening over shoals. Further research should also look into the iterative method in the solver for stationary solutions of the model equations to realize faster CPU time of a stationary problem. Although not established in this thesis, faster CPU time compared to a spectral model like SWAN should be possible based on the reduction of the solution space.

Preface

In the fall of 2013 I first came to Delft. I was halfway my BSc on a quest to find a study field suiting me for a MSc program. Not in the least was this move motivated as well by joining the training group of the rowing team which beat me in the development cup the year before. For two years I juggled with courses in Delft, Utrecht, a small detour to Texel, while actually putting all my energy into rowing practices and races. All this time I could not decide whether I preferred the analytical but abstract path of physics courses or the social relevance inherent to applications in civil engineering. The decision for the hydraulic engineering MSc track was made eventually in 2015, but only during this research project did it become clear to me this was the right choice. In this project I needed skills acquired in the field of physics and mathematics as well as in engineering, allowing me to enjoy aspects from all my study fields.

In that light, I would like to thank Martin and Ap for proposing this thesis topic to me, listening to the ups and downs in my progress and dropping hints along the way but letting me make my own discoveries. Thanks go to Dano for being able to pinpoint in no more than 20 minutes why I am stuck for weeks already, waving into the direction where to look afterwards. I owe a big thank you to Johan, whom I have asked for advice on modeling or programming on numerous occasions, at times feeling slightly distressed. After an extended coffee, I would have calmed down and seen the better sights of life (and project) again. Thanks to Ad, who completed the thesis committee as chair, enabling all of us to meet in his office such that I could practice my presentation skills in front of this ensemble of wise men.

In a year's time a lot can happen. I threw in the towel with my rowing career to focus with more energy on my study track, only to find out that my mind and my body don't share the same energy resource but rather like to be used in parallel for me to function well. My graduation buddies at Deltares (Anne, Bas, Bjarte, Cleo, Kamilla, Stef, Tim and Tim and of course all the others) will confirm with you that coffee break chatter would be as often about my new mania cycling as well as about frustration or epiphanies in our projects. Thanks for dragging my from my computer on these very necessary breaks!

Working on my MSc thesis at Deltares meant being surrounded by a lot of experts on various fields. I thank Alfons, Carolien, Mart en Sander for discussions which helped me to move forward with my research.

Last but not least thanks go to my parents, friends and Sander in particular for the support at moments that a nine month project appeared a bit daunting to me. You guys were right, of course I was going to make it to the end!

Marlies van der Lugt
Delft, September 2017

Contents

1 Introduction **1**
- 1.1 Motivation . . . 1
- 1.2 Problem statement . . . 2
- 1.3 Approach . . . 4
- 1.4 Research objective . . . 4
- 1.5 Outline . . . 5

2 Literature survey on wave generation **7**
- 2.1 Measurements of wave characteristics . . . 7
- 2.2 Wave growth per wave component . . . 13
- 2.3 Discussion . . . 15

3 Derivation of source term formulation **17**
- 3.1 HISWA approach . . . 17
- 3.2 Evolution relations . . . 19
- 3.3 The wave action balance . . . 20
- 3.4 Expanding the domain of applicability . . . 23
- 3.5 Depth limitations . . . 26
- 3.6 Summarizing . . . 30

4 Validation and properties in 1D **31**
- 4.1 HISWA comparison . . . 31
- 4.2 1D convergence . . . 34
- 4.3 Sink-Source balance in fully developed conditions . . . 36
- 4.4 Return rates to quasi-equilibrium . . . 38
- 4.5 Summarizing . . . 41

5 Implementation in 2D **45**
- 5.1 Directional distribution of wind input . . . 45
- 5.2 Adaptations to frequency prescribed wave drivers . . . 46
- 5.3 Robustness . . . 48
- 5.4 Validation cases . . . 49
- 5.5 Summarizing . . . 51

6 Field case **55**
- 6.1 Haringvliet storm hindcast . . . 55
- 6.2 Method . . . 56
- 6.3 Results . . . 57

6.4 Discussion 59

7 Conclusion and Recommendations **63**
7.1 Conclusion 63
7.2 Recommendations 64

8 List of Symbols **71**

A Period evolution under bottom friction **75**

B Calibration of friction coefficients **77**

C Additional figures Haringvliet assessment **79**

1. Introduction

1.1 Motivation

Storms in coastal waters give rise to storm surge. High surge levels can cause significant flooding, resulting in damage to property or ecosystems and possibly loss of life. Prediction of magnitude and geographic extent of surge is critical for impact assessment and timely emergency measure planning in case of forecasted storm conditions. Numerical modeling provides a means hereto.

Storm surge can be decomposed in set-up to the offshore water level induced by several processes. Aside from the tidal component, wind-induced set-up is the primary contributor. The wind induced set-up can be modeled in a hydrodynamic model. A second contributor is the wave climate in shallow water which generates stresses on the water column (Longuet-Higgins and Stewart (1964)). A decrease of radiation stresses in the surf-zone causes an additional set-up to the surge level named the wave-induced set-up. The wave-induced set up can be numerically modeled through a phase-averaged wave model which may or may not be coupled to a flow model. Wave climates in shallow water depend highly on the complexity of the bathymetry (e.g. Holthuisen (2007)). To resolve the breaking process, wave models require a finer computational grid than hydrodynamic models do. Moreover, recent years wave model approach has been to describe both linear and non-linear generation, dissipation and transfer processes in the wave spectrum explicitly (Booij et al. (1999), Benoit et al. (1996), Tolman (1991), WAMDI Group (1988)). This approach makes shallow water wave models very computationally demanding.

As storm surge is a natural hazard for coastal areas world wide, real-time forecasting of surge levels is an active field of research. Many model approaches to assessment of the wave-induced set-up have been investigated world wide. In the Netherlands the Storm Surge Warning Service (SVSD) forecasts in cooperation with the KNMI through the hydrodynamic Dutch Continental Shelf Model (DCSF), meanwhile assessing wave impact by means of wave models such as SWAN (Verlaan et al. (2005)) locally. On a larger regional scale hurricane waves and storm surge are jointly assessed for the US coast in coupled SWAN - ADCIRC models (Dietrich et al. (2011)). Under the condition of sufficient availability of computational cores (i.e. a supercomputer), this coupled flow-wave model can provide forecasts in real-time for the required domain.

If the scale is further increased, such as necessary to assess surge levels around the entire Australian coast, model approaches tends to assess the hydrodynamic component of the surge level numerically, while using location-calibrated stochastic models for the wave-induced set-up (McInnes et al. (2016)). This approach has been shown to overestimate storm surge in areas with complex bathymetry, possibly because bathymetry was not taken into account in the parametrization (O'Grady et al. (2015)).

As storms in open ocean affect several coastlines at once, present day storm surge models attempt to asses surge levels on a scale no smaller then regional. The Global Tide and Surge Model (GTSM, Verlaan et al. (2015)) is successful in real-time forecasting of the hydrodynamic component of storm surge on a global scale. With an unstructured model approach refinement of

the grid is only required in shallow water where the bathymetry prescribes the grid size. Implicit time-integration allows coarse time steps such that one simulation day requires just seven minutes of computations on a normal computer (one i7 processor with 4 cores). The wave-induced component however has not been included in the model yet. Wave modeling in a global model faces the challenge of the disparity between the scale of the model and the scale at which the wave processes in shallow water take place. This thesis investigates another wave model approach to contribute to the feasibility of real-time wave forecasting in a global model.

1.2 Problem statement

Spectral wave modeling in third generation wave models are important tools in understanding wave physics. If (computational) time is available they are also used for design and assessment purposes as wave models are very computationally demanding. This computational complexity is partly due to the numbers of dimensions used to describe a wave state in a full spectral model.

Dimensions of a wave field

The wave field in spectral wave models is expressed in five dimensions: time (t), 2D horizontal location (x, y), frequency (f) and propagation direction (θ). The solution space is hence five-dimensional. In the case where stationary conditions are assumed, the time-dimension can be eliminated and four dimensions of the solution space remain. In comparison, to model currents on a similar domain only the 2D horizontal location (x, y) is strictly necessary. In some hydrodynamic models the distribution of the flow-profile over the depth is additionally included (z). Suppose the spectral component of the solution space in the wave model is discretized: $\{f_i\}_{i=1}^{m}$, $\{\theta_i\}_{j=1}^{n}$. The description of a wave state in comparison to a 2D flow state on the same discrete grid $\{(x_k, y_l)|k = 1 \dots K, l = 1 \dots L\}$ then requires a factor KL more computer memory. Additionally, the systems of equations solved in the model is enlarged by the same factor. This increases the demand on fast solution algorithms greatly.

Wave models generally describe a wave state at location (x, y) by a two dimensional wave spectrum (θ, f). Radiation stresses however, can be derived from frequency integrated parameters ($E(\theta), n(\theta)$), where E is total wave energy and n is the ratio between group celerity and phase celerity of the waves (Dingemans et al. (1987)). Both these variables are defined on propagation space (x, t, θ). It is hypothesized that in the assessment of wave-induced set-up the distribution of wave energy over the frequency domain f is not of direct importance.

Therefore, this thesis will focus on a spectrally-integrated approach to wave modeling by eliminating f from the solution space. A three-dimensional solution space (x, y, θ) remains. This would make the model more appropriate for forecasting applications, because larger domains with a relatively fine grid can be modeled with similar problem-size and need for computer memory compared to spectral models.

Frequency integrated wave models

Commonly used phase averaged models are based on the wave energy or wave action balance. Wave action is conserved during wave propagation under ambient currents while wave energy is not (Bretherton and Garret (1969)). The wave action balance is given by:

$$\frac{\mathrm{d}A}{\mathrm{d}t} + \nabla \cdot (\vec{v}A) = S_A \tag{1.1}$$

in which $A = A(x, y, \theta, \sigma) = \frac{E(x,y,\theta,\sigma)}{\sigma}$ wave action density, ∇ is the three-dimensional differential operator over $(x, y, \theta)-$space, $\vec{v}$ is three-dimensional rate of change vector $\vec{v} = (c_{g,x}, c_{g,y}, c_\theta)^T$ and $S_A = S_A(x, y, \theta, \sigma)$ source terms. The group celerity is defined as $c_g = \dfrac{\partial \omega}{\partial k}$. The frequency ω is related to the wave number through the dispersion relation:

$$\omega^2 = gk \tanh(kh) \tag{1.2}$$

with k the wave number and h the height of the water column. The refraction rate follows from linear theory and consists of a bottom induced and a current induced refraction rate. Source terms in spectral wave models generally consist of:

$$S_A = S_{in} + S_D + S_{NL} \tag{1.3}$$

With S_{in} generation of waves by wind, S_D dissipation terms, which in deep water are dominated by white-capping (D_{wc}) while in coastal regions by bottom friction (D_f), and depth induced breaking (D_{br}). Transfer of action through the action spectrum is described by nonlinear wave-wave interactions S_{NL}.

An action density spectrum (σ, A) is reasonably represented by the bulk wave action and the peak frequency in case the spectrum is narrow banded and single-peaked. Under this assumption a frequency-integrated approach to the wave action balance is expressed as:

$$\frac{\partial A^*}{\partial t} + \nabla \cdot (\vec{v} A^*) = S_A^* \tag{1.4}$$

in which $A* = A(x, y, \theta) = \frac{\sum_\sigma E(x,y,\theta,\sigma)}{\overline{\sigma}}$ total wave action, $S_A^* = S_A(x, y, \theta, \overline{\sigma})$ source terms and $\overline{\sigma}$ a frequency representative for the spectrum. In this approach nonlinear wave-wave interactions are only described implicitly in the evolution of $\overline{\sigma}$ such that the source terms reduce to $S_A^* = S_{in}^* + S_D^*$.

Literature already describes some models with a frequency integrated approach. For example, HISWA (Holthuijsen et al. (1989)), Mase (2001), and, disguised as a storm impact assessment model XBeach (Roelvink et al. (2009)). The HISWA model solved a two-equation approximation to the wave action balance for the evolution of $(\overline{\sigma}, A^*)$ with a second generation process description for wind input S_{in} and dissipation D_f and D_{br}. White-capping (D_{wc}) was included implicitly in the wind input formulation. The second approximation equation to the wave action balance describes the peak period variations throughout the domain. Although no description of the nonlinear wave-wave interactions is available in HISWA, this second equation can be seen as a rudimentary description of spectral shape evolution. This model was operational for a number of years, but as the feasibility of spectral models for hindcasting purposes became greater throughout the years with the increase of computational power of the computer, focus shifted towards third generation wave models. HISWA-like generation mechanisms are still a process description option within the SWAN model (Booij et al. (1999)), but the two-equation approximation was completely abandoned there.

The XBeach model takes the narrow band assumption one step further. It assumes the attempted model domain is short in the direction of propagation of waves. The wave state in the interior of the domain is then dominated by the wave conditions provided on the offshore model boundary. These assumptions allow to reduce the complexity of the model:

- The wave period in prescribed throughout the whole domain and equal to the boundary prescribed value. This representative wave period can be either the moment-based mean period,

or the peak period, corresponding to the period of the significant wave. This computed wave period is assumed to be representative as wave period in the entire domain, hence acts as a constant in the wave celerity computation and the dissipation processes.

- All wave energy in spectra on the model boundary is positioned on the representative period and remains so when propagating into the domain.
- Because of the short travel time of waves in the interior of the domain, only dissipation processes are described and modeled. Local wave growth in short domains is assumed to be negligible.

XBeach-like wave drivers are currently also implemented as a wave-module in the unstructured finite volume flow model DFlow-FM (Reyns et al. (2016)). This implementation will be referred to as the Frequency Prescribed Model in FM (FPM-FM). An unstructured implementation has the advantage that generation of grids for complex bathymetry is easier and possibly more accurate with fewer grid cells as grid refinement can occur locally.

1.3 Approach

The approximation to the wave action balance in the HISWA model appears applicable to the real-time forecasting of wave-induced set-up in a large scale model because it reduces the solution space to propagation space: (x, y, θ) and the primary evolution processes are present. No currently operational implementation of the frequency integrated approach is available however. The XBeach wave drivers are operational, but the absence of a wave generation mechanism prevents its application to domains extending into water of intermediate depth and in regions sheltered from offshore wave conditions such as behind barrier islands and shoals.

Its unstructured version, FPM-FM, is operational in beta-release and provides a means to reduce the model problem size in contrast to the structured version because it allows local grid refinement. The additional advantage of D-Flow FM as the flow model coupled through wave-current interaction to the wave model is that the global model is also a D-Flow FM model. This makes the two models tightly coupled, which generally leads to a more efficient model (Dietrich et al. (2013)).

To make the FPM wave drivers in DFlow-FM suitable for application to larger domains and behind barrier islands, as is a requirement in regional modeling of storm surge, the objective of this thesis is narrowed down to the development of a wave generation mechanism for this model.

1.4 Research objective

The development process of a wave generation mechanism for a frequency integrated wave model can be divided into three parts: (1) Derivation of a source term formulation for wind input, (2) Implementation of the source term into FPM-FM wave drivers and (3) Validation of the model approach.

These are the research questions which follow from the objective:

1. (a) What should be the formulation of a wave generation mechanism in a frequency integrated approach?
   (b) How does the proposed source term relate to the wind input formulation in the HISWA model?

(c) How does the source term behave under wave states differing to the domain of wave states in the derivation?

2. (d) What steps are necessary to guarantee model robustness?
   (e) How does the wind input interact with other source terms in the wave action balance?

3. (e) How does the predictive skill of the model compare to a spectral wave model?
   (f) Does the model show reduced CPU time in comparison to a spectral wave model?

1.5 Outline

The structure of this thesis is as follows. Chapter 2 discusses literature on the topic of wave generation by wind. In Chapter 3 the derivation of a source term formulation is made. Convergence under ideal 1D conditions and properties of the derived sourve term are described in Chapter 4. The source term formulation is extended for implementation in a 2D model in Chapter 5. A validation of the 2D implementation by means of a hindcast is described in Chapter 6. Chapter 7 then reports on the research conclusions and provides some recommendations towards further research.

2. Literature survey on wave generation

Two approaches can be identified in literature to describe wave growth. The first is based on the description of evolution of integral characteristics. The second approach attempts to describe the evolution of wave components within the wave spectrum. Although the latter approach is geared towards spectral wave models while this thesis investigates a frequency integrated model approach, it is worthwhile to study its theory as it is today's state of the art. To that end this chapter first discusses literature on measurements of integral wave characteristics and then reports on the description of growth of wave components in Section 2.2. Section 2.3 discusses which properties from the spectral description of wave growth are relevant in a frequency integrated model.

2.1 Measurements of wave characteristics

Integral wave characteristics of the wave spectrum can be defined in a multitude of ways. Often, primary characteristics used are significant wave height and peak period (H_s, T_p), because visual wave observations can be related to these spectral quantities. In case the integral characteristics are derived from a measured signal, total wave energy and mean period (E_{tot}, T_{M01}) are preferable. The first observations of wave growth under wind forcing come from Sverdrup and Munk (1946) and Bretschneider (1952). They observed that wave characteristics respond similarly to wind forcing when the growth rates were compared in dimensionless form by scaling appropriately with a measure of the friction velocity and the gravitational constant. Measurements were taken in conditions that approximate an idealized scenario. In this stationary scenario (the conditions don't change in time) the wind blows offshore over deep water where the waves do not experience any bottom effects. This led to power law expressions as prediction relations for wind-generated waves as:

$$\widetilde{H}_{\mathrm{s}} = \mathrm{a}_1 \widetilde{F}^{\mathrm{b}_1} \tag{2.1}$$

$$\widetilde{T}_{\mathrm{p}} = \mathrm{a}_2 \widetilde{F}^{\mathrm{b}_2} \tag{2.2}$$

The tilde indicates a dimensionless variable, $\mathrm{a_i}, \mathrm{b_i}$ coefficients and F stands for fetch: the shore-normal component of the distance from the measurement point towards the upwind coast along the wind direction. The definitions of these dimensionless variables are given in Table 2.1. Strikingly, such power laws still form the basis of today's study of prediction relations, despite their basis on highly idealized conditions.

Kitaigorodskii (1962) developed theoretical arguments on growth and spectral shape based on self-similarity of integral characteristics of the spectrum. Pierson and Moskowitz (1964), using this similarity theory, described universal limits for the growth of sea states. The dimensionless wave energy in a fully developed sea state appeared constant due to a balance between generation and dissipation. Intuitively, this upper limits matches wave conditions with a phase celerity equal to the wind speed. Shear between the air- and sea layer diminishes and hence the energy transfer

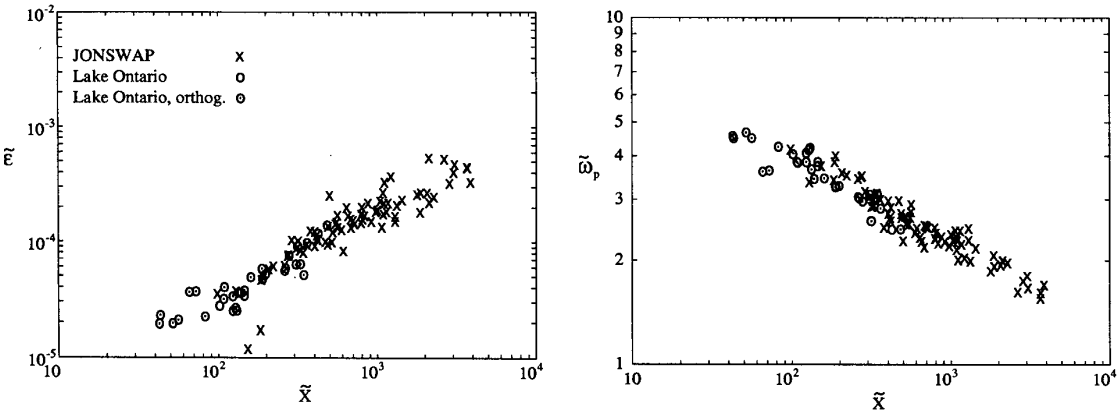

Figure 2.1: *Wave characteristics measurements from two field experiments on log-log scale. Left:wave energy $\widetilde{\epsilon}$ against fetch $\widetilde{x}$. Right: peak frequency $\widetilde{\omega}_p$ against fetch. All are made dimensionless.*

can't take place through a shear mechanism anymore. Cut-off values for the above given growth curves given as

$$\widetilde{H_\infty} = \mathrm{c}_1 \tag{2.3}$$

$$\widetilde{T_\infty} = \mathrm{c}_2 \tag{2.4}$$

Later, Hasselmann et al. (1973) analyzed field data of young sea states in the North Sea in a project called JONSWAP. Young sea states have wave climates which have not yet reached fully developed conditions and the energy transfer from air to sea is dominant over dissipation mechanisms. The JONSWAP project identified self-similarity not only in the integral characteristics but also in the shape of the young sea state wave variance spectrum. A universal shape of the spectrum was parameterized where the shape parameters are wave age dependent.

Quantification of growth curve coefficients

More field experiments were performed in the years after, amongst others the Bothnian Sea (Kahma (1981)), ARSLOE (Rottier and Vincent (1982)), Lake Ontario (Donelan et al. (1985)), Lake Marken (Bouws (1986)). The prediction relations these studies resulted in, were translated into prediction relations for the engineering community in for example the Shore Protection Manual (1984).

Although in each field experiment a clear correlation between fetch and wave energy and between fetch and wave period was observed, the quantification of coefficients in the best-fit parametrization of the growth curves in each of these field studies continued to show discrepancies. Growth curves with double steepness were observed in Kahma (1981) compared to Hasselmann et al. (1973).This led Kahma and Calkoen (1992) to (re)analyze a joint set of wave studies (JONSWAP, Bothnian Sea, Arsloe, Marken, Ontario and Qeii) in an attempt to identify the cause to these discrepancies.

The main conclusion from the analysis of the collected database of observations was that no single factor could explain the differences in growth curves observed at different sites. The particularly large differences between growth curves between the JONSWAP experiment and lake Ontario could be partially explained by assessing the state of stratification of the air-sea surface

Variable	units	scaling
Significant wave height	$[H_s]$=m	$\widetilde{H}_s = \frac{gH_s}{{u_{10}}^2}$
Bulk wave variance	$[m_1]$=m^2/m^2	$\widetilde{m}_1 = \frac{g^2 m_1}{{u_{10}}^4}$
Bulk wave energy	$[E]$= J m^{-2}	$\widetilde{E} = \frac{gE}{\rho {u_{10}}^4}$
Fetch	$[F]$=m	$\widetilde{F} = \frac{gF}{{u_{10}}^2}$
Period	$[T_p]$=s	$\widetilde{T}_p = \frac{gT_p}{u_{10}}$
Time	$[t]$=s	$\widetilde{t} = \frac{gt}{u_{10}}$
Group celerity	$[c_g]$=m/s	$\widetilde{c}_g = \frac{c_g}{u_{10}}$
Wave action	$[A]$=J s/m^2	$\widetilde{A} = \frac{g^2 A}{\rho u_{10}^5}$

Table 2.1: *Definitions of dimensionless variables. Conversion between the various variables expressing energy:* $H_s = H_{1/3} \approx H_{m_0} = 4.004...\sqrt{m_0}$ *and* $E = \rho\, g\, m_0$.

temperature. They propose different coefficients for the fetch power laws in the case of stable and unstable stratification in temperature between air and sea. Since not all field experiments reported on temperature and the distinction did not remove the disparities completely, they also provided a wave prediction relation for the composite dataset, the coefficients of which are given in Table 2.2. Equations (2.1) and (2.2) with coefficients given by Kahma and Calkoen (1992) are from here on referred to as KC1992 curves.

A second conclusion drawn from their analysis is the difference in predictive power of the scaling laws between wave energy and wave period. Correlations between dimensionless variables on log-log scale can be partially addressed to the dependence of the dimensionless values on the wind speed. This is especially the case when the measurement of the wind speed is inaccurate and the range of the dimensionless quantity is small in comparison to the wide range of the independent variable $\widetilde{\mathrm{F}}$, which is exactly the case for measurements of wave period. From this discussion they concluded that most attention should be given to the prediction relation of wave energy, and less to prediction of peak period, because spurious correlations have a smaller effect on the former.

Transition to fully developed sea states

The transition between fetch limited sea states and fully developed sea states has not been described by Kahma and Calkoen. To that end, Young and Verhagen (1996) prescribe the use of tanh-expressions that entail a continuous transition to fully developed sea states:

$$\widetilde{H} = \widetilde{H}_\infty \left(\tanh(k_1 \widetilde{F}^{m_1})\right)^p \tag{2.5}$$

$$\widetilde{T}_\mathrm{p} = \widetilde{T}_{\mathrm{p}_\infty} \left(\tanh(k_2 \widetilde{F}^{m_2})\right)^q \tag{2.6}$$

See Figure 2.2 for a comparison of Equations (2.1) - (2.6).

$\widetilde{H}_s$	$\widetilde{T}_p$
$a_1 = 2.88 \times 10^{-3}$	$a_2 = 0.459$
$b_1 = 0.45$	$b_2 = 0.27$
$c_1 = 0.24$	$c_2 = 7.69$
$k_1 = 4.41 \times 10^{-4}$	$k_2 = 2.77 \times 10^{-7}$
$k_3 = 0.343$	$k_4 = 0.10$
$m_1 = 0.79$	$m_2 = 1.45$
$m_3 = 1.14$	$m_4 = 2.01$
$p = 0.572$	$q = 0.187$

Table 2.2: *The coefficients for* (2.1), (2.2), (2.3), (2.4), (2.9) *and* (2.10) *based on the composite dataset as proposed by Kahma and Calkoen (1992) and with fully developed sea states described by coefficients of Pierson and Moskowitz (1964) as supported by Breugem and Holthuijsen (2007)*

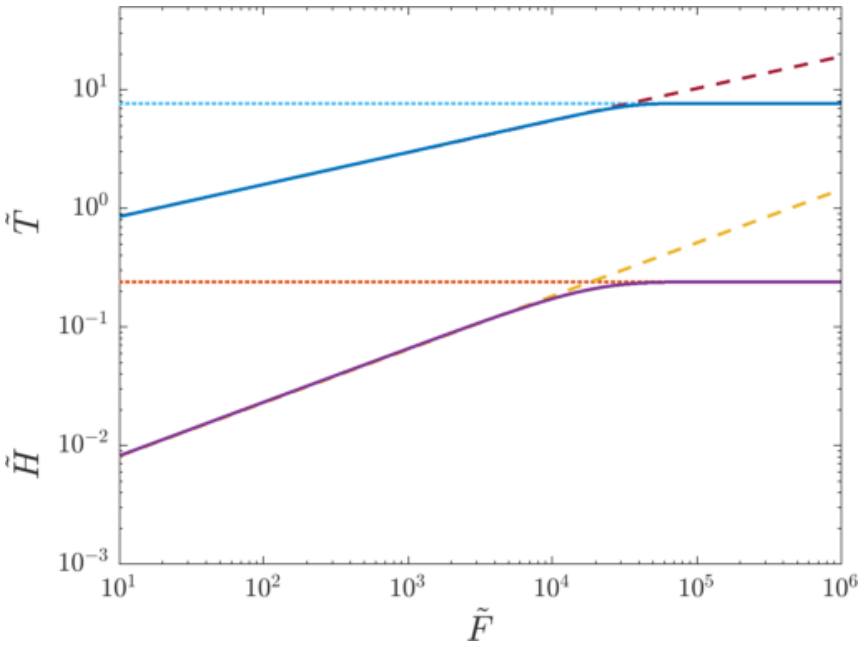

Figure 2.2: *The tanh fit of Young and Verhagen (1996) (full lines) to the Kahma and Calkoen (1992) curves (dashed lines) and the fully developed limit from Pierson and Moskowitz (1964) (dotted lines) on the growth curve for significant wave height (lower graphs) and peak period (upper graphs) as a function of fetch on log-log scale. Definitions of dimensionless variables can be found in Table 2.1.*

Finite depth effects

Apart from describing the transition to fully developed wave conditions, in the same paper Young and Verhagen (1996) acquired a new set of wave observations in lake George in Australia, in this measurement campaign focusing on the effect of depth limitations on wave growth. They expected the cut-off wave states in finite depth to scale with the water depth. This depth dependence was confirmed in their study, see Figure 2.3. Although a large scatter can be observed, a depth dependent upper bound was present in the data. Despite being slightly gentlier sloped, the relation for

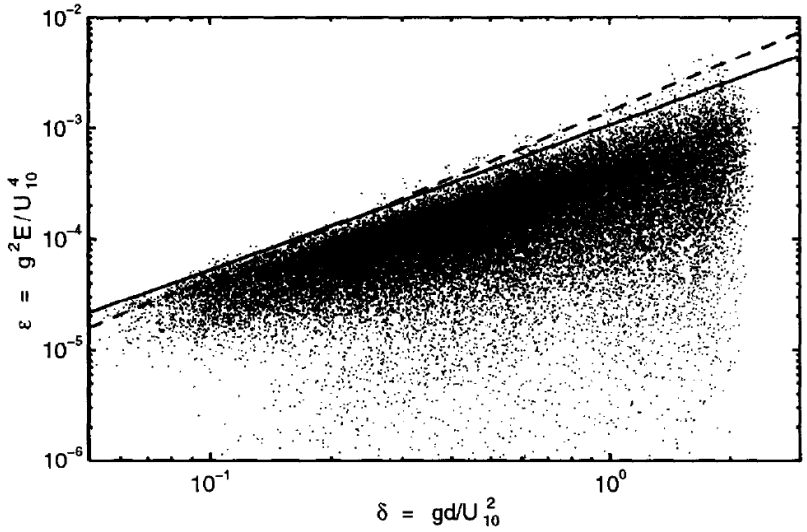

Figure 2.3: *A scatter plot wave observations in finite depth taken from Young and Verhagen (1996). The dimensionless wave energy ϵ is plotted against dimensionless depth δ. The upper-envelope (solid line) and the Lake Okeechobe result (Bretschneider (1978)) (dashed line).*

this upper bound is similar to a prediction relation already in 1978 by Bretschneider. The characterization of the depth effect on the fully developed criteria by Young and Verhagen (1996) was given by:

$$\widetilde{H_\infty} = \min\left(a_3\widetilde{h}^{b_3}, \widetilde{H_{\infty\,\text{deep water}}}\right) \tag{2.7}$$

$$\widetilde{T_\infty} = \min\left(a_4\widetilde{h}^{b_4}, \widetilde{T_{\infty\,\text{deep water}}}\right) \tag{2.8}$$

These relations are plotted for dimensional values in Figure 2.4. Young and Verhagen (1996) provided the growth curves with an additional tanh- expression to describe the transition between young sea states and fully developed sea states whilst also including a transition from shallow to deep water in a continuous manner:

$$\widetilde{H_\text{s}} = \widetilde{H_\infty}\left[\tanh(k_3\widetilde{h}^{m_3})\tanh\left(\frac{k_1\widetilde{F}^{m_1}}{\tanh(k_3\widetilde{h}^{m_3})}\right)\right]^p \tag{2.9}$$

$$\widetilde{T_\text{rep}} = \widetilde{T_\infty}\left[\tanh(k_4\widetilde{h}^{m_4})\tanh\left(\frac{k_2\widetilde{F}^{m_2}}{\tanh(k_4\widetilde{h}^{m_4})}\right)\right]^q \tag{2.10}$$

where

$$k_i = \left(\frac{a_i}{\widetilde{H_\infty}}\right)^{\frac{1}{p}} \text{ and } m_i = \frac{b_i}{p} \text{ for } i = 1,3 \tag{2.11}$$

$$k_j = \left(\frac{a_j}{\widetilde{T_\infty}}\right)^{\frac{1}{q}} \text{ and } m_j = \frac{b_j}{q} \text{ for } j = 2,4 \tag{2.12}$$

These relations are further referred to as YV1996. Breugem and Holthuijsen (2007) reanalyzed the lake George dataset and excluded all observations that were made under wind conditions from

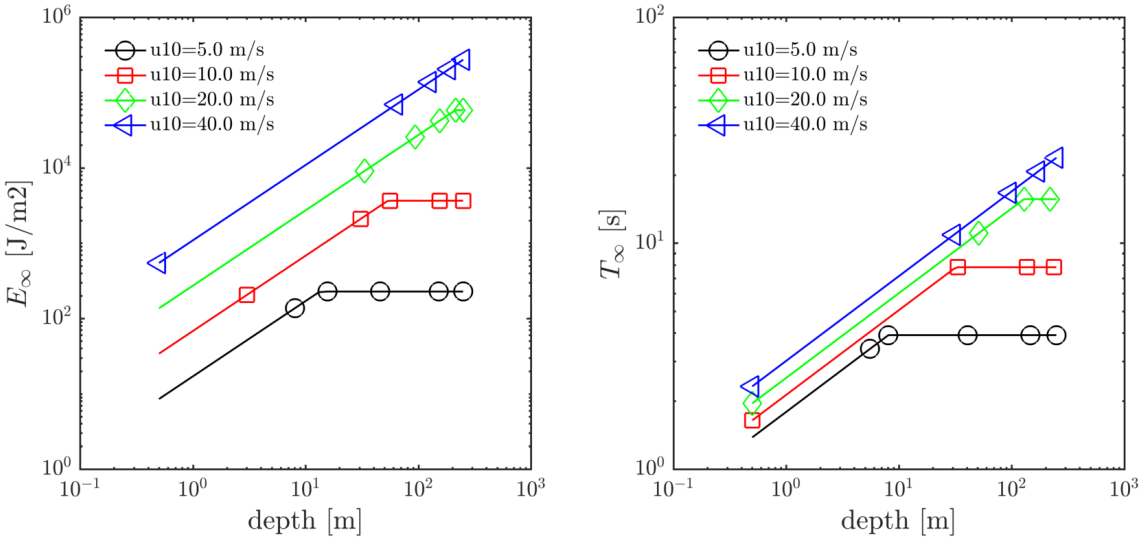

Figure 2.4: *The deep shallow water constraints on fully developed wave state as described by Young and Verhagen (1996), modified by Breugem and Holthuijsen (2007). Left: significant wave height against water depth. Right: wave peak period against water depth.*

the south, because they concluded that the lateral coastlines were influencing the sea state at the observation points for wind from this direction. They also re-examined the calculation of the fetch and excluded all calculations based on inferred fetch (deducing the fetch from the current wave state through an assumed relation). They replaced the inferred fetch calculations with the more traditional geometric fetch (the measured length of the shore-normal component of the distance towards the upwind shoreline). With the remaining observations they reconfirmed the Kahma and Calkoen composite prediction relation for deep water waves and reformulated the coefficients from Young and Verhagen (1996) for the depth-limited relations. See Table 2.2 for their quantification.

With these prediction relations, the interest in the quantification of fetch limited growth curves altered. Further studies focus on the evolution of the spectral shape or at the directional spreading of wind waves. For example, the wave spectrum in shallow water is observed to have a harmonic at slightly less then twice the peak frequency (Young and Babanin (2006)). In this paper additional shallow water wave measurements were included in the analysis, with which the shape parameters of the growth curve relations can be slightly modified to enhance the fit. With the general form of the prediction relations (2.9) and (2.10) in place, a starting point for the derivation of a source term is in place, the approach of which will not be altered by minor changes in the growth coefficients.

Correct wind speed scaling

There has been discussion about the best variable to scale dimensional variables with to make dimensionless ones. Kitaigorodskii et al. (1975) scaled the wave height, fetch and peak period with u_∞, the air velocity at the end of the boundary layer from where the wind field can be assumed uninfluenced by the waves. Hasselmann et al. (1973) and Kahma and Calkoen (1992) scaled the variables with the friction velocity u^*. This friction velocity is generally not measured directly, but inferred from a wind speed measured at some height above the water level through an assumed relation, the friction coefficient $C_D = \dfrac{u^{*2}}{u_{10}^2}$ for example. The friction coefficient can

include temperature stratification effects, wind speed, density differences, etc. One would expect that through a more detailed description the predictive skill of the power laws should improve. Young and Verhagen (1996) compared the use of u_{10} and u^* through investigating the scatter of the observations around the model line, and concluded that parametrization on u^* did not significantly decrease the amount of scatter. The latter does not prove that u_{10} would indeed be the best scaling variable, but merely indicates that the indirect measurement techniques for the friction velocity might not be adequate enough to show its effect, an argument also made by Yelland and Taylor (1996). For this reason, most recent studies parameterizing power laws as (2.1) and (2.2), such as Young and Verhagen (1996) and particularly Breugem and Holthuijsen (2007), scale directly with u_{10}.

The phase plane

The prediction relations for wave height and period are both explicit in fetch, which suggests that through equating those relations, a relationship should exist between the two wave parameters as well. A universal relation between dimensionless significant wave height and wave period was already given by Toba (1972):

$$\widetilde{H} = \beta \widetilde{T_{\mathrm{p}}}^{\gamma} \tag{2.13}$$

In Toba's argumentation $\gamma = 3/2$. With the Kahma and Calkoen expressions $\beta = a_1 \left(\frac{1}{a_2}\right)^{\frac{b_1}{b_2}} = 0.0105$ and $\gamma = \frac{b_1}{b_2} = 1.6667$. This relation is plotted in the f, E phase plane in Figure 2.5. Through variations in the wind speed, a local wave state may suddenly deviate from the equilibrium relation between energy and period. Non-linear transfer processes are expected to steer towards local equilibrium. This is in fact a quasi-equilibrium, since both wave energy and period continue to grow or dissipate but are in equilibrium with each other as long as they move along the equilibrium trajectory throughout phase space. Some of the first parametric wave prediction models described exactly this evolution (e.g. Hasselmann et al. (1976), Günther (1981)). The relaxation towards equilibrium as present in Hasselmann et al. (1976) is plotted as pointed trajectories in Figure 2.5. This model behavior can serve as a means of validation of the forcing towards quasi-equilibrium of the derived wind-input source term.

2.2 Wave growth per wave component

Besides wave observations in stationary conditions, there has been an extensive discussion in the literature on development of a source term formulation for spectral wave models in non-stationary problems. The development of wind induced waves on a flat water surface is first described by Phillips (1957), based on the principle of resonance between surface pressure fields and the celerity of free surface wave components. When some waves already exist, Miles (1957) concludes that these waves modify the air flow in the boundary layer, thereby enhancing the energy transfer from wind field to surface waves (Figure 2.6). Energy transfer takes place at the concave sea surface from wind field to surface waves. Growth is a positive-feedback mechanism: the rate of change is proportional to magnitude of present wave energy. Therefore:

$$\frac{\partial E(x,y,\sigma,\theta)}{\partial t} = \gamma E(x,y,\sigma,\theta) \tag{2.14}$$

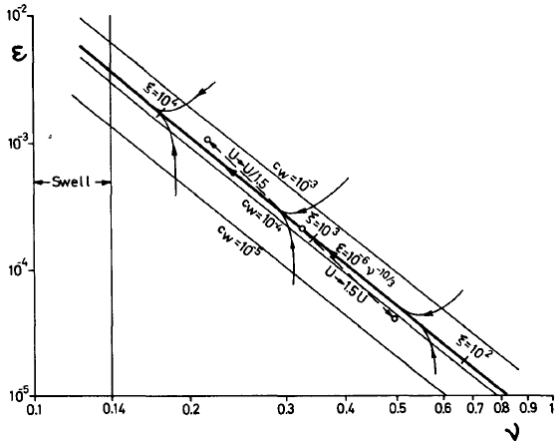

Figure 2.5: *The Hasselmann et al. (1976) quasi-equilibrium line in the ν, ϵ (dimensionless (f, E) plane. Left of the vertical line wave states can be considered uninfluenced by wind forcing (Swell). To the right trajectories from non-matching phases towards the quasi-equilibrium are drawn. The three lines marked by c_w indicate quasi-equilibria which would be find in case the drag coefficient would heave been a factor 10 more or less, hence gives a qualitative range for the likelihood of observing non-matching wave states. The three open dots connected by a dashed line indicate the jump of a wave state in the dimensionless phase plane in case the wind speed suddenly increases or drops by a factor 1.5.*

in which γ is a growth rate.

Measurements, amongst others Snyder et al. (1981) and Hasselmann et al. (1973), showed underestimation of wave growth with Miles' mechanism. This contributed to theoretical arguments stating that the mechanism as formulated by Miles oversimplifies the physics by assuming air flow is inviscid and turbulence is unimportant apart from maintaining the shear flows of air and water surface. Miles' theory however still forms the basis of the wind generation mechanism present in most of present days' wave models. Janssen (1989, 1991), following a proposal from Snyder et al. (1981), showed Miles' mechanism explained the growth rate of old sea states (sea states with fully developed wave spectra) reasonably well. He identified that the presence of waves not only influences their own direct boundary layer, but also the lower atmosphere in which the boundary layers of other waves lay. He argued the growth of young sea states can also be modeled through a Miles' like mechanism if the drag coefficient (a measure for the amount of friction between two shearing layers) is made wave age dependent. This approach was backed by observations from Donelan (1982) who found drag coefficients which were 50% higher for young sea states than for old ones. Taylor and Yelland (2000) later quantified the dependence of the sea surface roughness on the wave height and steepness.

The growth rate expression

The expression for the growth rate γ in Janssen's variation on Miles' mechanism is given by:

$$\frac{\gamma}{\omega} = \epsilon\beta \left(\frac{u_*}{c}\right)^2 \cos^2(\theta) \tag{2.15}$$

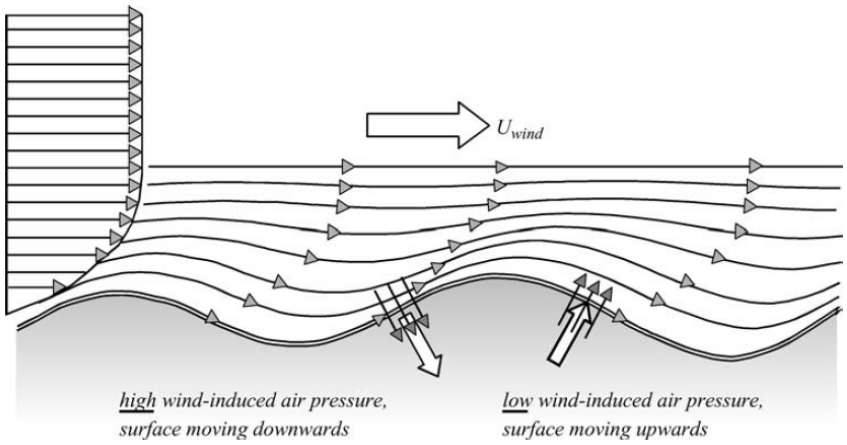

Figure 2.6: *Taken from Holthuisen (2007): The energy transfer mechanism at the concave sea surface from wind field to surface waves.*

with ω the wave frequency, ϵ the air-sea density ratio, u_* the friction velocity, θ the angle of the waves with the wave direction, c the wave celerity and β another growth rate provided by

$$\beta = \frac{1.2}{\kappa^2}\mu \ln^2(\mu) \tag{2.16}$$

Here, κ is the Von Kármán constant and μ a dimensionless critical height:

$$\mu = k(z_c + z_1) \tag{2.17}$$

This amounts to the addition of the critical height z_c, at which the resonance condition ($U_{wind} - c = 0$) is met, and the roughness length z_1 of the sea surface due to the presence and growth of short capillary waves, made dimensionless by multiplication with the wave number k. Janssen assumes that the wind profile is sufficiently described by a logarithmic profile, which enables him to rewrite μ into an expression in terms of z_0 (roughness length of the air flow) and z_1 (roughness length of the sea surface due to short capillary waves) instead of z_c (critical height) and z_1. This allows for the application of Charnock's relation:

$$z_0 = \frac{\alpha u_*^2}{g} \tag{2.18}$$

With α Charnock's constant, g the gravitational acceleration. The dependence on z_0 can then be eliminated and only z_1 remains. μ reduces to:

$$\mu = \left(\frac{u_*}{\kappa c}\right)^2 \Omega \exp[\frac{\kappa c}{u_* \cos(\theta)}] \quad , \quad \Omega = g(\frac{\alpha u_*^2}{g} + z_1)\frac{\kappa^2}{u_*^2} \tag{2.19}$$

Because of the implicit nature of the set of equations, they are solved for through the iterative procedure of Mastenbroek et al. (1992) in the most advanced wave models, (e.g. SWAN) .

2.3 Discussion

The theoretical work of above authors is the most accurate description currently available, thereby a logical candidate for a framework to develop a source term for the frequency integrated wave

drives. A major disadvantage is that the theory applies to the generation of wave-components of a sea state. This lends itself particularly well when the full wave spectrum is being discretized and modeled and only afterwards the integral wave properties are derived from the calculated wave spectra. As no information on the spectral shape is available in a frequency integrated model, the effect of growth of single wave components on the integral wave properties should be incorporated in the theory.

One approach would be to assume all spectra in a frequency integrated model to have a perfect JONSWAP shape. This way both integral wave parameters significant wave height and peak period of the spectrum could be back-engineered on which the wind input is calculated through the above described generation mechanism. Afterwards these calculated spectra can be converted back to integral wave parameters. Aside from the large amount of computations necessary in one source term update, does the wind input also rely heavily on non-linear wave-wave interactions to redistribute the wave energy input over the frequency range. Parameterizing the joint effect of these redistribution mechanisms with the growth mechanism from the state-of-the-art description of the mechanisms would come down to disguising a spectral model as a frequency integrated one.

The description of fetch-limited stationary wave states, however, takes the nonlinear transfers into account implicitly by describing the evolution of integral characteristics. Some information on the energy transfer is however lost. Integral characteristics of wave spectra are only appropriate measures if the spectrum is unimodal (e.g. well described by just one peak). Moreover, temperature or density stratification effects are ignored in the joined description of growth curves through (2.1) and (2.2). Last, the stationary solution as prescribed by the growth curves does not directly describe a growth rate. A growth rate description still needs to be derived. Janssen's formulation can then be used to prescribe some properties which a wind input formulation should conform to. In reference to (2.15):

- Growth of total wave energy is a positive feedback mechanism.
- The growth rate is wave age dependent.
- When the phase speed develops towards the wind speed, the energy transfer should diminish.
- The integral growth rate for bulk energy is dependent on the integral wave frequency.
- The directional distribution of wind input is described by $\cos^2(\theta - \theta_{wind})$.

As a concluding remark, it should be noted that the amount of scatter around all model lines through observations of integral wave characteristics is considerable. Some of the scatter can be attributed to the limited capability to measure the friction velocity, but this certainly does not explain all. Site specific influences remain unidentified. Using the prediction relations, the scatter around the model lines should always be kept in mind. A model which perfectly reproduces such growth curves does by no means have to exactly reproduce measurements at a new location.

3. Derivation of source term formulation

This chapter describes the derivation of a source term formulation for a frequency integrated wave model. First the available description from the HISWA model is discussed. In the section thereafter a different approach was adopted and described. Incorporation of wave growth in the wave action balance is discussed in Section 3.3. The domain of applicability is expanded in Section 3.4. Section 3.6 then summarizes the derived set of equations.

3.1 HISWA approach

Wave growth for a frequency integrated wave model was present in HISWA. Booij et al. (1999) presents dimensionless growth curves expressed as a function of time for the total wave energy $\widetilde{E}_1$ and the moment based mean frequency $\widetilde{\Omega}$:

$$\widetilde{E}_1 = \mathrm{a}\tanh(\mathrm{b}\,\widetilde{t}^{\,\mathrm{c}})^{\mathrm{d}} \tag{3.1}$$

$$\widetilde{\Omega}_1 = \mathrm{e}\widetilde{E}^{\mathrm{d}} \tag{3.2}$$

Where $\mathrm{a}-\mathrm{f}$ are mentioned to be model constants equal to $a = 3.6 \times 10^{-3}$, $b = 0.21 \times 10^{-21}$, $c = 4.667$, $d = 0.3$, $e = 0.04$ and $f = 0.283$. These coefficients were chosen to match the deep water wave growth of the prediction relations in the Shore Protection Manual of 1973 as closely as possible. The fitting method was not reported on. The SPM relations are:

$$\widetilde{\mathrm{H}}_s = 1.6 \cdot 10^{-3}\widetilde{\mathrm{F}}^{1/2} \tag{3.3}$$

$$\widetilde{\mathrm{T}}_p = 2.857 \cdot 10^{-1}\widetilde{\mathrm{F}}^{1/3} \tag{3.4}$$

which are equal in shape to (3.7) (3.8), with slightly different coefficients. Booij suggests taking a time derivative of (3.1) and (3.2) to obtain expressions for the source term for energy and wave period in terms of dimensionless time. (3.1) and (3.2) are then substituted in the expressions for the derivative in order to relate the rate of change of energy and frequency to their local value. In case a wave state does not conform to (3.2), the source term for the wave period is multiplied with a relaxation parameter:

$$C = \frac{\widetilde{\Omega}}{\left(e\widetilde{E}^{d}\right)^{m}} \tag{3.5}$$

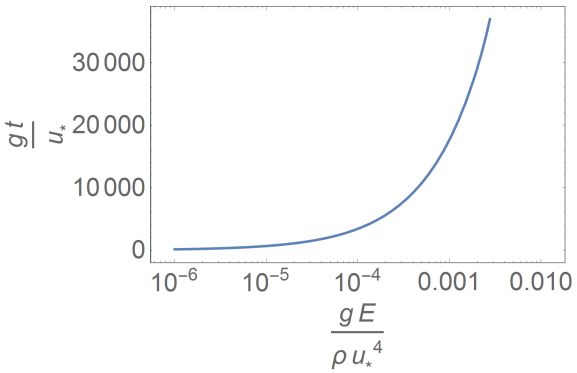

Figure 3.1: *The equivalent time derived from the local wave energy according to* (3.1).

In which m is a tuning parameter to influence the return rate of the model to (3.2). C returns the ratio between ideal wave period (i.e. following (3.2)) and the actual wave period observed:

$$C(\widetilde{E}, \widetilde{T_{\text{rep}}}) = \frac{f_{E-\omega}(\widetilde{E})}{\widetilde{\omega}} \begin{cases} = 1 & \text{wave state positioned on growth curve} \\ > 1 & \text{energy further developed than period} \\ < 1 & \text{period further developed than energy} \end{cases} \tag{3.6}$$

where $f_{E-\Omega}$ is the inverse of (3.2). In HISWA the relaxation is tuned to match Günther (1981) (as cited in Holthuijsen et al. (1989)), see Figure 2.5 or Section 2.1.

Some comments can be made regarding this wind input formulation:

- The wave energy and the representative period are not coupled by themselves in Booij's formulation. It requires a tuned relaxation factor to force growth towards a quasi-equilibrium (3.2).
- In Booij's wind input formulation, only the value of the local wave energy is included in the formulation while no spatial gradients of the wave state are taken into account. Therefore, the source term is not able to distinguish between fetch limited and time limited wave states.
- The fully developed mean wave frequency is equal to 0.1966 s^{-1} (mean period of 5.09 s). In Holthuijsen et al. (1989) a conversion factor of 1.2 between the peak period and the mean period is mentioned to be used in comparing Booij's growth curve to the SPM relations (3.3) and (3.4), which implies a peak frequency of $\widetilde{T_{\text{rep}}} = 6.1$ s. This does not equal any of the fully developed sea states described in literature (only approximates 2π, the value of wave period at which the group celerity is equal to the wind speed).
- The inverse of (3.1), is used to compute a rate of change corresponding to the current wave state. The inverse function is not defined at fully developed wave states, see Figure 3.1. Because of this, a value of the wind input term seizes to exist at wave states at fully developed or over-developed wave states. Booij does not address how to deal with these wave states. Alfons Smale and Mart Borsboom addressed source term behavior towards fully developed conditions by applying a limiter function to the value of the local energy to obtain finite rates of change on the entire domain (Smale and Borsboom (2016), personal communication).

A wind input formulation for the FIM-FM model should at least address these concerns.

3.2 Evolution relations

In this section, a slightly different approach to development of growth rate epxressions is adopted to circumvent fitting a duration-fetch relation to (Brettschneider-like) curves, because these are already empirical fits by nature. The growth curves described by Kahma and Calkoen (1992) with upper bounds described by Pierson and Moskowitz (1964) and depth limitations described by Breugem and Holthuijsen (2007) after Young and Verhagen (1996) in terms of significant wave height and peak period form the basis of this derivation. Repeating (2.1) and (2.2):

$$\widetilde{H}_{\mathrm{s}} = \mathrm{a}_1 \widetilde{F}^{\mathrm{b}_1} \tag{3.7}$$

$$\widetilde{T}_{\mathrm{p}} = \mathrm{a}_2 \widetilde{F}^{\mathrm{b}_2} \tag{3.8}$$

with quantification of coefficients $\mathrm{a}_1 = 2.88 \times 10^{-3}$, $\mathrm{a}_2 = 0.459$, $\mathrm{b}_1 = 0.45$ and $\mathrm{b}_2 = 0.27$. These growth prediction relations hold initially only in deep water and fetch limited conditions. Extension of their applicability towards these ranges is discussed in later sections. For now deep water wave conditions, non fully developed wave conditions and a one-dimensional scenario are assumed.

(3.7) and (3.8) can be rewritten explicitly in fetch:

$$\left(\frac{16\widetilde{E}}{{a_1}^2} \right)^{1/2b_1} = \widetilde{F} \tag{3.9}$$

$$\left(\frac{\widetilde{T}_{\mathrm{p}}}{a_2} \right)^{1/b_2} = \widetilde{F} \tag{3.10}$$

The conventional definition of fetch is generally the distance to the upwind shore, e.g. a geometric fetch. The fetch equivalent of a finite storm duration in case the geometric fetch is infinite is equal to the integral over the group celerity from the time wind starts blowing to the current time:

$$\widetilde{F}_{eq} \equiv \int_0^{\widetilde{t}} \widetilde{c}_{\mathrm{g}}(n, \widetilde{T}_{\mathrm{p}}, \widetilde{k}) \, \mathrm{d}t^* \tag{3.11}$$

The equivalent fetch can be interpreted as the fetch which would have lead to a stationary solution with an amount of energy equal to the energy currently present at given location under the idealized condition that wind has been blowing infinitely. Differentiating with respect to $\widetilde{t}$, the local rate of change of the equivalent fetch is then given as:

$$\frac{\mathrm{d}\widetilde{F}}{\mathrm{d}\widetilde{t}} = \widetilde{c}_{\mathrm{g}} \tag{3.12}$$

Therefore, when taking the time derivative of (3.9) and (3.10):

$$\frac{\mathrm{d}}{\mathrm{d}\widetilde{t}} \left(\left(\frac{16\widetilde{E}}{{a_1}^2} \right)^{1/2b_1} \right) = \widetilde{c}_{\mathrm{g}} \tag{3.13}$$

$$\frac{\mathrm{d}}{\mathrm{d}\widetilde{t}} \left(\left(\frac{\widetilde{T}_{\mathrm{p}}}{{a_2}^2} \right)^{1/b_2} \right) = \widetilde{c}_{\mathrm{g}} \tag{3.14}$$

These can be rewritten as:

$$f_1(\widetilde{E})\frac{\mathrm{d}\widetilde{E}}{\mathrm{d}\widetilde{t}} = \widetilde{c_{\mathrm{g}}} \tag{3.15}$$

$$f_2(\widetilde{T_{\mathrm{p}}})\frac{\mathrm{d}\widetilde{T_{\mathrm{p}}}}{\mathrm{d}\widetilde{t}} = \widetilde{c_{\mathrm{g}}} \tag{3.16}$$

in which the functions f_1 and f_2 are given as:

$$f_1(\widetilde{E}) = \frac{16}{2{a_1}^2 b_1}\left(\frac{16\widetilde{E}}{{a_1}^2}\right)^{1/2b_1-1} \tag{3.17}$$

$$f_2(\widetilde{T_{\mathrm{p}}}) = \frac{1}{a_2 b_2}\left(\frac{\widetilde{T_{\mathrm{p}}}}{a_2}\right)^{1/b_2-1} \tag{3.18}$$

Two coupled growth rates for dimensionless wave energy and peak period are then expressed as:

$$\frac{\mathrm{d}\widetilde{E}}{\mathrm{d}\widetilde{t}} = \widetilde{c_{\mathrm{g}}}/f_1(\widetilde{E}) \tag{3.19}$$

$$\frac{\mathrm{d}\widetilde{T_{\mathrm{p}}}}{\mathrm{d}\widetilde{t}} = \widetilde{c_{\mathrm{g}}}/f_2(\widetilde{T_{\mathrm{p}}}) \tag{3.20}$$

These two equations entail 3 unknown variables $(\widetilde{\mathrm{E}}, \widetilde{\mathrm{T}}_p, \widetilde{\mathrm{c}}_g)$. The dispersion relationship f_d establishes another relation between wave celerity and wave period:

$$\widetilde{c_{\mathrm{g}}} = f_d(n, \widetilde{T_{\mathrm{p}}}, \widetilde{k}) \tag{3.21}$$

$n = f(h, k)$, and $k = f_d(T_{\mathrm{p}})$ and wheref_d is given bt (1.2).

Therefore, the wind input is given by the three relations (3.19), (3.20) and (3.21) in the three unknown variables $\widetilde{E}$, $\widetilde{T_{\mathrm{p}}}$ and $\widetilde{c_{\mathrm{g}}}$ given the local flow information: water height h, and flow velocity $\vec{u}$.

3.3 The wave action balance

In this section (3.19) and (3.20) are converted to source terms for the wave action balance in one dimension. The total derivative of dimensionless wave action in 1D can be expressed in the derivatives of dimensionless energy and frequency as:

$$\frac{\mathrm{d}\widetilde{A}}{\mathrm{d}\widetilde{t}} = \frac{\mathrm{d}}{\mathrm{d}\widetilde{t}}\left(\frac{\widetilde{E}}{\widetilde{\sigma}}\right) = \frac{1}{\widetilde{\sigma}}\frac{\mathrm{d}\widetilde{E}}{\mathrm{d}\widetilde{t}} - \frac{\widetilde{E}}{\widetilde{\sigma}^2}\frac{\mathrm{d}\widetilde{\sigma}}{\mathrm{d}\widetilde{t}} \tag{3.22}$$

Under the assumption that any ambient currents are stationary in space and time, the rate of change of intrinsic frequency is assumed to be similar to the rate of change of absolute frequency:

$$\frac{\mathrm{d}\sigma}{\mathrm{d}t} \approx \frac{\mathrm{d}\omega}{\mathrm{d}t} \tag{3.23}$$

Therefore the rate of change of wave action can be written as:

$$\frac{\mathrm{d}\widetilde{A}}{\mathrm{d}\widetilde{t}} = \frac{1}{\widetilde{\sigma}}\frac{\mathrm{d}\widetilde{E}}{\mathrm{d}\widetilde{t}} + 2\pi\frac{\widetilde{E}}{\widetilde{\sigma}^2{\widetilde{T_{\mathrm{p}}}}^2}\frac{\mathrm{d}\widetilde{T_{\mathrm{p}}}}{\mathrm{d}\widetilde{t}} \tag{3.24}$$

The rate of change of wave action is governed by the rates of change of wave energy (3.19) and wave period (3.20). The dimensionless formulation must be converted to a dimensional source term. This conversion is given by:

$$\frac{\mathrm{d}A}{\mathrm{d}t} = \frac{\rho {u_{10}}^4}{g} \frac{\mathrm{d}\widetilde{A}}{\mathrm{d}t} \equiv f_{\widetilde{A}-A}(\widetilde{A}) \tag{3.25}$$

Here and in the following, the projection function from dimensionless to dimensional quantities is named as $f_{\widetilde{\mathcal{Q}}=\mathcal{Q}}(\overline{\mathcal{Q}})$. The wave action balance is in conservative form, i.e. wave action is conserved in any arbitrary control volume when no sink or source terms are present. The total rate of change of wave action is equal to the sum of source terms:

$$\frac{\partial A}{\partial t} + \frac{\partial}{\partial x}\left(c_{\mathrm{g}} A\right) = S(A, t, x, \ldots) \tag{3.26}$$

The evolution of wave action as described in (3.25) however, is expressed in nonconservative form:

$$\frac{\mathrm{d}}{\mathrm{d}t} = \frac{\partial}{\partial t} + \frac{\mathrm{d}x}{\mathrm{d}t}\frac{\partial}{\partial x} \equiv \frac{\partial}{\partial t} + c_{\mathrm{g}}\frac{\partial}{\partial x} \tag{3.27}$$

Therefore, the cross-component of the gradient of $c_{\mathrm{g}}A$ needs to be added to the source term. The wave action balance with wind-input as the only source term, is then given as:

$$\frac{\partial A}{\partial t} + \frac{\partial}{\partial x}\left(c_{\mathrm{g}} A\right) = \frac{\mathrm{d}A}{\mathrm{d}t} + A\frac{\partial c_{\mathrm{g}}}{\partial x} \tag{3.28}$$

in which $\frac{\mathrm{d}A}{\mathrm{d}t}$ is according to (3.25) with (3.30), $\widetilde{c_{\mathrm{g}}}$ from (3.21) and $\widetilde{E}$, $\widetilde{T_{\mathrm{rep}}}$ follow from Table 2.1. The first term on the right hand side of (3.28) will be nonzero in each local wave state below the fully developed wave conditions. In an infinite domain with uniform wave field, these are the duration-limited wave states. The second term, the gradient of the group celerity, is only non-zero in those wave states in which spatial differences are present. In an ideal scenario of a constant wind blowing over a domain, this term will only be non-zero for fetch-limited wave states, since those wave states lie on the curves (3.7) and (3.8).

When a wave state under consideration is forced to always comply with the wave prediction relations (3.7) and (3.8), the wave period is a property of the total energy (or vice versa). Equating (3.9) and (3.10), $\widetilde{T_{\mathrm{rep}}}$ can be expressed in terms of $\widetilde{E}$ along the growth curve:

$$\widetilde{T_{\mathrm{p}}} = a_2 \left(\frac{16\widetilde{E}}{a_1^2}\right)^{b_2/2b_1} = f_{E-T_{\mathrm{p}}}(\widetilde{E}) \tag{3.29}$$

See also Section 2.1. The group celerity then follows from the wave period and wave number (obtained through the dispersion relationship). Also the group celerity therefore is a property of the wave energy along the growth curve. Hence, to study the evolution of the action balance as an initial condition problem matching (3.29), it is sufficient to assess just the action balance and let the period be a property of the total wave energy through (3.29).

Generally speaking however, a boundary value problem in shallow water has boundary wave states which do not necessary match (3.29). It is incorrect to overwrite the boundary conditions and force the peak period to match the young sea state energy through (3.29). At the same time, the win input within the domain is such that it forces a wave state to (3.29). To correctly resolve both processes, an additional evolution relation for the wave period is necessary where the advection scheme correctly combines the wave periods of adjacent cells.

In absence of ambient currents

Although the derivation of the wind source term describes the evolution of peak period (T_p), the spectral mean period ($T_{M-1,0}$) is a more appropriate period as propagation of wave period essentially comes down to an energy averaging of the wave period in two neighboring grid cells. Therefore, the representative period (T_{rep}) describes the spectral mean period instead of the spectral peak period from here onwards.

If ambient currents are absent, (3.22) reduces to:

$$\frac{\mathrm{d}\widetilde{A}}{\mathrm{d}\widetilde{t}} = \frac{1}{2\pi}\left(\widetilde{T_{\text{rep}}}\frac{\mathrm{d}\widetilde{E}}{\mathrm{d}\widetilde{t}} + \widetilde{E}\frac{\mathrm{d}\widetilde{T_{\text{rep}}}}{\mathrm{d}\widetilde{t}}\right) = \frac{1}{2\pi}\left(\frac{\widetilde{T_{\text{rep}}}\widetilde{c_{\text{g}}}}{f_1(\widetilde{E})} + \frac{\widetilde{E}\widetilde{c_{\text{g}}}}{f_2(\widetilde{T_{\text{rep}}})}\right) \tag{3.30}$$

Although (3.20) gives an explicit source term for the wave period, wave period by itself is not a conserved quantity and hence can't be advected in the same manner as total wave action throughout the domain. For this reason, a complementary evolution relation must be solved for. Moments of the wave action spectrum provide a means hereto. The n-th moment of the wave action spectrum is defined as:

$$m_n^A = \int_0^\infty \omega^n A(\omega)\,\mathrm{d}\omega \tag{3.31}$$

In the absence of background currents the relative and absolute frequency are equal: σ=ω, and hence a mean wave period in terms of wave action spectral moments can be derived from the more well known expressions in terms of wave energy spectral moments ($m_n^E = \int_0^\infty \omega^n E(\omega)\,\mathrm{d}\omega$):

$$T_{\text{rep}\,M^E_{-1,0}} = \frac{2\pi}{\omega_{M^E_{-1,0}}} \equiv 2\pi\frac{m^E_{-1}}{m^E_0} = 2\pi\frac{\int_0^\infty \frac{E}{\omega}\,\mathrm{d}\omega}{\int_0^\infty E\,\mathrm{d}\omega} = 2\pi\frac{\int_0^\infty A\,\mathrm{d}\omega}{\int_0^\infty \omega A\,\mathrm{d}\omega} = 2\pi\frac{m^A_0}{m^A_1} \equiv T_{\text{rep}\,M^A_{01}} \tag{3.32}$$

From here onwards a spectral moment is taken from the wave-action spectrum and the superscript A is dropped, unless otherwise specified. The total wave action is equal to the first order moment of the wave action spectrum, and in absence of currents the first spectral moment is equal to the total wave energy. Therefore the wave action balance (3.28) is complemented with a wave energy balance:

$$\frac{\partial E}{\partial t} + \frac{\partial}{\partial x}\left(c_{\text{g}}E\right) = \frac{\mathrm{d}E}{\mathrm{d}t} + E\frac{\partial c_{\text{g}}}{\partial x} \tag{3.33}$$

in which:

$$\frac{\mathrm{d}E}{\mathrm{d}t} = \frac{{u_{10}}^3}{\rho}\frac{\mathrm{d}\widetilde{E}}{\mathrm{d}\widetilde{t}} \tag{3.34}$$

where $\frac{\mathrm{d}\widetilde{E}}{\mathrm{d}\widetilde{t}}$ according to (3.19), $\widetilde{E}$ and $\widetilde{c_{\text{g}}}$ follow from Table 2.1. The representative period is then calculated from $2\pi\frac{A}{E}$.

Further on, reference is made to the Frequency Prescribed Model (FPM) in case the wave period is prescribed thus constant (the XBeach approach) while Frequency Integrated Model (FIM) refers to the derived two-balances approach in which the wave period evolves.

Ambient currents

This section investigates to what extent the presence of ambient currents affects the derived source term. In the presence of background currents, a distinction arises between the absolute wave frequency, as would be observed by a fixed observer, and the relative frequency, which is measured by an observer moving with the background current. The wave periods that follow from the prediction relations are absolute, since they are best-fit curves through a scatter of wave height and period observations (which are generally made on a fixed location). This has consequences for the above derivation.

First, the first order moment of the wave-action spectrum does no longer equal total wave energy, since it gets multiplied by the ratio between mean absolute and mean relative frequency: $m_1 = \frac{\omega}{\sigma} \cdot E$, where $\sigma = \omega - \vec{k} \cdot \vec{u}$. The stronger the current, the larger the deviation from total wave energy. Hence it would better to refrain from naming the first order moment total wave energy but rather refer to it simply as the first spectral moment in case ambient currents are taken into account.

The measure of mean period which is obtained from dividing the zeroth spectral moment by the first is no longer identical to $T_{\text{rep}_{M_{-1,0}}}$. The relation only holds in zeroth order approximation:

$$\begin{aligned} T_{\text{rep}}{}^{A}_{M_{01}} &= 2\pi \frac{m_0^A}{m_1^A} \\ &= \frac{\int A \,\mathrm{d}\omega}{\int \omega A \,\mathrm{d}\omega} \\ &= \frac{\int \frac{1}{\omega - \vec{k}\cdot\vec{u}} \,\mathrm{d}\omega}{\int \frac{\omega}{\omega - \vec{k}\cdot\vec{u}} E \,\mathrm{d}\omega} \\ &= \frac{\int \frac{E}{\omega} \left(1 + \frac{\vec{k}\cdot\vec{u}}{\omega} + (\frac{\vec{k}\cdot\vec{u}}{\omega})^2 + \dots\right) \mathrm{d}\omega}{\int E \left(1 + \frac{\vec{k}\cdot\vec{u}}{\omega} + (\frac{\vec{k}\cdot\vec{u}}{\omega})^2 + \dots\right) \mathrm{d}\omega} \end{aligned} \tag{3.35}$$

It does however still produce a measure of mean absolute period, but because of the weighting by the action spectrum instead of the energy spectrum it can not be linked to the conventional energy weighted measure. Before the two-equation approach is adopted in ambient-current problems, the validity of the approach should be investigated further. One recommendation is made for this situation. The mechanism of energy exchange through the boundary layer on the water-air interface is believed to be driven on velocity gradients between the wind speed and the wave speeds. When a background current is present, the wave speeds are dependent on the relative frequency, such that the wave speed is either greater or smaller than in the absence of a background current. Therefore, the magnitude of wind speed should be corrected with the parallel component of the background current when used to calculate the wind input.

3.4 Expanding the domain of applicability

So far, the derived growth rates (3.19) and (3.20) are able to describe wave growth in deep water for young sea states. To expand the range of applicability of the source term, the transition to fully developed conditions is described and two approaches to deal with finite-depth effects are suggested in this section.

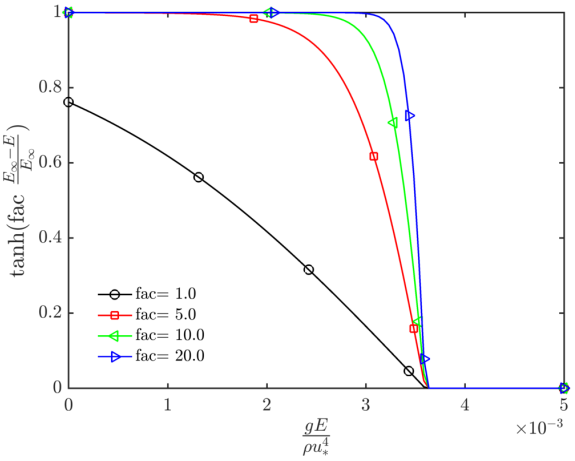

Figure 3.2: *The behavior of the tapering function χ_E (3.36) for energy as a function of dimensionless wave energy.*

Transition to fully developed conditions

Fully developed wave conditions are physically very rarely realized, because of the extremely large lengths of aligned, open water necessary to obtain the required dimensionless fetch. Only when the wind speed suddenly drops, thereby increasing the dimensionless value of the fetch, would fully developed conditions be encountered in a nearshore model. With this scenario in mind, it is important to also describe the behavior of the source term on the transition to fully developed conditions (2.7) and (2.8). Hence the solution of an idealized set-up of the model should converge to (2.5) and (2.6) in deep water. This can be realized by multiplying the source term with a tapering function:

$$\chi_i(\widetilde{\mathcal{Q}}_i) = \max\left[\tanh\left(\text{fac}_i \frac{\widetilde{\mathcal{Q}}_{i,\infty} - \widetilde{\mathcal{Q}}_i}{\widetilde{\mathcal{Q}}_\infty}\right), 0\right] \tag{3.36}$$

Where $i \in \{E, T_{\text{rep}}\}$ and $\mathcal{Q}$ dummies either for E or T_{rep} . This tapering function ensures that in fully developed wave states the total wave energy and the representative wave period do not grow further, while for wave states close to fully developed wave conditions the amount of wind input is reduced to zero continuously for stability reasons. With the tuning factors fac_i it is possible to mimic the smoothened behavior of (2.5) and (2.6) in the transition region (Figure 2.2). See Figure 3.2 for the behavior of χ_E for different values of the tuning factor. For energy values larger than the fully developed criterion the taper function is always equal to zero.

The best-fit parameters for fac_i were found by minimalizing the mean relative error on 4 locations in the transition region between the model output and the relations (2.5) and (2.6), see figure Figure 3.3. The best fit was found for $\text{fac}_E = 2.0$ and $\text{fac}_T = 8.5$.

Range of the source term

Robustness of the system of equations regardless of the initial conditions it is provided with is important. This section investigates the range (co-domain) of growth rates (3.19) and (3.20) as a function of its domain. Since the mapping from dimensionless to dimensional variables is strictly monotone, it is sufficient to asses any asymptotic behavior in dimensionless space to cover the entire domain of energy, wave period and wind speed.

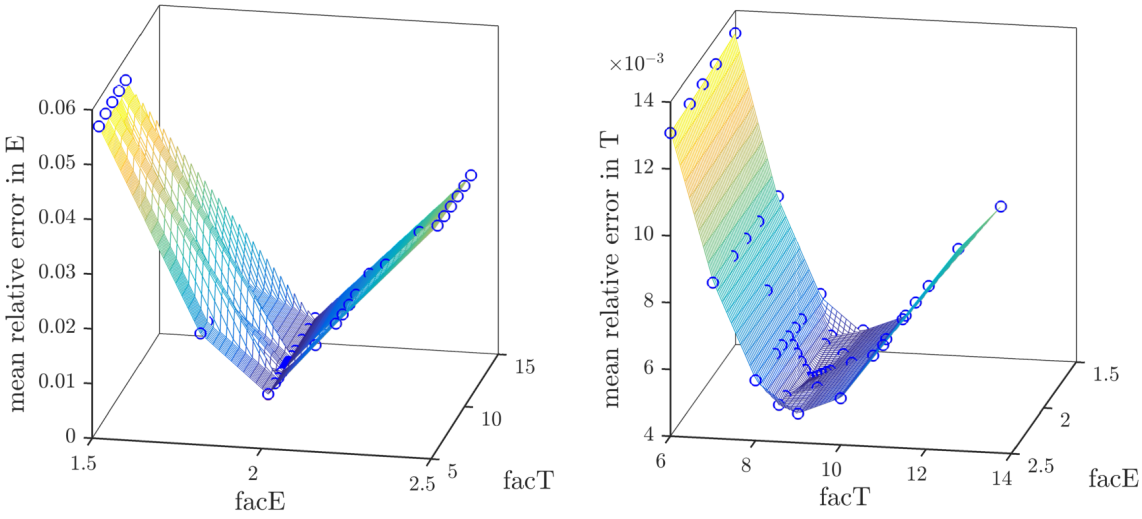

Figure 3.3: *Bisection of a surface plot of the mean relative error on four locations in the transition region towards fully developed wave conditions* (2.9) *and* (2.10) *against the tuning factors facE and facT. Left: mean relative error in growth curve of wave period, Right: mean relative error in growth curve of wave energy.*

First, in Figure 3.4, the magnitude of the source terms in case the wave energy and wave period match the quasi-equilibrium (3.29) as suggested by the growth curves is displayed for both growth to the Kahma and Calkoen (1992) curves (top panels) as well as tapered growth to the Young and Verhagen (1996) curves. Differentiation is made between a duration-limited scenario in which no spatial gradients are present (displayed in blue circles) and a scenario in which the spatial gradients in the group celerity are equal to those along an ideal growth curve, i.e. a fetch limited scenario (red circles). The additional growth in a fetch limited scenario is considerable at around 20% of the local rate of change. When stronger gradients in the group celerity are present, this increase in growth rate can be even larger and without limiter could tend to infinity ($\frac{\mathrm{d}E}{\mathrm{d}t} \propto \frac{\partial c_g}{\partial x}$ therefore $\lim_{\frac{\partial c_g}{\partial x} \to \infty} (\frac{\mathrm{d}E}{\mathrm{d}t}) \to \infty$). A numerical implementation of the generation mechanism should limit this behavior. More on proposed limiters is described in Section 5.3.

Asymptotic behavior potentially occurring in regions of the phase space far away from the quasi-equilibrium relation between energy and period, (2.13) and the white dashed lines in Figure 3.5, needs to be addressed. Figure 3.5 plots the magnitude of (3.19) and (3.20) in the absence of spatial gradients in the complete domain of wave energy and period. Paneling is similar to Figure 3.4. In the left column of the figure the tapering of the source term to the Young and Verhagen (1996) curves is shown to remove the discontinuity in the source term around the fully developed wave energy cut-off. The rate of change of the period (right column) shows asymptotes around $\widetilde{\mathrm{E}} = 0$ and $\widetilde{\mathrm{T}} = 0$. In a numerical model with integration through an arbitrary time step such as the quasi-time stepping approach to the stationary iterative solver, such as the FPM-FM, the change of action per time step needs to be bounded. Again, more on a proposed upper bound is given in Section 5.3.

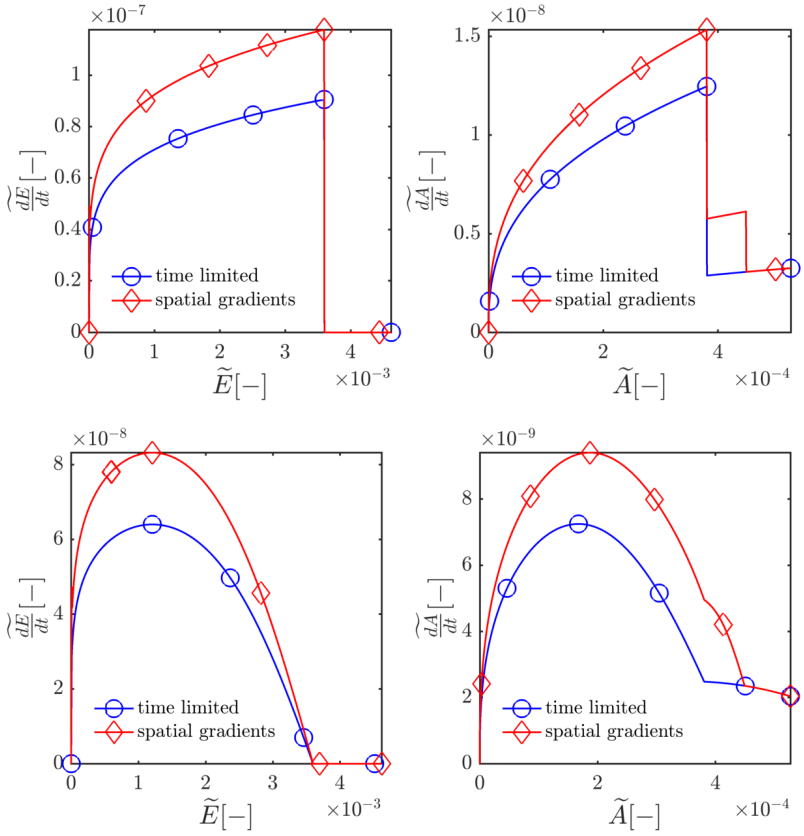

Figure 3.4: *The dimensionless magnitude of the derived source terms for both the action balance (right panels) and the energy balance (left panels). The top row shows the magnitude of the source term from the derivation from Kahma and Calkoen (1992) curves, while the bottom row shows the magnitudes for the source terms that have been tapered towards Young and Verhagen (1996) curves through* (3.36) *with* $fac_E = 2$ *and* $fac_T = 8.5$*. The red diamond marked line includes the spatial gradient term in* (3.28) *and* (3.33) *while the blue circle marked line assumes a spatially uniform wave field where no spatial gradients in group celerity are present. Since the evolution of action and energy is a coupled system of equations through the group celerity, the wave energy and wave period comply to the quasi-equilibrium that is suggested by the growth curves in producing these figures to eliminate a degree of freedom.*

3.5 Depth limitations

Wind waves on water with finite depth develop to smaller heights than on deep water. Physically, this height limitation will be due to dissipation or friction processes. The shallow water measurements on which the depth limited growth curves from literature are fitted however, entail all field generation and dissipation processes available. Up until this point, the wave balance with just one source term was discussed:

$$\frac{\partial A}{\partial t} + \nabla \cdot (\vec{v}A) = S_A \tag{3.37}$$

S_A was formulated to correctly reproduce wave growth in deep water. In growth scenarios the shallow water effect can be incorporated by evaluating at each cell the depth restricted fully developed wave conditions described in (2.7) and (2.8) and substituting these for $\widetilde{Q}$ in (3.36). Thus avoiding a need for explicit description of any dissipation processes and being able to match the shallow water curves from literature exactly. The influence of these depth limitations on the mag-

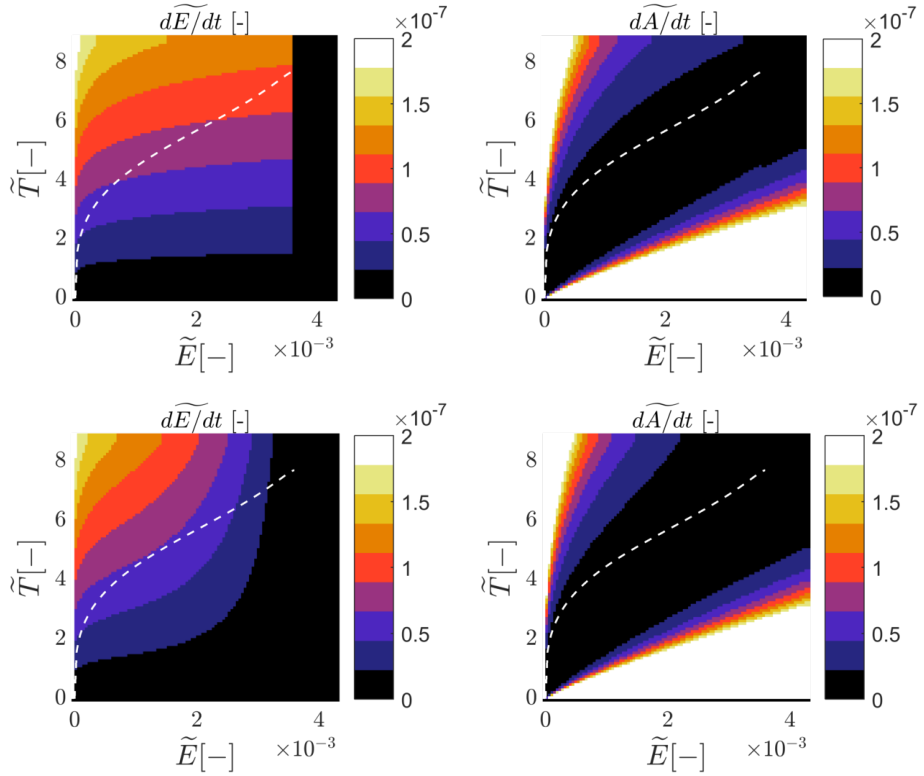

Figure 3.5: *the dimensionless magnitude of the derived source term for both the action balance (right panels) and the energy balance (left panels) in the absence of spatial gradients, that is, an infinite uniform domain. The top row shows the magnitude of the source term from the derivation from Kahma and Calkoen (1992) curves, while the bottom row shows the magnitudes for the source terms that have been tapered towards Young and Verhagen (1996) curves though* (3.36) *with* $fac_E = 2$ *and* $fac_T = 8.5$*. Generally speaking the wave energy and period need not comply to the quasi-equilibrium suggested by the growth curves (dashed white lines), hence these contour plots show the behavior in the entire dimensionless phase space.*

nitude of the growth term are drawn in Figure 3.6. Implicitly, the effect of bottom friction (D_f) is then incorporated in S_{in}. This approach prevents locally generated wave energy from overdeveloping. However, as S_{in} is strictly positive, it can't dissipate wave energy which is overdeveloped compared to the water depth. To do that, an explicit description of bottom friction is necessary.

Suppose that the wind input tapered to correct depth is simply added to the FPM-FM energy balance:

$$S_A(u_{10}, d, E, T) = D_f(d, E, T) + D_{br}(d, E, T) + S_{in}(u_{10}, d, A, E) \tag{3.38}$$

As S_{in} decreases with decreasing water depth and D_f increases with decreasing water depth, finite depth effects are counted double in the effective source term S_A. The growth rate of waves in shallow water is hence under predicted. Therefore, the description of wave generation and depth effects is ideally decoupled by removing the depth dependence from the wind input term:

$$S_A(u_{10}, d, E, T) = D_f(d, E, T) + D_{br}(d, E, T) + S_{in}(u_{10}, A, E) \tag{3.39}$$

As the FPM-FM model keeps the wave period constant and equal to the boundary provided value, no evolution of period under dissipation is currently present. Finite depth affects both the fully developed value of wave energy as well as the magnitude of its corresponding wave period. Therefore, if depth effects are to be taken out of the source term formulation in FIM-FM, an evolution

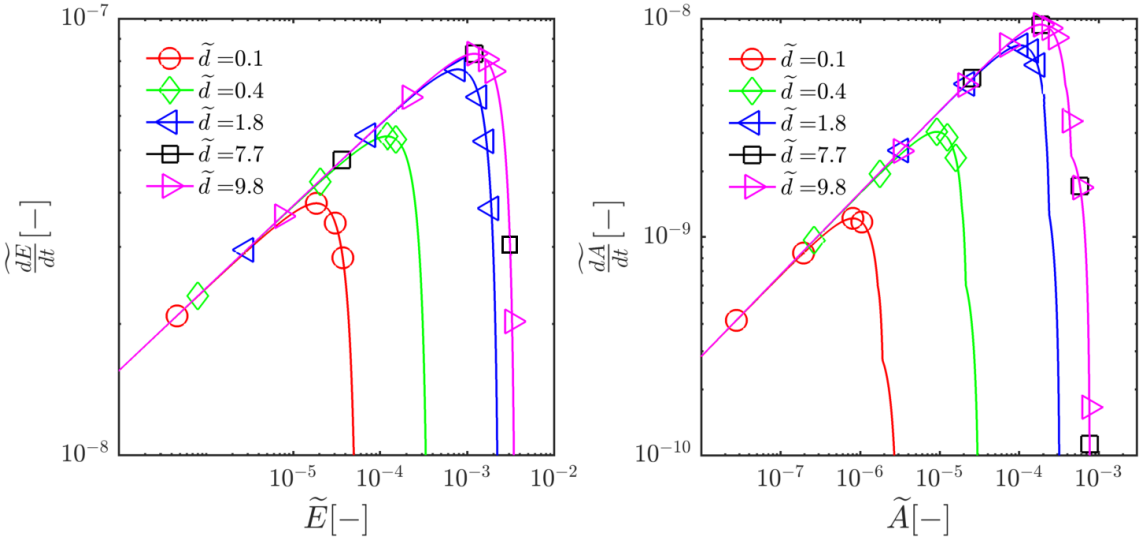

Figure 3.6: *The dimensionless magnitude of the source term in shallow water as a function of dimensionless wave energy and different water depths (left) and as a function of dimensionless wave action and various water depths (right).*

mechanism for the wave period under dissipation processes must be incorporated. Eldeberky (1996) observed that the general shape of the wave spectrum remains constant under depth induced breaking such that the breaking-induced dissipation can be distributed over the frequencies in proportion to the local spectral energy. The representative period can thus be assumed constant under wave breaking. What remains is the coupling of wave period evolution under bottom friction. The representative wave period T_{rep} changes under bottom friction because waves with large periods undergo more dissipation than waves with smaller periods. As evolution of T_{rep} is thus essentially a result of dissipation of waves energy, the change of T_{rep} can be coupled to the magnitude of D_f.

Parameterizations of bottom friction

FPM-FM currently models bottom friction on the bulk wave energy after Roelvink and Stive (1989):

$$D_f = \frac{2}{3\pi}\rho f_w \left(\frac{\pi H_{rms}}{T_{m01}\sinh(kh)}\right)^3 \tag{3.40}$$

In which T_{m01} is a mean wave period based on the zeroth and first moment of the energy spectrum, H_{rms} the root mean square wave height and f_w a friction coefficient (which is a measure of the bottom roughness). A description of evolution of wave period under dissipation is presented in Booij et al. (1999), and repeated for completeness in Appendix A. The obtained relationship between D_f and evolution of wave period (D_T) is given by:

$$\left(\frac{\partial T}{\partial t}\right) = C_T \frac{T^2}{2\pi(1-n)} c_g k_p \frac{1}{E}\left(\frac{\partial E}{\partial t}\right) \tag{3.41}$$

With shape parameter $n = 3$ in the derivation by Booij, which means that the high wave number tail of the wave number-variance spectrum is described there by $E \propto k^{-3}$. Introducing the coefficient C_T, the evolution of T_{rep} can be tuned to account for varying shapes of the spectral tail. The

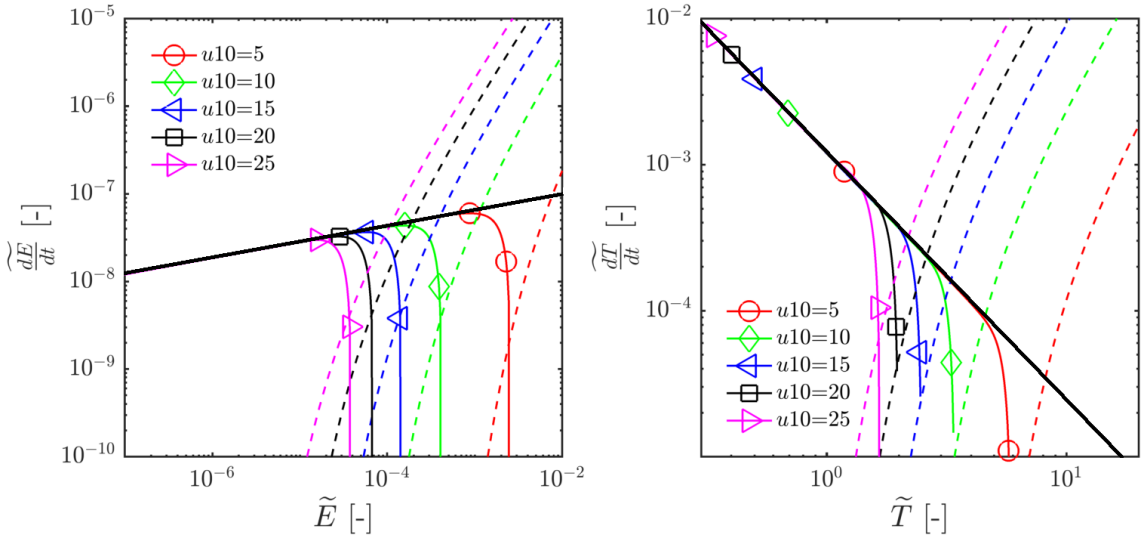

Figure 3.7: *Dimensionless rates of change of wave energy (left) and wave period (right) assuming energy and period are related through quasi-equilibrium (Section 4.4). Deep water solution in solid black line. Dimensionless rates of change in colored solid lines. Dimensionless bottom friction scaled with the friction coefficient* $\frac{D_f}{f_w}$ *in dashed colored lines for varying wind speed. Figure drawn for* $d = 5$*m.*

coupling between dissipation of wave energy and wave period is two-way. Because D_f depends negatively on $Tm01$ the wave energy dissipation mechanism is coupled back to the wave period field.

Balance of S_{in} and D_f

A balance between S_{in} and D_f can only hold if both reach similar order of magnitude at the appropriate shallow water upper limits. Qualitatively, this is investigated in Figure 3.7.

Here, the magnitude of the wind input without depth effects is plotted as black thick solid lines in dimensionless variables, in case the wave energy and period match the quasi-equilibrium (2.13). When finite depth effects are included in the source term formulation by assuming a finite depth (in this particular figure $d = 5$m), the rates of change become wind speed dependent (the marked colored sold lines). This is due to a varying dimensionless water depth, such that fully developed conditions are met at lower dimensionless wave energy for higher wind speeds[1].

The dashed lines, in color corresponding to the various wind speeds, represent the dimensionless bottom friction dissipation rate $\widetilde{\frac{D_f}{f_w}}$ (left) and $\widetilde{\frac{D_T}{f_w}}$ (right). Although the match is not exact, the dissipation mechanisms obtain non-negligible values at a range of wave energy and period where the depth limited wind-input starts to deviate from the depth-independent wind input. From these wave states onwards, the dissipation mechanisms grow more relevant and eventually dominate over the wind input. Identifying the correct friction coefficients, a balance between the dissipation and depth-independent source term should account to correct depth limited growth curves. It is

[1] Note this leads to larger rates of change for higher wind speeds in the dimensional world, something that is not directly obvious from the dimensionless figure! The smaller waves [small wind speeds] are influenced by bottom effects in shallower water than large waves [large wind speeds] are, which is why in this dimensionless plot the lower wind speeds deviate at larger dimensionless wave energy from the depth-independent wind input

further investigated which magnitude of f_w is necessary to reach a balance between S_{in} and D_f at the literature described upper limits in Section 4.3.

3.6 Summarizing

In the above derivation, a source term for the wave action balance was formulated that should match the prediction relations by Kahma and Calkoen (1992), or, when a smooth transition to fully developed conditions is preferred, the relations described by Young and Verhagen (1996). Because the group celerity varies along these growth curves, it became apparent that a second evolution relation was necessary to solve the evolution of the mean wave period over the domain. The evolution of the first order moment of the wave action spectrum, complementary to the zeroth order moment, was found able to provide a measure for the wave period. In the absence of ambient currents, this first order moment can be interpreted as the bulk wave energy, and the ratio between action and energy is then equal to the commonly known $T_{\text{rep}}{}^{E}_{M_{-1,0}}$. In this and other scenario's, the ratio between action and energy will be referred to as T_{rep}. Correct upper limits on depth-limited growth curves are achieved through an explicit balance between the wind source term and bottom friction or, in local growth-dominated scenario's, by taking the dissipation effects into account implicitly in the source term formulation.

Including all the aspects above, the evolution relations of spectral bulk properties in 1D are given by:

$$\frac{\partial A}{\partial t} + \frac{\partial}{\partial x}\left(c_{\text{g}} A\right) = \mathcal{S}_A(T_{\text{rep}}, E, c_{\text{g}}) + D_{\text{A}}(x,t) \tag{3.42}$$

$$\frac{\partial E}{\partial t} + \frac{\partial}{\partial x}\left(c_{\text{g}} E\right) = \mathcal{S}_E(E, c_{\text{g}}) + D_{\text{E}}(x,t) \tag{3.43}$$

D_{A} and D_{A} entail bottom friction and breaking sink terms and:

$$\mathcal{S}_A = \frac{1}{2\pi} f_{\widetilde{A}-A}\left(\chi_E(\widetilde{E})\frac{\widetilde{T_{\text{rep}}}\widetilde{c_{\text{g}}}}{f_1(\widetilde{E})} + \chi_{T_{\text{rep}}}(\widetilde{T_{\text{rep}}})\frac{\widetilde{E}\widetilde{c_{\text{g}}}}{f_2\left(f_{E-T_{\text{rep}}}(\widetilde{E})\right)}\right) + \chi_E(\widetilde{E})A\frac{\partial c_{\text{g}}}{\partial x} \tag{3.44}$$

$$\mathcal{S}_E = f_{\widetilde{E}-E}\left(\chi_E(\widetilde{E})\frac{\widetilde{c_{\text{g}}}}{f_1(\widetilde{E})}\right) + \chi_E(\widetilde{E})E\frac{\partial c_{\text{g}}}{\partial x} \tag{3.45}$$

$f_{\widetilde{A}-A}$, $f_{\widetilde{E}-E}$, f_1, f_2 and χ_i are defined in (3.25), (3.34), (3.15), (3.16) and (3.36) respectively. $\widetilde{E}$ and $\widetilde{T_{\text{rep}}}$ follow from E and T_{rep} according to Table 2.1 and $T_{\text{rep}} = 2\pi\frac{A}{E}$.

4. Validation and properties in 1D

The validity of the derived source term formulation in 1D tests is described in this chapter. First the derived source term is compared with the HISWA source term in Section 4.1. Section 4.2 shows convergence of the system of equations to the correct growth curves. Calibration of a correct sink source term balance in depth limited conditions is described in Section 4.3. Section 4.4 assesses the strength of the return to quasi-equilibrium is. The chapter closes with a summary of the properties of the derived source term formulation that were investigated.

4.1 HISWA comparison

Booij's source term formulation provides a means of validation for the derived source term. To properly compare the behavior of the derived wind input formulation and Booij's formulation, only time limited wave states (no spatial gradients) can be addressed since Booij's source term can not distinguish between time and space limitations. Therefore, the assumption of a time limited wave state must also made for the derived source term. Furthermore, the comparison is only made for values of the wave energy and wave period that match the wave steepness prescribed by the respective growth curves: (3.2) for Booij, (3.29) for the derived growth rates. This means that at all times, the wave period can be expressed in terms of wave energy and vice versa through the prediction relations.

A duration-limited wave state has no spatial gradients. Therefore the derived source term for wave energy and period are (as compared to (3.44) and (3.45)):

$$\mathcal{S}_{E,\text{time limited}} = f_{\widetilde{E}-E}\left(\chi_E(\widetilde{E})\frac{\widetilde{c_\text{g}}}{f_1(\widetilde{E})}\right) \tag{4.1}$$

$$\mathcal{S}_{T_\text{rep},\text{time limited}} = f_{\widetilde{T_\text{rep}}-T_\text{rep}}\left(\chi_{T_\text{rep}}(\widetilde{T_\text{rep}})\frac{\widetilde{c_\text{g}}}{f_2(\widetilde{T_\text{rep}})}\right) \tag{4.2}$$

The rates of change of wave energy and period compared to Booij's formulation are plotted in Figure 4.1. First the left panel is analyzed. The rate of change of the derived source term at small wave energies is larger than Booij's source term. This results in a quicker growth of very young sea states. In time limited conditions, Booij's rate of change increases more strongly for more developed wave states. Both source terms vanish at the same condition for fully developed wave energy. In the right panel, again the rate of change of wave period for the derived source term is larger than for Booij's source term. This difference in rate of change reduces for more developed wave states, but Booij's rate of change never takes over. Because for this comparison it was chosen to express the value of the wave period in terms of wave energy, the wave period never quite reaches fully developed conditions, since the steepness relation is only valid for wave energies below fully developed conditions. To that end does the rate of change of period never

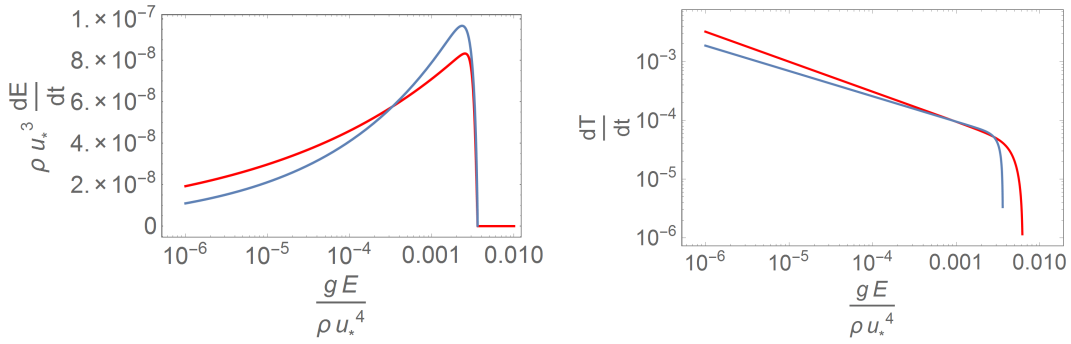

(a) Rate of change of bulk energy

(b) Rate of change of peak period

Figure 4.1: *The dimensionless rates of change of wave energy and representative period as a function of local dimensionless energy and period. Booij et al. (in blue) and the derived growth rates (in orange), in case of a duration limited wave field.*

completely reach zero. It is clear that the asymptotic behavior of Booij's source term and the derived source term do not occur at the same wave energy.

The growth curve expressed as a function of time based on the KC curves in a time limited wave state (i.e. the evolution of the wave energy and period at a fixed point in an infinite open domain) is given by the system of equations:

$$\widetilde{E}'(\widetilde{t}) - \mathcal{S}_{E,\text{time limited}}(\widetilde{E}(\widetilde{t}), \widetilde{T_{\text{rep}}}(\widetilde{t})) = 0 \tag{4.3}$$

$$\widetilde{T_{\text{rep}}}'(\widetilde{t}) - \mathcal{S}_{T_{\text{rep}},\text{time limited}}(\widetilde{T_{\text{rep}}}(\widetilde{t})) = 0 \tag{4.4}$$

These can be numerically integrated to obtain an explicit relation for $\widetilde{E}$, $\widetilde{T_{\text{rep}}}$ as a function of $\widetilde{t}$. The integration constant was chosen such that the resulting curve matched Booij's curve at $t = 1$ s. The result is plotted in Figure 4.2. Several differences between the two growth curves can be observed.

First, it can be concluded that both formulations converge to the same value for dimensionless fully developed wave energy (3.6×10^{-3}). Booij's formulation however, arrives there slightly faster (approximately 1.4 hours earlier). The rate of change of energy in the first hour in the KC derivation is faster than in Booij's growth curve. At later moments, the rate of change in Booij's formulation overtakes the KC derivation slightly.

The peak period for Booij's growth curve was obtained by multiplying the relation for the moment based mean period by a factor 1.2. This does not remove the discrepancy between the two fully developed wave periods. The derived growth curve continuous to grow further where Booij's growth curve levels off. Similar to wave energy, the wave period grows faster in the derived formulation than in Booij's formulation in young sea states, and again, at later moments, the rate of change in Booij's formulation catches up with the derived rates of change.

Developing fetch-limited wave conditions

In a half-infinite domain with on upwind side a land boundary, fetch-limited wave conditions are expected to develop. The derived source term included a term dependent on the gradient of the group celerity. This term is zero in any infinite domain with translation invariant wave conditions, but is positive when spatial gradients in group celerity are present. This results in a nett increase of the local rate of change of wave energy (See Figure 3.4). The difference between Booij's source

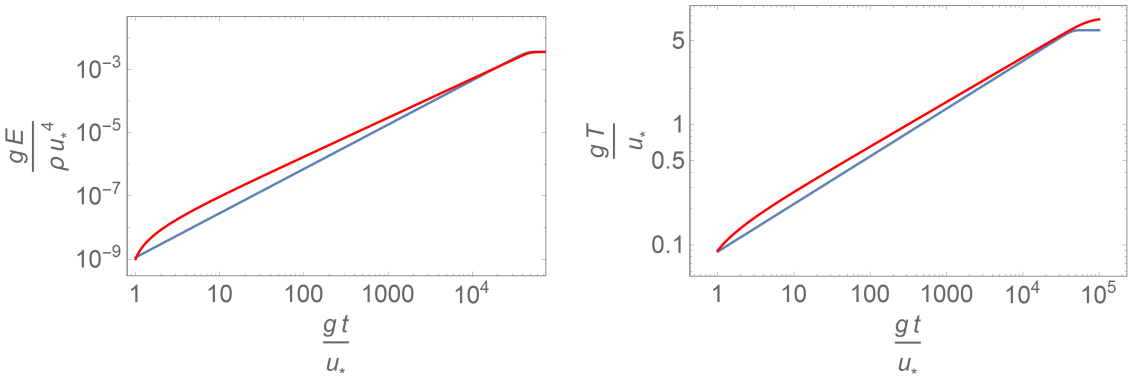

(a) Bulk energy **(b)** Peak period

Figure 4.2: *The duration limited growth curve from the KC derivation compared to Booij's growth curve relations. Booij et al. (in blue) and the derivation from KC curves (in red). The peak period for Booij's growth curves was obtained by multiplying the relation for the moment based mean period by a factor 1.2*

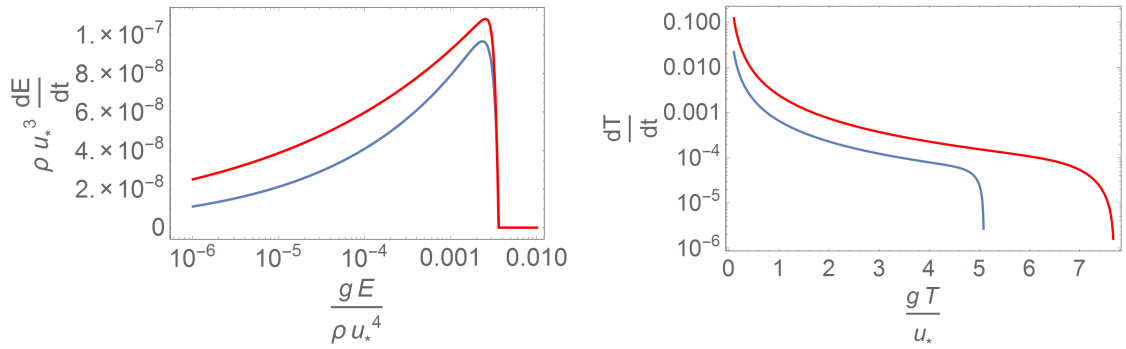

(a) Rate of change of bulk energy **(b)** Rate of change of peak period

Figure 4.3: *The dimensionless rates of change of wave energy and representative period as a function of local dimensionless energy and period in case wave field is fetch-limited: spatial gradients on the growth curve are present. Booij et al. (in blue) and the derived growth rate (in red).*

term and the fetch-limited values of the derived source term are plotted in Figure 4.3. In the left panel the rate of change of energy in the derived source term is seen to stay larger than Booij's source term over the entire domain. Likewise, the rate of change of period in the derived source is larger over the entire domain.

The derived growth rates can thus distinguish between fetch- and duration limited scenario's. The rates of change in young sea states is greater than Booij's formulation. As the source terms differ quantitatively from the HISWA source terms, it should be validated whether the derived source term does in fact reproduce the growth curves it was based on.

4.2 1D convergence

A 1D model is set up to study the behavior of a numerical model which solves the evolution of the zeroth and first order moment of the wave action balance with the derived wind input term. A 1D model allows for an extensive analysis of the performance of the source term in non-ideal conditions without complications from the flow model, before further investigating two-dimensional behavior.

Discretization

The formulations (3.28) and (3.33) are supplemented with a first order upwind discretization for advection in the absence of dissipation terms. The time integration method used is explicit Euler. Discretization is performed in anticipation of the staggered grid approach in FM:

$$\mathcal{Q}_i^{n+1} = \mathcal{Q}_i^n + \mathcal{L}(c_\mathrm{g}, \mathcal{Q}) + \mathcal{S}_\mathcal{Q}(c_\mathrm{g}, \mathcal{Q}) \tag{4.5}$$

$$\mathcal{L}(c_\mathrm{g}, \mathcal{Q}) = -\frac{\Delta t(t^n)}{\Delta x(x_{i+1/2})}\Big(I^n_{i+1/2}{c_\mathrm{g}}^n_{i+1/2}\mathcal{Q}^n_i - I^n_{i-1/2}{c_\mathrm{g}}^n_{i-1/2}\mathcal{Q}^n_{i-1} + (I^n_{i-1/2}-1){c_\mathrm{g}}^n_{i-1/2}\mathcal{Q}^n_i - (I^n_{i+1/2}-1){c_\mathrm{g}}^n_{i+1/2}\mathcal{Q}^n_{i+1}\Big) \tag{4.6}$$

where indicator function I distinguishes the upwind from downwind direction: $I^j_i = 1$ if ${c_\mathrm{g}}^j_i \geq 0$ and $I^j_i = 0$ if ${c_\mathrm{g}}^j_i < 0$. The wind input formulation for energy and action is discretized as:

$$\mathcal{S}_A(c_\mathrm{g}, A, E) = \Delta t(t^n)\chi_E(E^n_i)\left[\frac{|{c_\mathrm{g}}^n_{i+1/2} + {c_\mathrm{g}}^n_{i-1/2}|}{2}\frac{1}{2\pi}\left(\frac{\chi_T(T^n_i)}{\chi_E(E^n_i)}\frac{\widetilde{\mathrm{T}}^n_i}{f_1\left(\widetilde{E}^n_i\right)} + \frac{\widetilde{\mathrm{E}}^n_i}{C(\widetilde{E}^n_i, \widetilde{T^{-}_{\mathrm{rep}_i}}^n)^m f_2\left(f_{E-T_\mathrm{rep}}(\widetilde{E}^n_i)\right)}\right) + A^n_i\frac{I^n_{i+1/2}{c_\mathrm{g}}_{i+1/2} - I^n_{i-1/2}{c_\mathrm{g}}_{i-1/2}}{\Delta x(x_{i+1/2})}\right] \tag{4.7}$$

$$\mathcal{S}_E(c_\mathrm{g}, E) = \Delta t(t^n)\chi_E(E^n_i)\left[\frac{|{c_\mathrm{g}}^n_{i+1/2} + {c_\mathrm{g}}^n_{i-1/2}|}{2}\frac{1}{f_1\left(\widetilde{E}^n_i\right)} + E^n_i\frac{I^n_{i+1/2}{c_\mathrm{g}}_{i+1/2} - I^n_{i-1/2}{c_\mathrm{g}}_{i-1/2}}{\Delta x(x_{i+1/2})}\right] \tag{4.8}$$

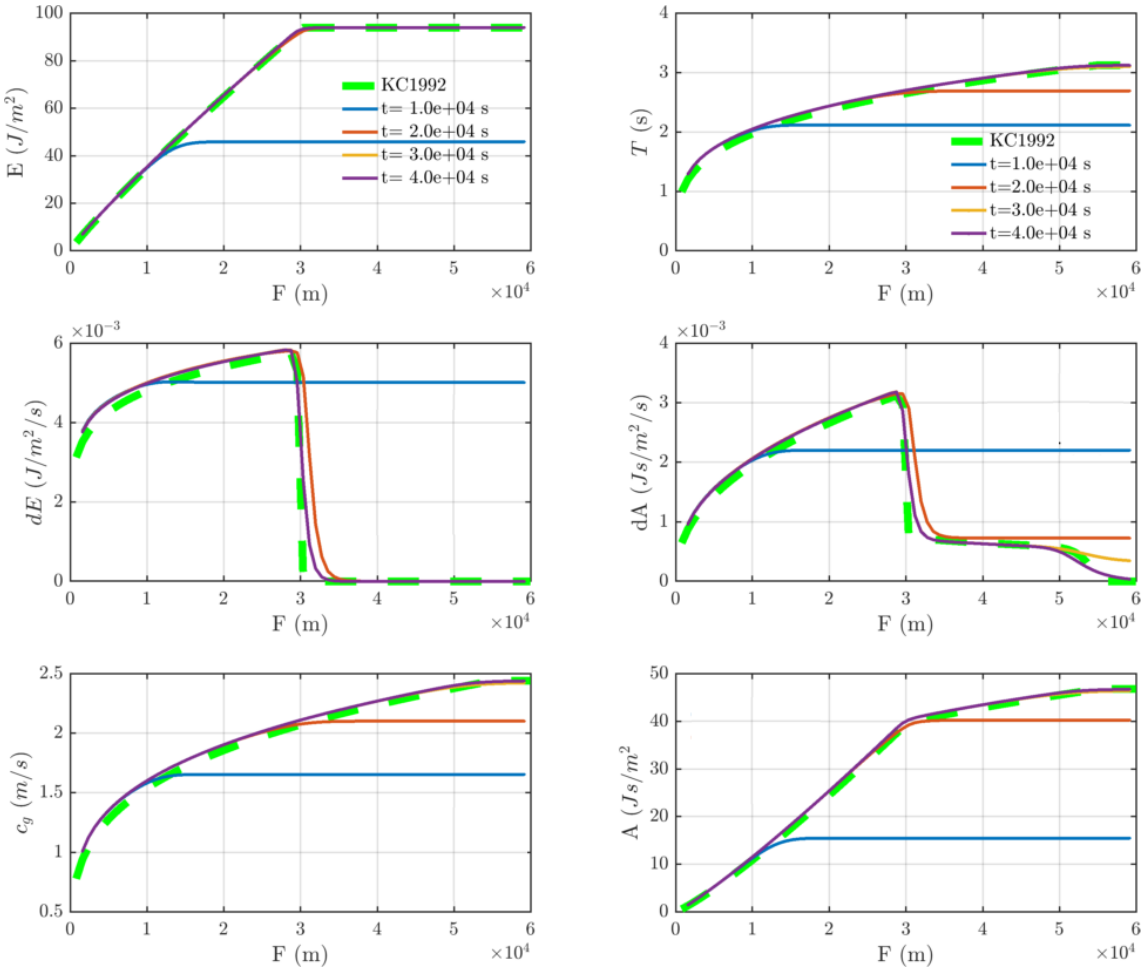

Figure 4.4: *1D Matlab model output for a deep water growth curve. Advected variables E (top left corner) and A (bottom right corner). Their rate of change in the center row. Growth curve for T in top right corner, with the resulting evolution of c_g bottom left.*

Deep water solution

To confirm that the formulations in Section 4.2 indeed converge to growth curves (3.7) and (3.8) in the absence of sink terms and background current, the deep water solution was assessed in a test model. In the absence of a current, ω=σ. Therefore, the deep water group celerity in the test model is given by:

$$c_{\mathrm{g}} = \frac{1}{2}\frac{gT_{\mathrm{rep}}}{2\pi} \tag{4.9}$$

which can be made dimensionless using Table 2.1:

$$\widetilde{c_{\mathrm{g}}} = \frac{1}{2}\frac{\widetilde{T_{\mathrm{rep}}}}{2\pi} \tag{4.10}$$

1D space is discretized uniformly: $\Delta x = C$, $x_i = x_0 + (i-1)\cdot\Delta x$, $i = 1\ldots M$ while time is discretized not necessarily uniform: $t_n = t_0 + \sum_1^n \Delta t(n)$, $n = 1\ldots N$, where $\Delta t(n) = t_{\mathrm{fac}} \cdot \frac{\Delta x}{c_{\mathrm{g}}(i,n)}$. t_{fac} is a constant strictly smaller than 1 in order to comply to the CFL condition arising from an explicit time integration.

The first test entails convergence in the case of ideal boundary- and initial conditions. At x_1 a Dirichlet boundary condition is specified: $\widetilde{E}_1^t = \frac{a_1^2}{16} {x_0}^{2b_1}$, $t = 1 \dots N$ and at x_n a homogeneous Neumann boundary condition: $\left(\widetilde{E}_{,x}\right)_M^t = 0$, $t = 1 \dots N$. The initial condition is chosen to match the Dirichlet condition at x_1:

$$\widetilde{E}_i^0 = \widetilde{\mathrm{E}}_1$$
$$\widetilde{T_{\mathrm{rep}_i}}^0 = f_{E-T_{\mathrm{rep}}}(\widetilde{E}_1)$$
$$\widetilde{c_{\mathrm{g}_i}}^0 = f_{T_{\mathrm{rep}}-c_{\mathrm{g}}}(\widetilde{T_{\mathrm{rep}_1}})$$

with $f_{E-T_]}$ and f_{E-c_g} according to (3.29) and (4.10).

When N is chosen sufficiently large, the 1D-model output indeed appears to model the growth curves on which the source term formulation was based correctly. Graphically, this is confirmed in Figure 4.4. The stationary solution as well as several intermediate time steps have been plotted. In the top row the growth curves for wave energy (left) and period (right) against fetch. Auxiliary model output plotted in the windows below. The stationary solution for wave energy is reached faster than the stationary solution for wave period, approximately in 3.5 and 8.3 simulated hours respectively, because the fully developed conditions are met at shorter fetch. The source term, as plotted in the center row windows, grows as a function of time and is tapered abruptly to zero as the local wave state approximates fully developed conditions. The rate of change of wave action shows a two-step jump to zero input at fully developed conditions. The first step can be associated to the fetch at which the wave energy reaches fully developed conditions. The second, more gentle step corresponds to the fetch at which the wave period becomes fully developed.

The actually convergence of the model-solution to the real growth curves is expected to be linear in Δx and Δt, since the upwind scheme for advection and explicit Euler for time integration are of first order. This has been confirmed when the model was run for several spatial step sizes, and the relative error is plotted against the step size, see Figure 4.5.

Hasselmann et al. (1976) distinguishes between fetch- and duration-limited growth rates in his model. In the intermediate output of the 1D matlab model of Figure 4.4, time-space equivalence, which formed the basis of the derivation, is confirmed. The wave state for the intermediate time steps shows to be time limited. The *equivalent fetch* (3.11), is graphically found by tracing the energy along the fetch-axis back to the geometrical growth curve.

4.3 Sink-Source balance in fully developed conditions

Upper limits on growth curves in shallow water are established through a balance between wind input and dissipation, as described in Section 3.5. Appropriate values for the bottom friction coefficient f_w are addressed in this section for varying wind speed and water depths. As the depth limited growth curves as described in literature are upper envelopes to many wave state observations, the friction coefficients required to reproduce these upper bounds act as lower bounds for application in field cases. There can be other factors, such as a rough bottom as on coral reefs, or highly evolving sand bars, which influence the actual calibration of the friction coefficients. Choosing greater coefficients as the ones described in this section is no problem, but choosing smaller friction coefficients could lead to over-development of literature described fully developed conditions.

Two calibrating parameters are identified: the friction coefficient f_w in (3.40) and the multiplication coefficient for the magnitude of period evolution C_T in (3.41). Both serve different roles and are explained on the basis of Figure 4.6. In this figure the depth limited literature prescribed

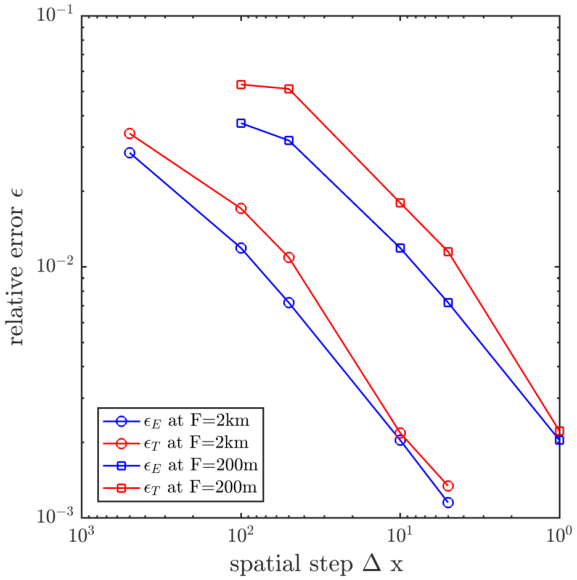

Figure 4.5: *The convergence behavior of the first order upwind advection of action and energy with source term for wind input The errors in energy ϵ_E and in period ϵ_T were measured at a dimensionless fetch of $F = 200m$ and $F = 2km$, and the time step was reduced together with the spatial step by choosing the time step according to certainly match the CFL condition: $\Delta t = 0.5 \cdot \frac{\Delta x}{\widetilde{c}_g}$*

growth curves for energy and period are plotted as black solid lines, while the colored, marked lines are growth curves obtained through a 1D model in which depth-independent wave growth is balanced by bottom friction. Each marked line represent another configuration of the calibration parameters f_w and C_T. Since both the dissipation of wave energy and wave period are directly related to f_w, f_w can be used to steer both growth curves towards higher or lower upper bounds. These are the lines marked with $\triangleright$, $\square$ and $\triangleleft$. Increasing the friction coefficient lowers the upper bounds of both wave energy and period.

Fine-tuning can then happen through C_T since this parameter has the opposite effect on both growth curves. Increasing C_T increases dissipation of wave period, which results in a decrease of the upper bound of wave period, compare the lines marked by $\circ$, $\diamond$ and $\square$. Since the wave energy dissipation mechanism is effected by C_T only through an inverse dependence on the representative wave period, a lower upper limit for wave period results in a higher upper limit for wave energy.

Figure 4.7 show computed growth curves at four wind speeds for one arbitrary depth. In black, the literature prescribed growth curves are plotted. The marked lines are model output. As this comprises a local growth test on a bottom of constant depth (of 5 meters), no wave breaking was present. For all wind speeds, it was possible to approximate the correct fully developed conditions through a balance of bottom friction and wind input. However, the friction coefficient had to be varied. A doubling of the wind speed requires the friction coefficient to be reduced by two.

More growth curves for a range of wind speeds and water depths were assessed. For each, f_w and C_T were varied and the distance of the computed upper bounds to the shallow water growth curves was computed. This distance is minimized in the best calibrated model. See Appendix B for a graphical assessment. The following trends were identified in the required calibration parameters regarding water depth and wind speed:

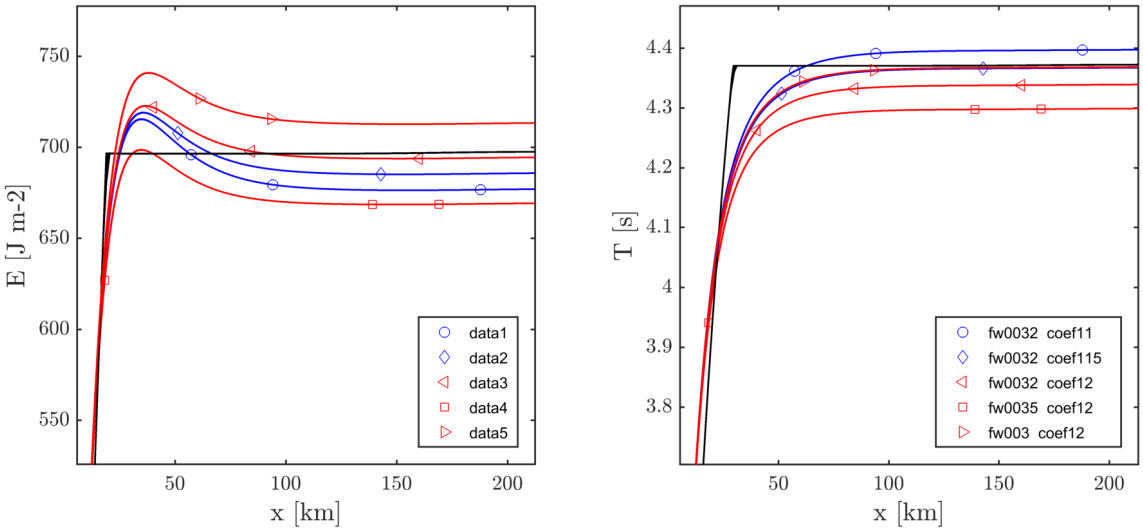

Figure 4.6: *Effect of calibration parameters on upper bounds wave energy (left) and period (right) at a depth $d = 5$m and wind speed $u_{10} = 12$ m/s.*

Depth dependence

In the range of water depths from 3-18 m, f_w ranges 0.02-0.07 and C_T ranges 0.9-1.3. In linear approximation the friction coefficient f_w increases by 0.008 ($\uparrow$) for an increase of water depth of 1 meter ($\uparrow$). C_T on the other hand decreases ($\downarrow$) for increasing water depth ($\downarrow$). This depth dependence of the friction coefficients will inevitably lead to less propagation of offshore boundary conditions into the breaker zone, as these dissipate more. This increase of bottom friction corresponds to prescribing a constant Nikuradse roughness k_s throughout the domain while the friction coefficient is modeled after Soulsby (1997):

$$f_w = 1.39 \left(\frac{u_{orb}}{\omega z_0} \right)^{-0.52} \tag{4.11}$$

with u_{orb} wave orbital velocity and bed roughness $z_0 = \frac{k_s}{33}$ in which k_s is the Nikuradse roughness. This is a modeling approach not uncommonly adopted in simple models (Roelvink and Reniers (2011)).

Wind speed dependence

In the range of wind speeds from 8-20 m/s, f_w equally ranges 0.02-0.07 and C_T ranges 1-1.2. On the investigated domain, the required f_w halves ($\downarrow$) when the wind speed doubles ($\uparrow$). C_T decreases slightly ($\downarrow$) for increasing wind speed ($\uparrow$). As the wind speed increases, the surface wave amplitude increases and hence also the orbital velocity at the bottom. If the friction coefficient would be modeled after (4.11), an inverse relationship between the friction coefficient and the wind speed is then also expected.

4.4 Return rates to quasi-equilibrium

So far this chapter discussed properties of the wind input formulation which assumed the wave energy and representative period to math the quasi-equilibrium (2.13), either in deep water (Section 4.2) or in shallow water (Section 4.3). A violation of the quasi-equilibrium (2.13) can arise

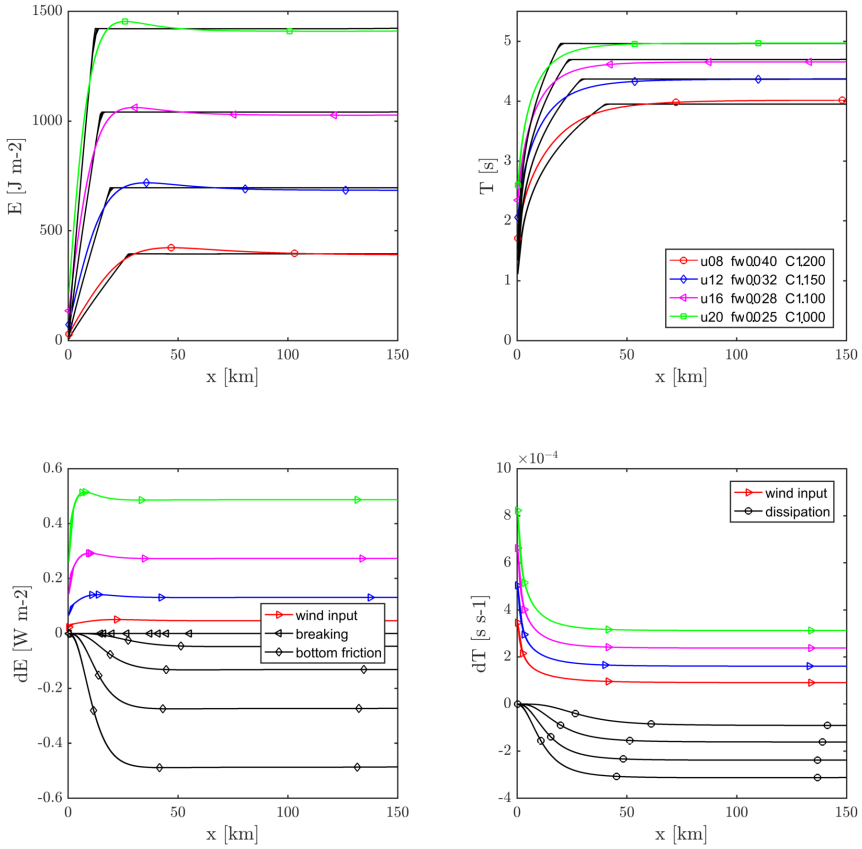

Figure 4.7: *Calibration of growth curves through a balance of wind input and bottom friction for a limited depth of $d = 6$m and varying wind speed at constant $C_T = 1$. Top row: Energy (left) and period(right) against fetch. In black solid line the Kahma and Calkoen curve with finite depth effect, colored marked line the model result. Bottom row, source terms for energy (left) and period (right) as a function of fetch.*

through numerous processes. Mere wave propagation, wave breaking, other interactions with the bottom profile or non-matching boundary conditions imposed on the model boundary are all potential causes for non-matching sets of wave energy and period on local points in the interior of the domain.

Two out-of-equilibrium scenario's are identified that provide insight in the rate at which the source term forces a return to the quasi-equilibrium. First, the dimensionless deep water growth curves with on the upwind model boundary not an infinite coast but out-of-equilibrium boundary condition. Secondly, an infinite domain responding in unison to spatially uniform wind forcing.

Last, it is pointed out that the above described method removes the need for a tapering function on S_{in} to account for finite depth effects. The taper function (3.36) should however remain present to account for fully developed conditions in deep water as bottom friction is negligible in deep water. In absence of a white capping dissipation mechanism, the wind input should diminish when fully developed wave conditions are approached.

Spatial return to quasi-equilibrium

This test comprises of a 1D matlab model which has nonzero Dirichlet boundary conditions on the upwind coast that deviate from quasi-equilibrium. While propagating into the domain, these

wave conditions develop and the wave state develops. Figure 4.8 plots the wave state evolution for three sets of wave conditions: matching, underdeveloped and overdeveloped wave energy and wave period. In Subfigure (a) the wave energy is varied around matching boundary conditions while in Subfigure (b) the wave period is altered.

The growth rate of the wave energy is positively influenced by an overdeveloped wave period, as a natural outcome of the linear dependence of (3.19) on group celerity thereby dependence on T. The group celerity actings as a coupling mechanism in the source term for the two wave properties.

The growth rate of the representative wave period is independent of the available wave energy, as a natural result of the absence of wave energy in (3.20). The small deviations that are visible in the graph can be explained by the means of advection of representative wave period as a function of two orders of moment of the wave action spectrum: total wave action and total wave energy.

For each of the energy or period under- or over development, the return to the growth curve occurs asymptotically. Only at fully developed wave states at far fetch do the trajectories with different boundary conditions meet completely. To quantify the rate of return to quasi-equilibrium a so called relaxation length could be defined; the distance required to reduce the deviation from equilibrium by e.g. one half. To the best of the author's knowledge, there is little literature available on an appropriate relaxation length to describe the rate of return in the spatial dimension. Several early wave models have reported on rates of return in their presentation papers, be it in the time dimension instead of the spatial dimension. To allow comparison with these sources, the dynamical system is also analyzed in the time domain in the next section.

Time to return to quasi-equilibrium in infinite domain

As a second test a 1D model is set up with a uniform domain and a Neumann upwind boundary in order to mimic an infinite domain. The domain is provided with matching initial conditions and with overdeveloped and underdeveloped wave energy (Subfigure (a) in Figure 4.9) or representative wave period (Subfigure (b) in Figure 4.9).

In the time evolution test similar behavior is observed as in the fetch limited test; deviations from quasi-equilibrium in the initial wave period influences the growth curve of the period as well as of wave energy. Deviations in initially present wave energy only influence the energy growth curve. When the wave energy is underdeveloped in comparison with the wave period the wind input for wave energy is increased compared to matching initial conditions and vice versa (Subfigure (a)). The evolution of wave energy when the wave period is still underdeveloped lacks behind compared to the matching initial conditions case (Subfigure (b)).

The rates of return for various trajectories from non-matching initial conditions is compared to the rate of return in the HISWA model, which in its turn is calibrated on return rates described by Günther (1981), see Figure 4.10. In the bottom figure taken from Holthuijsen et al. (1989), the equilibrium relation is represented by $\widetilde{\mathrm{E}} = 6.45 \times 10^{-6} \widetilde{\mathrm{f}}_p^{\,-10/3}$ which is a predecessor of the Kahma and Calkoen growth curve based on Hasselmann et al. (1973). The equilibrium relation for the derived model (top figure), is (2.9) and (2.10) generated with equal fetch. Qualitatively these two descriptions of quasi-equilibrium don't differ, only the transition towards the fully developed wave state shows disparities. Similar initial conditions have been chosen to set out trajectories towards the quasi-equilibrium.

The rate of return in the HISWA model is significantly stronger then through the derived wind input, which can be seen in the curvature of the trajectories. In the HISWA model the rate of return in the model is calibrated towards such a strong response through (3.6) based on wave steepness in the absence of any other coupling mechanism. In the derived rates of change coupling is already

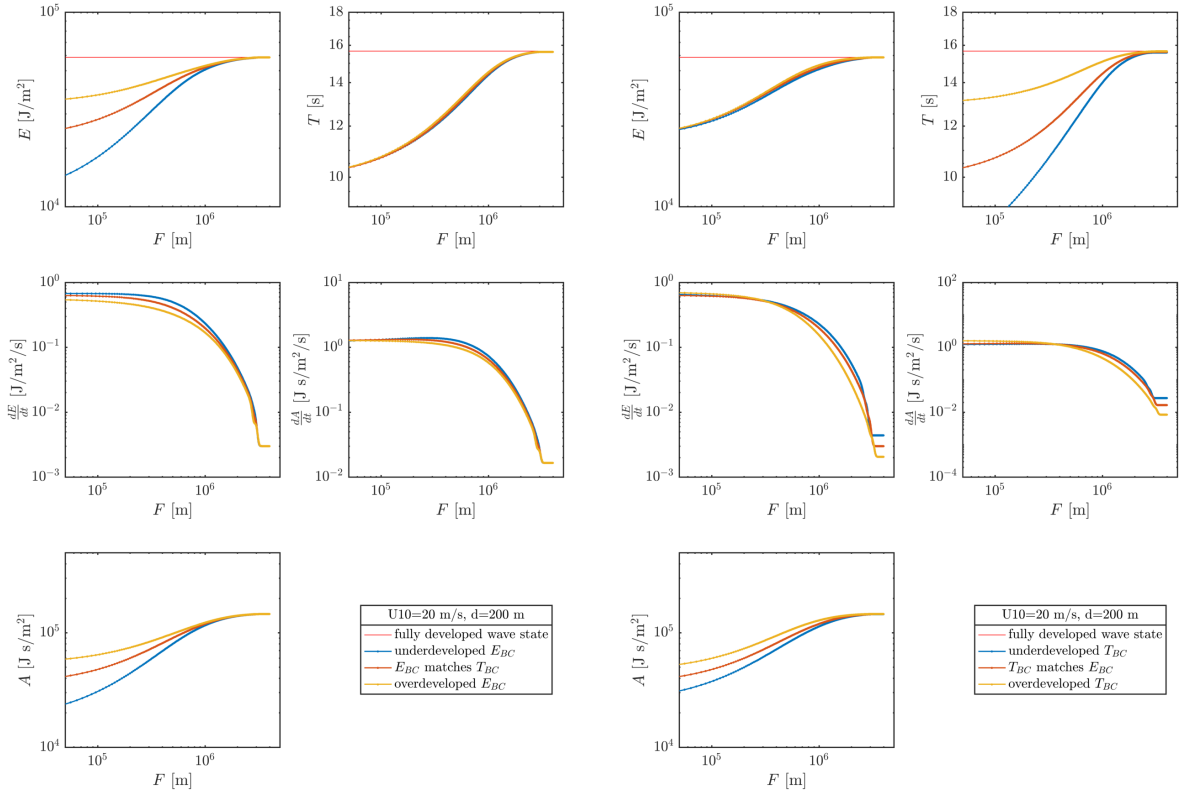

(a) Wave energy deviates from quasi-equilibrium

(b) Wave period deviates from quasi-equilibrium

Figure 4.8: *Two test cases that display the propagation and evolution of non-matching boundary conditions into a 1D domain. In (a) the wave energy is varied by constant wave period boundary conditions while in (b) the wave period is varied for constant wave energy at the boundary. The top rows show the variables of interest wave energy E and representative period T, the center row show the magnitude of the source terms in the wave action and wave energy balance and on the bottom row the wave action is displayed, as this is the principle variable in the dynamical system.*

present through the group celerity. Clearly, this does present different return rates. Both Günther (1981) and Hasselmann et al. (1985), which together formed the basis of the return rates in the HISWA model, do not base their return rates on data. Therefore it was decided that no additional relaxation coefficient is currently implemented in the derived wind input formulation. In case this is felt necessary on the basis of measurements or on a theoretical basis, it is possible to do so in the future.

4.5 Summarizing

In this chapter, the derived rates of change due to wind input were shown to be qualitatively similar to the HISWA rates of change, but differ quantitatively at very young sea states and towards fully developed conditions. HISWA wind input does not distinguish between duration limited and fetch limited conditions as it has no dependence on spatial gradients in the wave field, which the derived source term does. The convergence of the derived wind input formulation to the deep water Kahma ad Calkoen growth curves gives confidence in the validity of the approach.

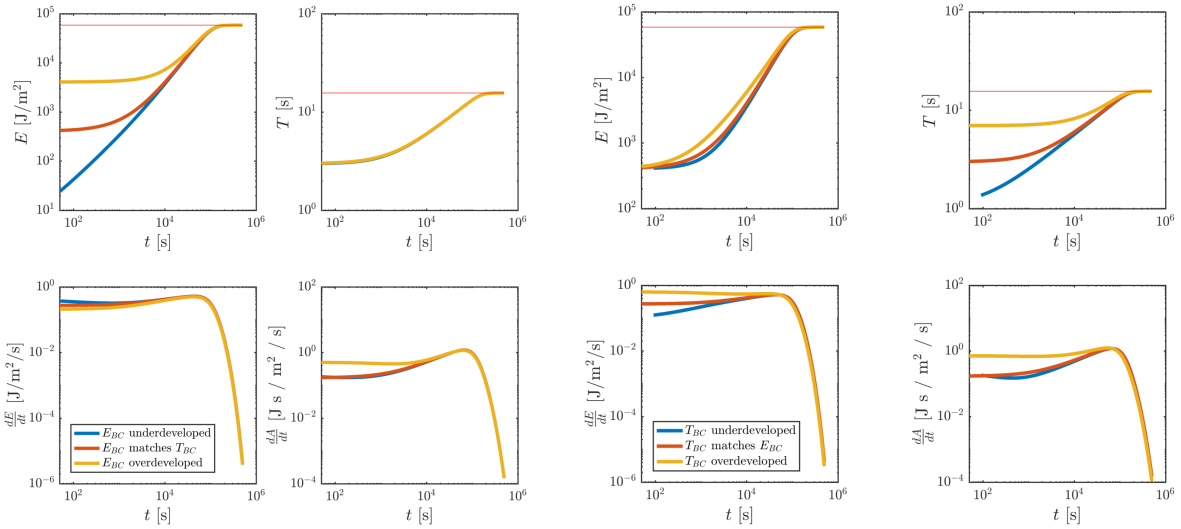

(a) Wave energy deviates from quasi-equilibrium

(b) Wave period deviates from quasi-equilibrium

Figure 4.9: *Two test cases that display the evolution in time of a uniform wave state with varying initial conditions. In (a) the initial wave energy is varied by constant wave period while in (b) the initial wave period is varied for constant wave energy. the top rows show the variables of interest wave energy E and wave period T while the bottom rows show the magnitude of the source terms both as a function of time. Both test were carried out in a model with a depth of 200 meter and wind speed of 20 m/s.*

The range of applicability of the source terms can be extended into shallow water by a correct balance of wind input and bottom friction. The required bottom friction coefficients f_w and C_T to obtain correct fully developed conditions are not constant for varying wind speed or water depth. The friction coefficients required in this calibration lie within a physically feasible range $0 - 0.1$ (Roelvink et al. (2016)). The friction coefficients presented here as calibration parameters can serve as lower bounds. In case the bottom is found to be rougher than the upper limit described in literature, stronger dissipation is defensible with lower upper bound values on energy and period as a consequence.

A mechanism is present in the derived system of equations to force growth trajectories in f, E space towards the quasi-equilibrium relation between E and T. This mechanism is driven by the shared linear dependence of the source term on the group celerity. The rate of return in the derived dynamical system is much weaker than can be found in wave models of Gunther and Rosenthal (1979) and Holthuijsen et al. (1989), which have wave steepness as the driving mechanism to return to equilibrium and calibrated towards strong convergence. Until convincing arguments become available that require such strong rates of return, the currently present mechanism through group celerity is assumed to be sufficient.

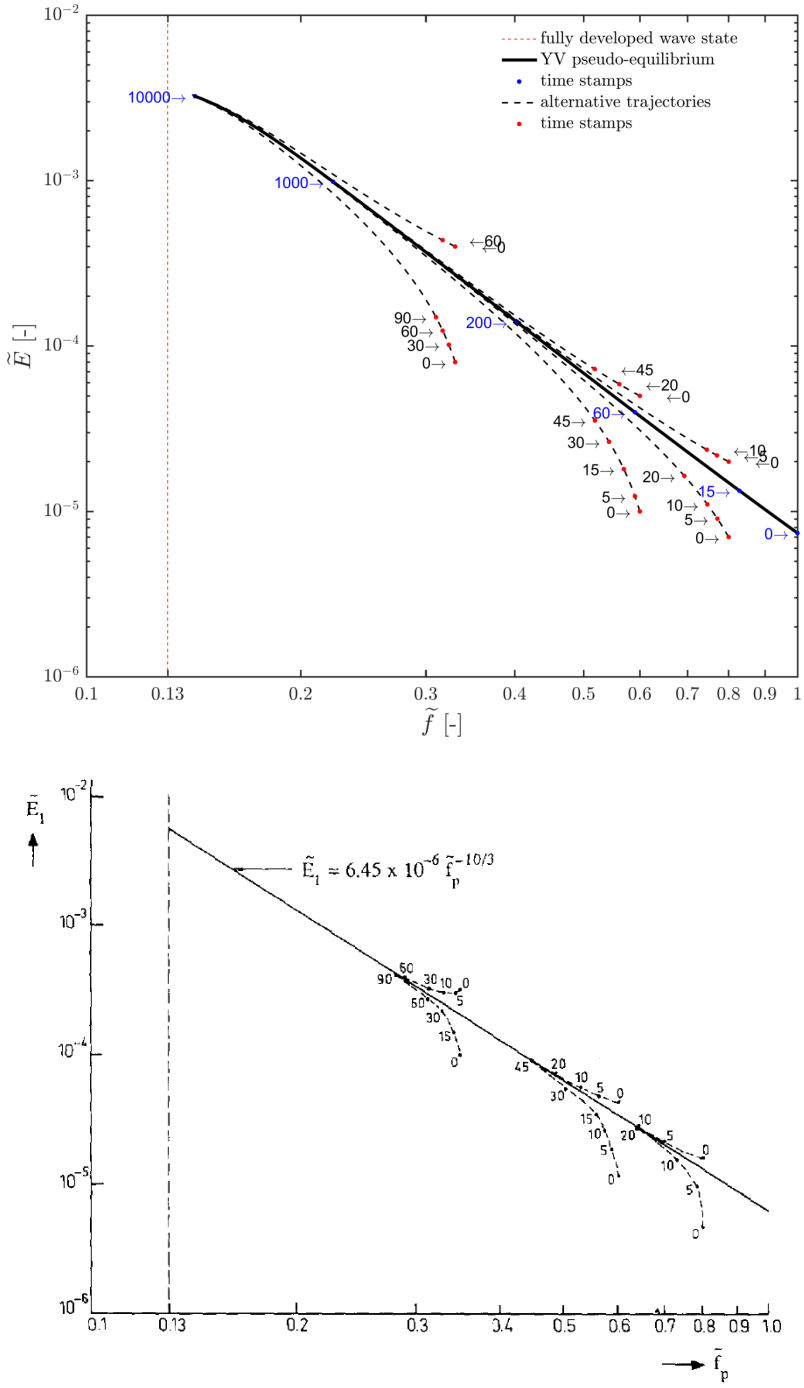

Figure 4.10: *Trajectories in the dimensionless f, E plane. Top: The trajectories in the derived model for wave growth of scenario's with initial conditions deviating from the quasi-equilibrium path suggested by the Young and Verhagen growth curves. Bottom: Return trajectories in the HISWA model as presented in Holthuijsen et al. (1989). All time stamps are in dimensionless minutes (i.e. scaled according to Table 2.1).*

5. Implementation in 2D

So far, only 1D growth curves have been discussed in parallel to 1D balances. In 2D the generalized action balance solved by the dynamical system in the absence of ambient currents is given by

$$\frac{\partial A}{\partial t} + \nabla(\vec{c}_g A) = \frac{\mathrm{d}A}{\mathrm{d}t} + \max(A\nabla\vec{c}_g \cdot \frac{\vec{u}_{10}}{||\vec{u}_{10}||}, 0) \tag{5.1}$$

$$\frac{\partial E}{\partial t} + \nabla(\vec{c}_g E) = \frac{\mathrm{d}E}{\mathrm{d}t} + \max(E\nabla\vec{c}_g \cdot \frac{\vec{u}_{10}}{||\vec{u}_{10}||}, 0) \tag{5.2}$$

with a three dimensional differential operator: $\nabla = (\frac{\partial}{\partial x}, \frac{\partial}{\partial x}, \frac{\partial}{\partial \theta})^T$. Here the growth rate enhancing term $\mathcal{Q}\nabla\vec{c}_g$ is only accounted for when positive and acts only in the wind direction. The directional distribution of the wave action density is discretized. Since x, y space as well as the directional spreading θ are discretized in a 2D implementation, a distribution mechanism of the wave energy over $\theta-$space must be developed. Section 5.1 discusses approaches to distribute wind input over the action density directional distribution. Further sections in this chapter describe changes that were implemented in the XBeach wave drivers to include a wave generation process. To allow evolution of wave period throughout the model domain, Section 5.2 describes the adaptation of the advection mechanismin FPM-FM. The additional robustness measures for the two-equation approach is described in Section 5.3. In Section 5.4 a qualitative argument is made for the suitability of this approach. The conclusions from the 2D implementation are summarized in Section 5.5.

5.1 Directional distribution of wind input

Young sea states have a wide directional distribution, but its shape is not well known. Often it is theorized to be

$$D_{ideal} = A\cos^n(\theta - \theta_{wind}) \tag{5.3}$$

with $n = 2$ after Pierson et al. (1964), a relation which for frequencies not too far away from the peak frequency is also found in wave observations (Ewans (1998)).

The wave generation mechanism is derived in one dimension, in which all wave energy has a propagation direction aligned with the wind direction. There, the wind input is based on the total wave energy available at location (x, y). In a two dimensional energy density spectrum in which frequency space is parametrized by a representative period, total energy at a location (x, y) is the integral of the energy density over $\theta-$space. In the HISWA model the wind input is made $\theta-$dependent on the basis of a directional decoupling (Holthuijsen et al. (1989)). This approach is described in Section 5.1. Another approach is described in Section 5.1, in which the wind input in varying direction is coupled.

HISWA decoupling of wave directions

The wind input for each propagation direction is calculated independently from other directions (Holthuijsen et al. (1989)). A fixed directional distribution is assumed ($D_{ideal} = A\cos^n(\theta - \theta_{wind})$ with A a normalization function, θ the propagation direction of interest and θ_{wind} the mean wind direction. For young sea states $n = 2$). The energy density at θ: $ee(\theta)$ is then converted to an equivalent total wave energy through division by D_{ideal}. The wave period in the HISWA model generally is $\theta-$dependent. In computing the wind input however, a moment based average wave period over $\theta-$space is used as equivalent wave period. This equivalent wave energy $E^*(\theta)$ and $\overline{T(\theta)}$ then serve as input for the wave generation mechanism, after which the amount of energy input $dE^*(\theta)$ is multiplied with D_{ideal} to find the contribution to $ee(\theta)$ and $\overline{dT}$ is distributed over directional space with the energy density $ee(\theta)$ to contribute to $T(\theta)$.

Nodal approach

An alternative to the HISWA approach is suggested, which couples the evolution of wave energy and period in $\theta-$space for evolution of a two dimensional energy density. In analogy with the one dimensional formulation, the wind input at a location (x, y) is based on the integral of wave energy over $\theta-$space. The amount of generated energy is distributed over the respective propagation directions through (5.3). The shape of the locally generated wave field is thus prescribed. Accordingly, the wave generation mechanism acts as a restoring force towards the ideal directional distribution. Continuing the notation as used in Section 5.1; the wind input is computed based on E^* and T^* independent of propagation direction at each (x, y) with $E^* = \int ee(\theta)\,\mathrm{d}\theta$ and $T^* = \overline{T(\theta)}$. The computed energy input is distributed over the propagation directions through multiplication with the spreading function D_{ideal}: $dE(\theta) = D_{ideal} \times dE^*$. Rate of change of wave period per propagation direction: $dT(\theta) = dT^*$.

Although both approaches have been implemented as options in the FIM-FM wave drivers, the nodal approach has been given preference. Two main arguments support this choice.

First, coupling of evolution of wave energy in $\theta-$space is present in the frequency prescribed wave drivers through the formulations of the dissipation mechanisms of bottom friction and wave breaking. Both dissipation rates are described in terms of total wave energy and wave period at location (x, y) since wave breaking is determined by the total wave height. In case a directional decoupled approach is believed to be more correct, the decoupling should be present in all source term formulations in the frequency integrated model. The only coupling mechanism would then be refraction. A directionally decoupled model is only viable when this directional decoupling is possible in each of the source terms.

Secondly, as wave observations confirm the shape of the directional distribution D_{ideal}, particularly in fetch limited conditions (Ewans (1998)), a restoring mechanism should be present in dynamical system. When decoupling the wind input in $\theta-$space, such a mechanism is absent.

5.2 Adaptations to frequency prescribed wave drivers

The derived wind-wave generation mechanism is implemented in the frequency prescribed wave drivers in FM. Aside from the implementation of a subroutine which computes wave generation, Chapter 3 also identified the need to solve a second evolution relation to reproduce correct growth curves through (3.44) and (3.45). Therefore the model has been extended considerably and several subroutines were amended to change the model into a frequency integrated approach.

Varying wave period

	frequency prescribed	frequency integrated
action	$\frac{ee(x,y,\theta)}{\sigma(x,y)}$	$aa(x,y,\theta)$
energy	$ee(x,y,\theta)$	$m_1 = (\sigma \times aa)(x,y,\theta)$
wave period	T_{BC}	$T(x,y,\theta)$
relative frequency	$\sigma(x,y)$	$\sigma(x,y,\theta)$
wave number	$k(x,y)$	$k(x,y,\theta)$
wave celerity	$c(x,y)$	$c(x,y,\theta)$
refraction celerity	$c_\theta(x,y)$	$c_\theta(x,y)$

Table 5.1: *Effect of varying wave period on dimensions of variables in XBeach wave drivers*

In the frequency prescribed wave drivers in FM (FPM-FM) the wave period is a constant but is no longer the case in the two-equation approach (FIM-FM). The solution space for several variables was increased. For an overview of these variables, see Table 5.1. The wave dissipation mechanisms were revised to replace dependence on wave characteristics which used to be direction independent, by direction averaged wave characteristics:

$$f\left(\{\mathcal{Q}_i(x,y)\}\right) \longrightarrow f\left(\left\{\overline{\mathcal{Q}_i(\theta)}(x,y)\right\}\right) \tag{5.4}$$

where f dummies a dissipation mechanism and $\mathcal{Q}$ dummies for wave period, relative frequency, wave number or (group)celerity.

Advection of wave period

FPM-FM discretizes time integration into an advection step followed by an Euler step that evaluates the source terms. Wave energy density is scaled with relative frequency before applying the advection step. Wave action is converted back to wave energy before applying the Euler step, because the dissipation mechanisms are expressed in terms of energy. After the combined time integration step, the wave celerities are updated.

In the FIM wave drivers, the two step approach to time integration is maintained. Before applying the advection step, wave action density is computed by scaling wave energy density with relative frequency. In the advection step both wave energy density as well as wave action density are propagated. The relative frequency and wave period are updated by a scaling of wave energy density by wave action density, after which the wave celerities are updated. The wave period distribution and wave energy density form the principle variables of the Euler step. After evaluation of this second step the wave celerities need to be updated again, because the wave period will have changed.

5.3 Robustness

Complex bathymetry in shallow water requires a robust model. After first implementation, it was found that the following steps were necessary to perform stable model runs which are (more or less) invariant under initial conditions.

1. Each time step, at least one division of energy density by action density or vice versa has to be done. To prevent floating-point overflow, a minimum energy density and wave period need to be present. The values of which can be communicated to the model by the user through the params.txt file, but are default set at ee_{min} =0.1 J/rad/m^2 and T_{min} =0.1 s. ee refers to the total energy in a directional bin. This ensures there is always enough available energy to initiate some growth. Furthermore, an option is included to calculate the minimum amount of wave energy and wave period on the basis of the grid coarseness and the wind speed such that it matches the growth curve at a fetch equal to the grid coarseness.

2. A limiter on change in energy density and period per computational step was included. Similar to Hersbach and Janssen (1998), this limiter is dependent on the time step such that it will remain part of the source term when the limit $\Delta t \rightarrow 0$ is taken. The need for this limiter is particularly noticable for coarse grid resolution for which the Courant criterium allows large time steps. Because of the highly non-linear behavior of the wave period source term for really short waves the limiter prevents overshoot. The limiter has been set to

$$(\Delta ee_i)^{t_j}_{max} = \left(\left[\frac{\partial ee_i}{\partial t} \right]^{t_j} \Delta t \right)_{max} = ee_i^{t_j} \tag{5.5}$$

$$(\Delta T_i)^{t_j}_{max} = \left(\left[\frac{\partial T_i}{\partial t} \right]^{t_j} \Delta t \right)_{max} = T_i^{t_j} \tag{5.6}$$

   The severeness of this limiter, or other forms of limiters, remain to be investigated apart from some qualitative test cases which were for successful at very young sea states and showed no effect in other scenario's (which is the desired behavior of the limiter).

3. Already in the FPM-FM model a limiter was present for the amount of wave energy through $gammax$ in limited depth on physical grounds. The root mean square wave height is cut of at twice the water depth. All excess wave energy is removed. The underlying assumption of this limiter is that the bathymetry is too coarse in some cases to model the dissipation processes correctly.

   In a test case in which waves approached a spatially non-uniform beach, the need for a similar limiter on wave period became apparent. As wave period is an advected property in the new approach, it bunched against the beach but could not propagate further (nor back seawards, since $\theta-$space is often only discretized in the directions with a positive normal component to wind direction or shore).

4. Wave celerity varies much more strongly throughout the model domain in the new approach where wave period varies throughout the model domain. The front of wave energy propagating from the model boundary into a domain where waves are nearly completely absent, carries energy density as well as information on its own propagation speed. In case the advection of wave period lags the propagation of wave energy, bunching of energy at the propagation front can occur.

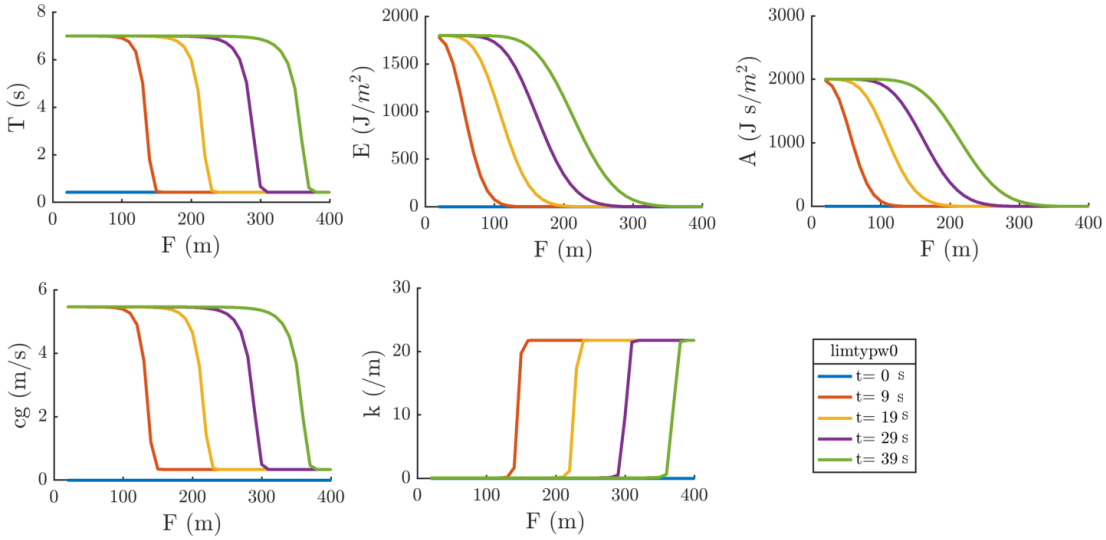

Figure 5.1: *The propagation of waves energy from the boundary into a wave-less domain in a semi-1D FIM-FM model with first order upwind discretization of advection. Top row: wave period T (left), total wave energy E (center) and wave action A (right), all against distance (F). Bottom row: group celerity c_g and wave number k against distance.*

In an unstructured approach a higher order discretization of the advection mechanism is not straightforward, because each node only has information on the location and connectivity to its direct neighbors. The default discretization in FPM-FM is therefore first order upwind. There are however higher order approximations available that make use of limiter types from the D-Flow FM flow module (Deltares (2016)). Their use triggered dispersion on the propagation front. Further research on the cause of the latter type of dispersive peaks is necessary before use of any limiter types other than $limptypw = 0$.

5.4 Validation cases

Propagation of period from boundary

Propagation of boundary conditions into the domain with the 2-equation under various higher order approximations of the discretization of the advection term was investigated, as described in Section 5.3. In Figure 5.1 the first time steps of propagating wave front are shown for limiter type 0 (no higher order approximation). The wave period front (top left panel) leads the wave energy front (top center panel), thereby ensuring the entire energy front propagates with the same celerity.

Next, the propagation of boundary conditions is combined with wave growth. As displayed in Figure 5.2, the wave front appears very dispersive. This unphysical peak at the wave front does propagate through the domain after which the trailing growth curve appears correct. Spin-up time of this model is hence equal to the time necessary for the boundary waves to travel throughout the entire domain to enter at the outflow boundary. In case the wave growth needs to be studied in an instationary setting, the source term, parallel to the boundary condition for wave energy, can be linearly tapered from zero at the start of the computation to its true value.

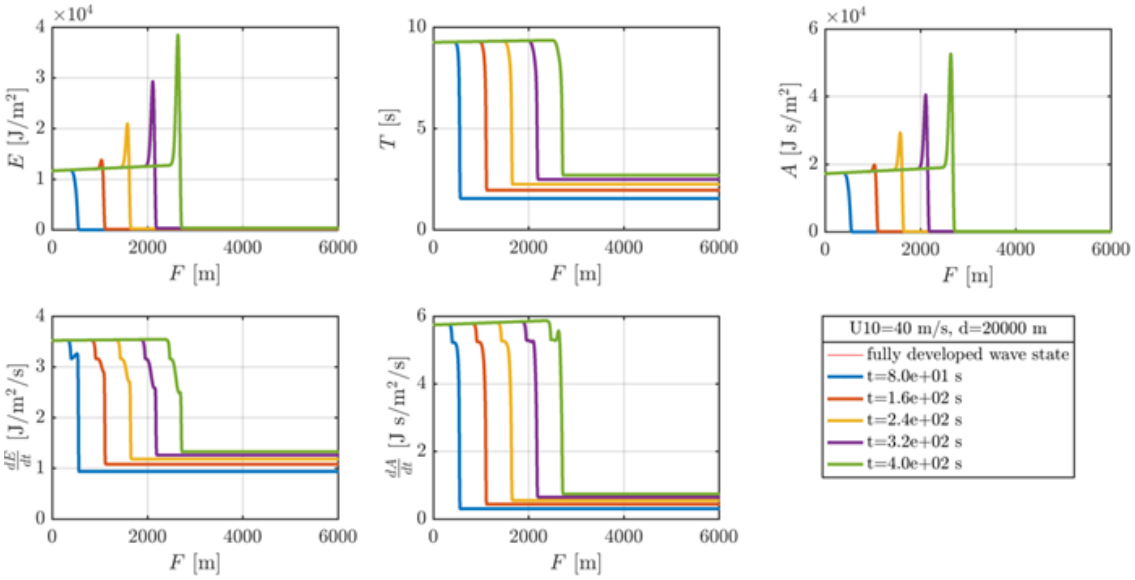

Figure 5.2: *Propagation of waves energy from the boundary into a wave-less domain in a semi-1D XBeach D-Flow FM model with first order upwind discretization of advection and wind input.*

Propagation around an Island

A 2D model for propagation around an island has been set up to compare FIM-FM to FPM-FM. No local wave generation is considered. See Figure 5.3 for a plot of the resulting (H_s, T) fields. The wave period field in the frequency prescribed version is off course constant and equal to the boundary prescribed value. In the modified version, the field shows sheltering behind the island. Moreover, since this model was run with a relatively coarse directional discretization, streaks of the influence lines of boundary conditions are visible in this sheltering area, while these are not present in the wave height field. An explanation to this could be that directional distribution of total wave energy occurs at the Dirichlet boundary, while the wave period prescribed at the Dirichlet boundary is constant in wave direction. Therefore streaks in the wave period field are much stronger than in the wave height field, because the angles away from mean propagation direction weight equally to the mean propagation direction.

Furthermore, the island appears to provide much less sheltering in the frequency integrated model in comparison to the frequency prescribed model, a result which is obtained through the modified wave celerity field as a result of the altered wave period field. Because wave energy travels more slowly trough the sheltering area in the modified model, more wave energy is present at a given time.

1D growth curves

A 1D test similar to the 1D Matlab test of Section 4.2 is performed on the FIM-FM wave drivers. This test is performed on a semi-1D grid (3x750) at a finite depth of 20 meters under a wind speed of $u_{10} = 20$m/s. The tapering of the source terms to Young and Verhagen (1996) growth curves as described in Section 3.4 is also included. Dissipation processes are turned off. The stationary solution as well as output at some intermediate time steps is plotted in Figure 5.4 on log-log scale. The slight deviation of the wave period growth curve from the literature prescribed curve

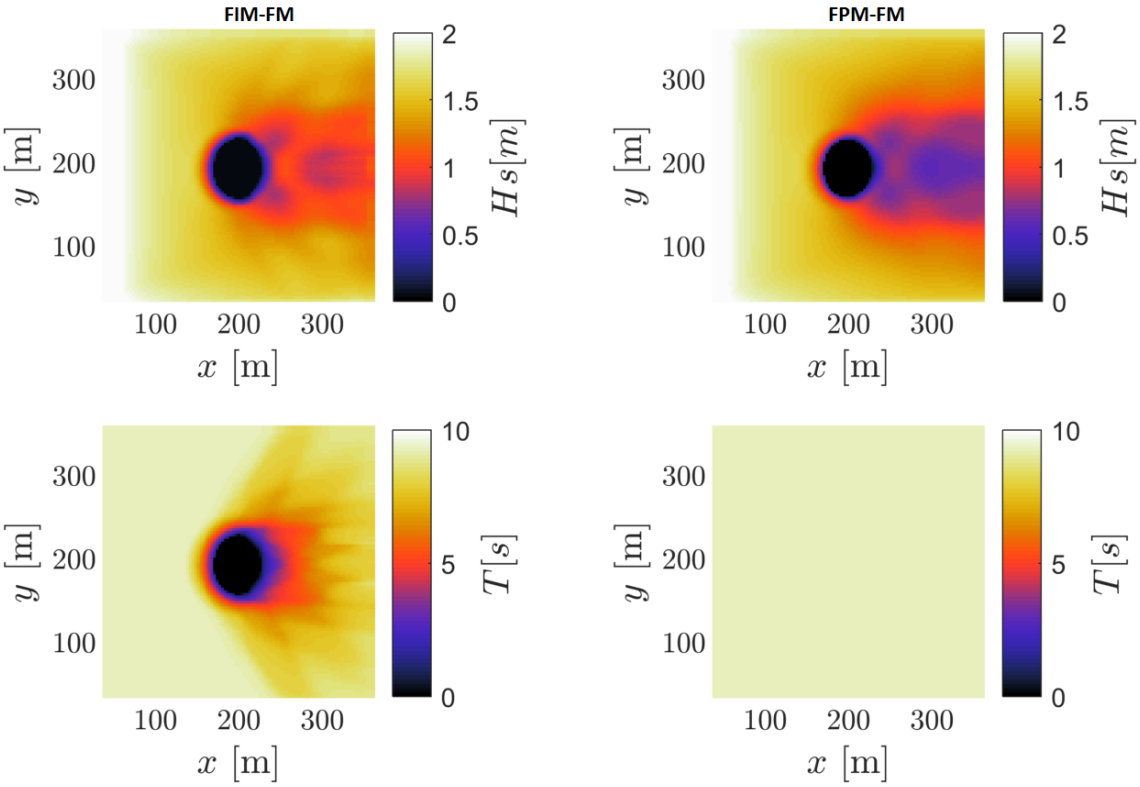

Figure 5.3: *A comparison of the refraction pattern around an island between FIM-FM approach (left) and FPM-FM approach (right). The top row plots significant wave height H_s, the bottom row plots representative period T.*

is attributed to the relatively coarse grid. The taper on the source term toward fully developed conditions correctly reproduces the tanh-transition as proposed by Young and Verhagen (1996).

5.5 Summarizing

The wave generation mechanism derived in Chapter 3 was implemented in the unstructured XBeach-like wave drivers in D-Flow FM (FPM-FM). To that end the formulation of the source term had to be generalized to two dimensions and a distribution mechanism of the wave input over the propagation directions was identified. Because wave observations suggest a distribution of wave energy over the propagation directions by $D_{ideal} = A\cos^n(\theta - \theta_{wind})$ (Ewans (1998)), a direction-integrated approach (the nodal approach) was adopted. Some limiters had to be imposed on the behavior of the wave period in very shallow water and on the time integration step for very young sea states on coarse grids. From the described test cases three recommendations can be given on the use of the two-equation propagation model:

1. The effect of higher order approximations to the discretization of advection need to be investigated further before used.

2. The spin-up time of an instationary solution is equal to the travel time of the wave front on the inflow boundary to the outflow boundary. During this spin-up time the model output is unphysical and should not be taken into account.

3. The discretization in $\theta-$ space needs to be fine to reduce the presence of streaks of wave period in sheltered areas of the domain. The number of bins is dependent on the interest in the wave field in the sheltered area. Roelvink et al. (2016) suggests discretizing the direction-domain with a resolution of at least one bin per 20 degrees and this is thought to be sufficient.

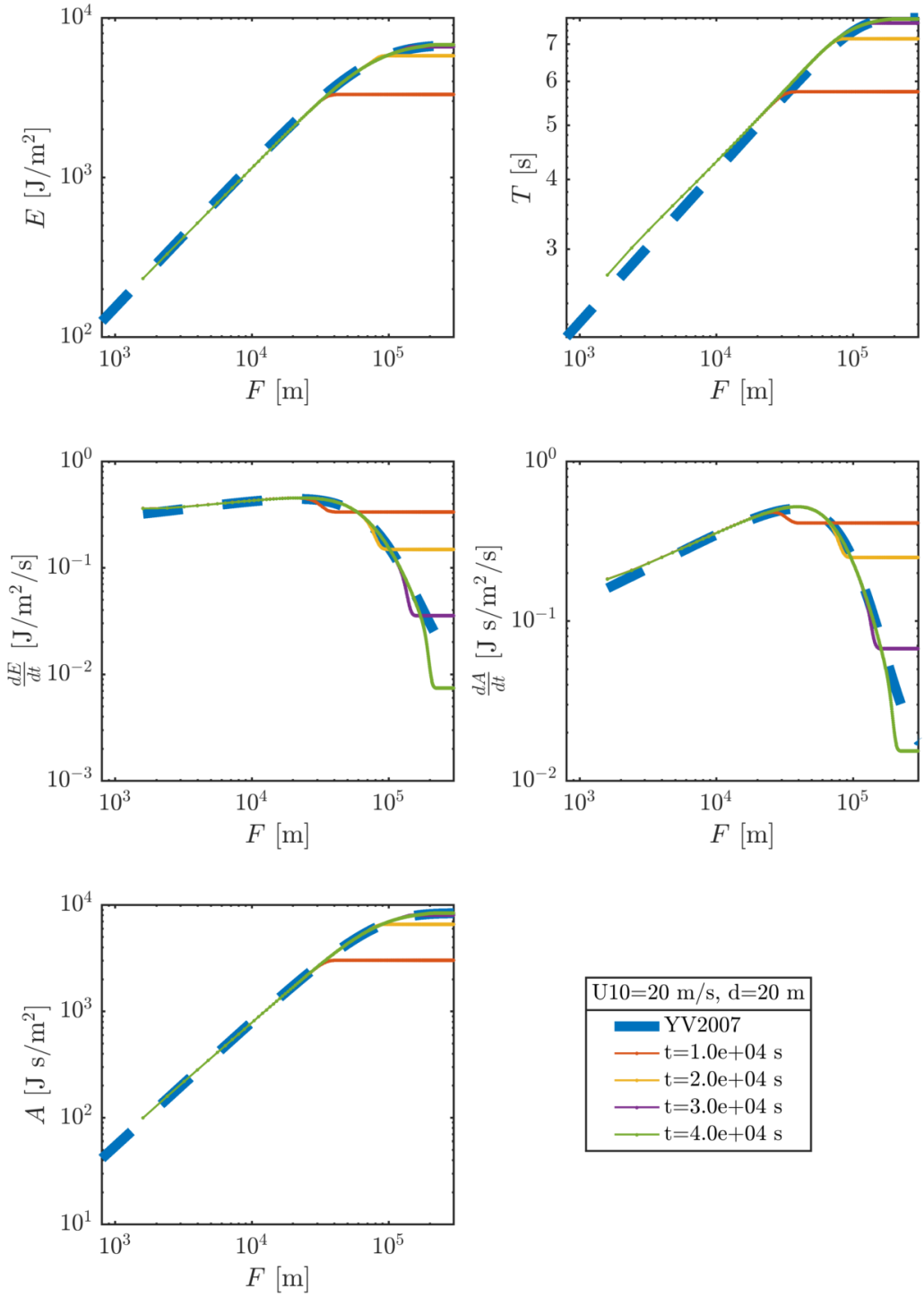

Figure 5.4: *semi-1D FIM-FM output for wave growth due to a constant wind speed of* $20m/s$ *on a grid with a resolution of 80m. Top left: wave energy, top right: wave period, center left: local rate of change of wave energy, defined by the group celerity, period and wave energy at beginning of time step, center right: local rate of change of wave action, bottom left: wave action. In each graph, the final equilibrium solution is shown as well as the output as intermediate time steps, see the legend. Both the prediction relations for wave energy and wave period from Young and Verhagen (1996), corrected by Breugem and Holthuijsen (2007) are matched by the final solution.*

.

6. Field case

So far, only idealized test cases were analyzed. In this chapter the interaction of the wave generation mechanism with the other source terms is challenged on a real discretization of a physical bathymetry, modeling a historic storm. A hindcast provides also a means to test correct behavior of the wave boundary conditions in the two-equation approach for advection. In the derivation of a source term formulation, it was already mentioned that reproduction of the literature described growth curves would not be exact in the case currents are present. The implementation of frequency prescibed wave drivers into D-Flow FM is still work in progress, and wave-current interaction is not operational as of yet. Therefore it was not possible at this stage to evaluate the effect of currents on the computed growth curves. To that end, a field case was chosen which has been used in a validation study of SWAN before, in which currents were assumed to be absent. This provides a means to compare model skill between the two wave models. The chapter starts with introduction of the field case. The validation method is discussed thereafter. Section 6.3 reports on the results from the validation. Section 6.4 raises some discussion points with regard to the model method and the relevance of various wave processes.

6.1 Haringvliet storm hindcast

The inlet of the Harinvliet, a Rhine-estuary between Westvoorne and Goeree-Overflakkee in South-Holland is separated from the Rhine-branch by sluices. On the sea-side of the sluices lies a shoal named the Hinderplaat. The Haringvliet is relatively shallow, and the area behind the shoal is partly sheltered from offshore boundary conditions such that local generation of waves becomes relevant. Because of the presence of the sluices, currents are largely absent. See Figure 6.1 left panel for a contourplot of the bathymetry of the domain. A measurement campaign on wave conditions was performed in 1982 by Rijkswaterstaat (Andorka Gal (1982)). The measurement set is obtained through the SWIVT database. The database includes a BOTKAR network of the bathymetry of the Haringvliet in 1982 with a resolution of 250x250 m. These measurements have served already other model validation purposes (Dingemans (1983), van der Westhuysen et al. (2012)). As such, a performance comparison of FIM-FM against SWAN can be made.

The measurement campaign reports on wave spectra at eight locations during four hours of storm conditions on 14-10-1982. These locations are marked in Figure 6.1. The storm duration was split by hour, after which hourly average wave spectra were reported. See Table 6.1 for an overview of the physical parameters in the four cases. The normalized wave spectra (normalized variance density against frequency) of the first storm hour are plotted in the right panel of Figure 6.1. The shape of the wave spectra at the first four locations shows a clear spectral peak and approximates the JONSWAP shape. The spectral shapes at locations five to seven are all in some degree affected by the sheltering effect of the Hinderplaat. The spectra are wider and the spectral peak is less defined. Especially the wave spectrum right behind the shoal at location five is very wide and all energy at the spectral peak has dissipated. At location eight a distinct second peak can

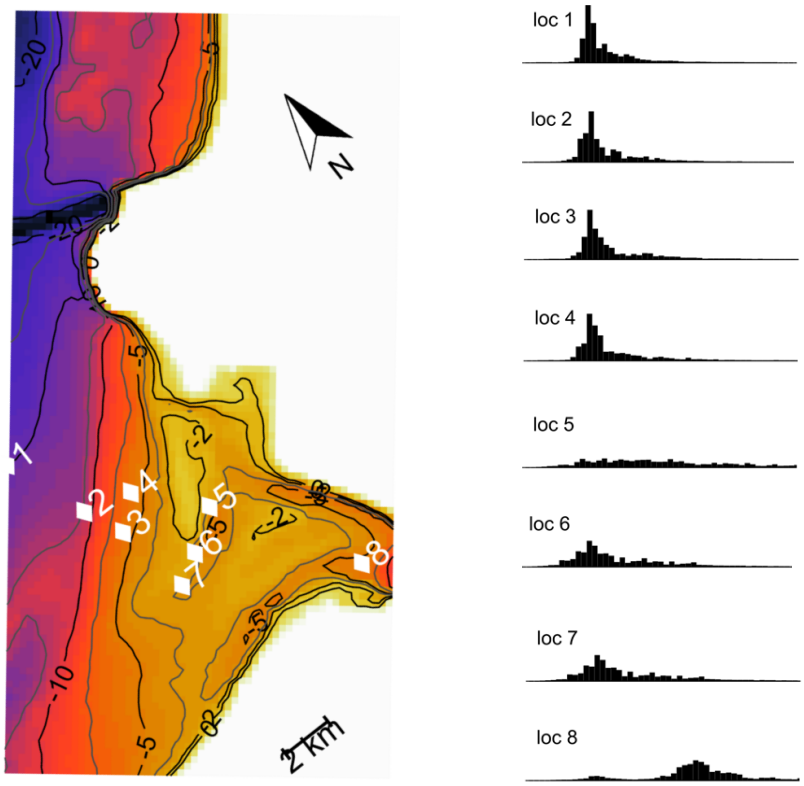

Figure 6.1: *LEft panel: Contour plot of bathymetry of the Haringvliet with eight measurement locations in white. Right panel: Shapes of the wave spectra(normalized variance density against frequency) during the first storm hour at the eight locations.*

be distinguished in the spectrum at much higher frequency. At this location the locally generated waves are present and noticeable.

6.2 Method

Each of the four hours of storm was simulated with stationary boundary conditions. In the wave generation mechanism, bottom friction is assumed to account for finite-depth effects. Wave breaking is modeled through Baldock et al. (1998). The significant wave height H_s and mean period T_{m01} from location one were used as wave boundary conditions on the entire offshore boundary.

The spectral characteristics of location two and three in the second model case were used to calibrate the friction coefficient f_w in the bottom friction formulation (Equation (3.40)) to $f_w = 0.03$ and C_T (in Equation (3.41)) to 7. The second model case is more representative for the other cases in comparison to case 001 because of the increasing water level throughout the four hours of storm. This friction coefficient was assumed constant for the entire domain in absence of information on bottom roughness.

Model skill at the seven remaining locations is assessed by looking at the difference from computed wave height and period to the imposed boundary conditions. As such, measurement locations far away from the model boundary are plotted far away from the origin of the scatter plot in Figure 6.2. This matches the intuition that a numerical model has better skill if it models the *evolution* of boundary condition well, rather than it merely advecting these wave boundary conditions unaltered through the domain. The two measurements of most interest for the regeneration

Table 6.1: *Physical parameters in Andorka Gal (1982). wind speed and direction according to nautical convention. Time in UTC. The Author acknowledges the use of the SWIVT database, kindly provided by Deltares through http://swivt.deltares.nl*

Case nr.	Time [hh:mm]	Water level [m]	Wind (U_{10}) [m/s]	Direction [°]
001	21.00 hrs	+0.30	12	330
002	22.00 hrs	+0.90	17	330
003	23.00 hrs	+1.70	14	330
004	24.00 hrs	+2.10	15	330

of waves within the domain, locations five and eight, are then located furthest away of the origin of the scatter plot.

The model skill is quantified through the evaluation of the scatter index (SCI), the relative bias and the Brier skill score (BSS). Reference is made to Van Dongeren et al. (2003) for a summary on their computation. These performance indicators only become significant when sufficient data is available. Since there are just seven stations modeled in a total of 4 model cases, these performance indicators provide a means to quantify the model fit to the data, but the superiority of one model over the other can't be concluded from their values through statistical rejection.

6.3 Results

The performance of FIM-FM in simulating the wave conditions at the eight measurement locations is plotted in Figure 6.2 along with its skill scores. Positive relative bias indicates a general over prediction of wave characteristics, a negative relative bias an under prediction. A higher scatter index suggests a wider scatter around the bias line. A skill score of 1 would imply perfect model skill. Positive skill scores imply that the model performs better than the no-model alternative (assuming boundary conditions everywhere in the model domain).

Appendix C gives an overview of the wave field and source term magnitudes for the reader interested in the greater picture of the wave field apart from the quantification at the measurement stations.

The model skill of FIM-FM is compared to simulations performed with SWAN 41.10. The process description and model parameters for SWAN were taken from the SWIVT database. For the calculation of the SWAN skill scores, stations two to eight from all four storm cases were included. For the FIM-FM skill scores, the second and third station of case 002 were additionally excluded as these were used in the calibration of the friction coefficient.

Most noticeable is the difference in relative bias in the wave period between FIM-FM and SWAN. SWAN tends to systematically under predict the mean period, where the frequency integrated model over predicts the mean period. Both models have very little bias in predicting the significant wave height, but the scatter around the perfect model skill line is in both models is still significant. Both models have problems in predicting the change in wave conditions between location three and four. Although the measurements suggest differently, both models predict a similar wave state at the two locations. This could possibly be explained by the relatively coarse grid of the BOTKAR network. A local variation in the bottom profile could induce refraction or dissipation. On a coarse grid, this could go unnoticed.

It must be kept in mind that the skill scores are based on only 26 data pairs (for FIM-FM, 28 for SWAN).

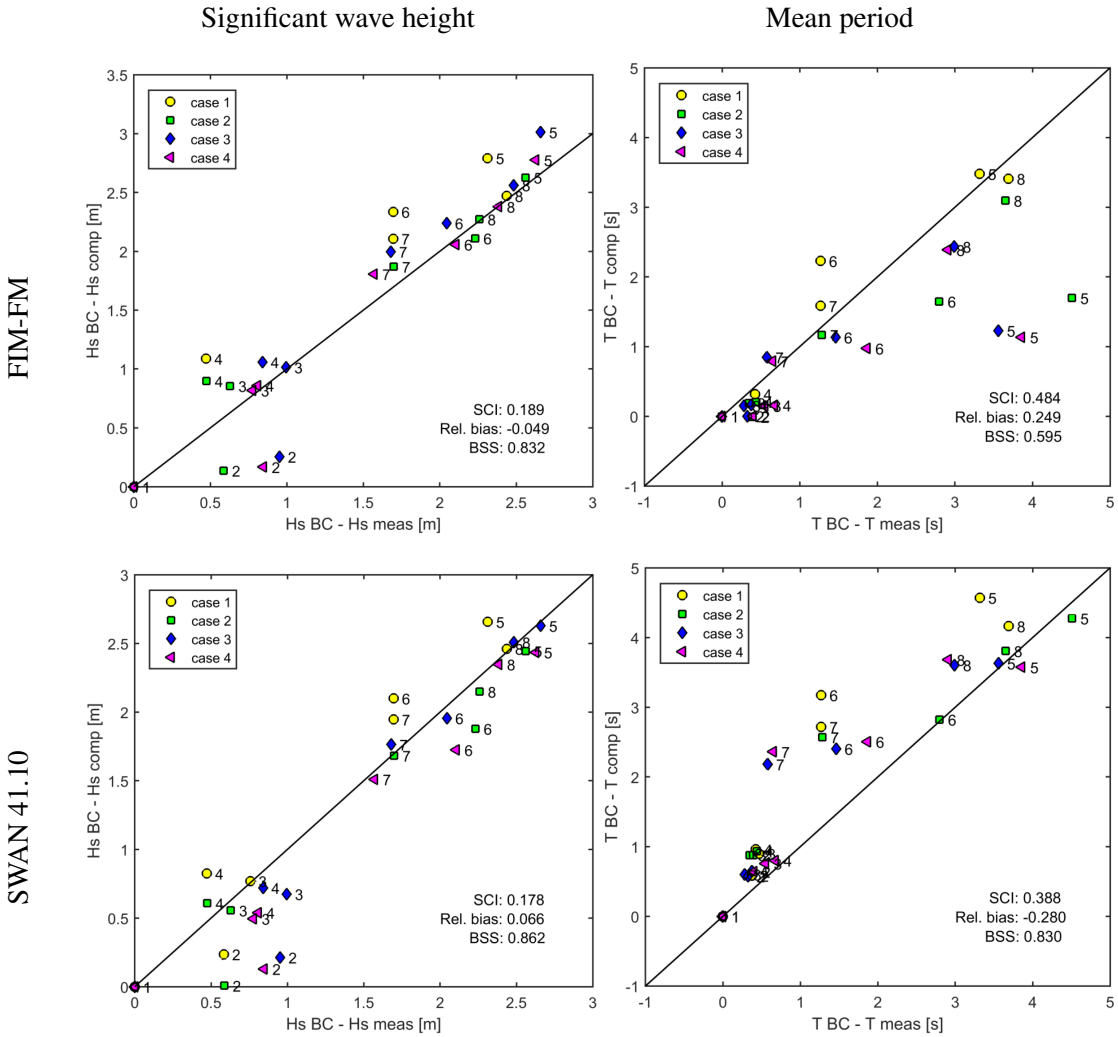

Figure 6.2: *The model skill of the FIM-FM (top row) in comparison to SWAN (bottom row) for significant wave height (left column) and mean period (right column). Scatter plot of deviation of computed wave height and period from the imposed boundary condition against deviation of measured wave height and period from wave state at measurement location one. The black solid line indicates perfect model skill. Skill scores computed combining computations from all four storm cases.*

Table 6.2: *Skill scores for storm case 001 for three model runs assessing the influence of three processes: dissipation of wave energy, dissipation of wave period and generation of both wave energy and period.*

Processes	SCI		Rel. Bias		BSS	
	H_s	T_{M01}	H_s	T_{M01}	H_s	T_{M01}
Wave breaking (Br)	0.24	0.71	-0.08	0.51	0.74	0.43
Br + bottom friction (Df)	0.45	0.38	-0.30	-0.02	0.43	0.67
Br + Df + wind input	0.19	0.48	-0.05	0.25	0.83	0.60
Br + depth limited wind input	0.17	0.77	0.02	-0.59	0.85	0.42
SWAN	0.18	0.39	0.07	-0.28	0.86	0.83

6.4 Discussion

To identify which process is dominant in describing the wave field, the effect of different processes (Figure 6.3) is compared with complete process description (Figure 6.2). Wave dissipation by depth induced breaking was present in all model runs. The skill scores are summarized in Table 6.2. As the combined skill scores for wave energy and representative period suggest, the wave field is best reproduced when all three processes are included in the simulation. To further understand the roles of the respective processes, some comparisons between model runs are discussed below.

First, the effect of bottom friction on the propagation of offshore boundary conditions is exemplified by Figure 6.3: Subfigure (a) (only wave breaking) and Subfigure (b) (wave breaking and bottom friction). Both the wave energy as well as wave period are significantly lower in the domain of (b). The wave energy shows a trend of under prediction in the absence of local wave generation. The wave period however shows very little bias towards under- or over prediction. This suggests that the evolution under bottom friction, which was calibrated on case 002 for two relatively offshore points, might not be strong enough in the rest of the domain.

This is confirmed when Subfigure (b) is compared with Figure 6.2 (top row) (complete process description). The wave period is overestimated when dissipation and local growth are combined. This is especially the case for location 5 right behind the Hinderplaat. Either the evolution of period under bottom friction over the shoal is too little or the local growth is too strong. The wave energy however, improves its predictive skill greatly by combining bottom friction and local generation.

Next, the model skill behind the Hinderplaat is closer inspected. In Figure 6.2 (top row) as well as Figure 6.3 Subfigure (b) the performance of the model at position 5 (right behind the Hinderplaat) for case 002-004 is very different from case 001, as the wave period in cases 002-004 is much over predicted. The water depth on top of the Hinderplaat varies strongly between the four model cases, from a few decimeters in case 001 to 2.5 meter in case 004. The measurements show that propagation over the shoal steepens waves more strongly than wave energy is dissipated, but this behavior is not reproduced by FIM-FM. In the model, either the advection of wave period over the shoal is too strong, the local generation of wave period is too strong (wave period grows most strongly in very young sea states), or the prescribed wave steepness with fixed friction coefficients through the evolution relation after Booij is unable to predict the steepening. Arguments can be made to point to the last of these potential causes.

When the performance of the four model cases in predicting wave period are inspected individually, each of them accounts to a different bias compared to the perfect-model-skill-line. Case 001 generally just under predicts wave periods at the measurement locations. In cases 002-003 the bias changes to an over prediction. This over prediction is then strongest in case 004. Since

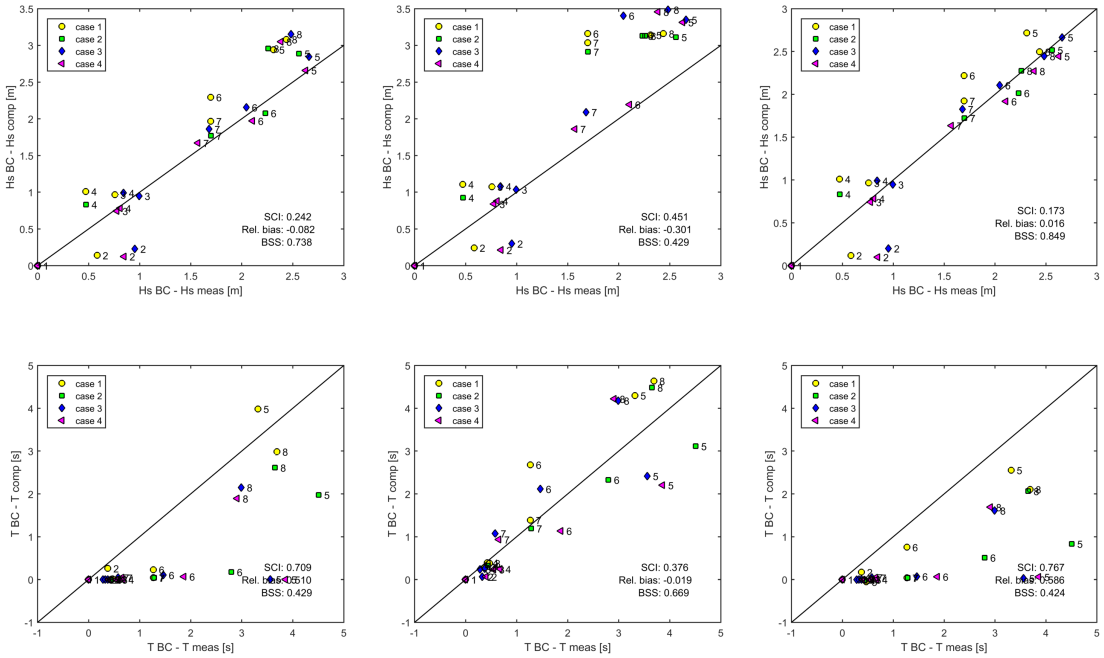

(a) Wave breaking (BR)

(b) Br + Bottom friction

(c) Br and Depth-limited growth

Figure 6.3: *Scatter plots of the computed wave heights (top row) and period (bottom row) against the measurements. In (a) bottom friction and local generation was turned off, only depth-induced breaking is included. In (b) bottom friction was included next to depth induced breaking. Subfigure (c) shows the alternative approach in which bottom friction is neglected and the growth rate is depth-dependent (Section 3.5)*

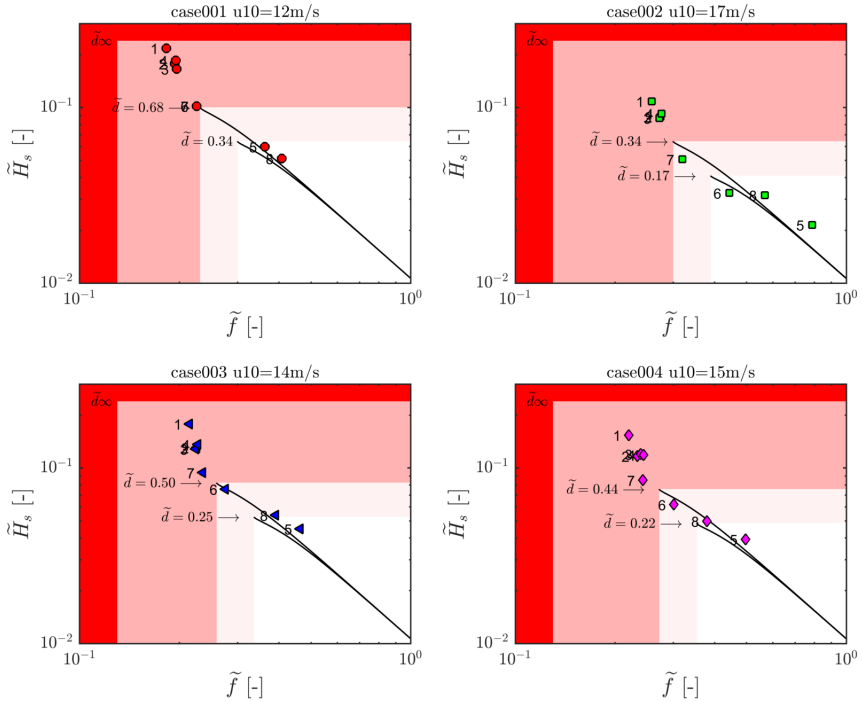

Figure 6.4: *Dimensionless measured significant wave height against dimensionless mean frequency (markers with label of the measurement location) for all four storm cases. In black solid line the Young and Verhagen growth curves for dimensionless water depths corresponding to d=5m, d=10m. The red colored zones indicate overdeveloped conditions for deep water (dark red) d=10m, (lighter red) and d=5m (lightest red).*

the model cases differ the most from each other in the mean water level, this suggests that friction coefficients should be depth-dependently prescribed. This approach is not further pursued in this field case since enough data points should remain for validation purposes after eliminating some data points for calibration. Only 26 data points were available for validation purposes in this field case.

The alternative option regarding depth limitations on the model approach, were bottom friction is only incorporated implicitly through limiting the local growth, was tested on the Haringvliet as well, in Figure 6.3 Subfigure (c). In comparison to full process description (Figure 6.2 (left)) the wave energy is predicted really well, but mean wave periods are severely overestimated. It is very clear from these results that some sort of evolution of wave period for offshore wave conditions is necessary to obtain reasonable local periods.

This arguments is supported in a further study of the measured wave spectra in the dataset. In the analyzed storm scenario's the wind speed varied from 12 m/s to 17 m/s. With these wind speeds, a dimensionless water depth of $\widetilde{d} = 1$ equals dimensional water depths in the range $d = 20.0$ m to $d = 29.5$ m. The measurement stations two to eight all lie in relatively shallow water where the water depth does not exceed 15 meters. In Figure 6.4 the measured significant wave height and mean frequency are made dimensionless and plotted on the $\widetilde{f}, \widetilde{H_s}$ phase plane. The equilibrium trajectories described by Young and Verhagen (Equations (2.9) and (2.9)) are plotted as well for three dimensional water depths. An infinite dimensionless depth accounts to deep water conditions. All wave observations lie around equilibrium trajectories with $\widetilde{d} = 2$ and even $\widetilde{d} = \infty$. Since the water depth in the Haringvliet typically accounts to dimensionless water depths well below $\widetilde{d} = 1$, the measured waves heights are overdeveloped with respect to the literature

described fully developed conditions in shallow water. Hence the joined contribution of bottom friction with local wave generation should have a nett sink effect, and an explicit bottom friction mechanism is really necessary to allow sink terms for wave period.

FIM-FM shows promising results in predicting the significant wave height throughout the Haringvliet hindcast through an accurate balance between generation of waves and dissipation. Location 5 directly behind the Hinderplaat strongly reduces the model skill of predicting wave period. In the model cases in which the remaining water depth on top of the shoal was >1 meter, the wave period is extremely over predicted. It appears that the steepening of waves in the model is not sufficient to describe the steepening occurring in the measurements. Either the evolution under bottom friction after Booij is not appropriate in this case, or the friction coefficients should be made depth dependent. Since wave steepening in case 001 was modeled correctly, the latter approach is recommended for further research in a hind cast where more data is available for calibration.

7. Conclusion and Recommendations

In this chapter the main results of this project are summarized and the research questions from Section 1.4 are addressed (Section 7.1) Conclusions were written separately for the three parts in which the development process was divided. Recommendations for further steps towards an operational shallow water wave forecasting model are given (Section 7.2).

7.1 Conclusion

Derivation of a spectrally integrated wave generation mechanism

Literature describes power laws relating total wave energy and period to fetch. These power laws are expressed in dimensionless variables. Dimensionless description of wave characteristics generalizes wave observations, as it renders the power laws independent of the wind speed. These power laws form the basis of the derived source term. Fetch and duration serve an equivalent role in describing the degree to which waves can develop. With this insight, wave growth rates can be related to local group celerity and wave energy. Evolution of wave energy over time and space is described by the wave action balance. As wave period determines to a large extent the group celerity, it needs to evolve too in a dynamical model that describes the energy growth curve. Wave period is not a conserved quantity under wave propagation. As such, it must be advected in a wave model by an auxiliary wave quantity. This quantity was identified as the first moment of the action density spectrum: wave energy. With two balance relations in place, one for wave action and one for wave energy, the evolution of wave energy is indirectly coupled to the evolution of wave period through the wind input. The coupling is such that ideal wave steepness is achieved both over time and after propagation in the spatial dimension.

Implementation

The additional evolution relation as well as the wind input term were extended to apply in two dimensions and concurrently implemented in frequency prescribed wave drivers in D-Flow FM. Limiters, some of which were already present for wave action, were introduced for wave energy. The interaction of the wind input formulation with bottom friction in limited water depth was furthermore studied. The conventional bottom friction formulation present in XBeach only dissipates wave energy. A coupling of the evolution of the representative period to dissipation of wave energy was additionally implemented. Growth curves for varying water depths and wind speeds were reproduced by a balance of wind input and bottom friction. The required bottom friction coefficients to obtain correct fully developed conditions are not constant for varying wind speed or water depth, but do vary in a physically correct range. In case bottom friction is not explicitly incorporated in the process description, the wind input can be tapered to prevent over development of shallow water growth curves.

Validation

The model approach was validated both through highly idealized 1D test cases as well as a hindcast study. Convergence with decreasing grid size towards idealized growth curves was established in test cases without dissipation processes. A hindcast study of the Haringvliet compared the model skill of the frequency integrated approach to the spectral model SWAN. The frequency integrated FM model shows a bias towards higher wave periods, whereas SWAN is generally biased towards lower wave periods. Model skill similar to SWAN was reported in the prediction of significant wave height. The evolution of wave period under bottom friction behind the shoal (Hinderplaat) in the model prediction was not sufficient to model the increase of wave steepness present in the wave observations in case the remaining height of the water column above the shoal was more than one meter. For the other measurement stations scatter around perfect model line for the frequency integrated model was of similar magnitude to SWAN.

7.2 Recommendations

Recommendations can be given regarding two aspects. Further development of process description in the model is discussed first, after which some recommendations for further steps towards an operational shallow water wave forecasting model are given.

Process description

In the derivation of the source term the validity of the two-equation approach to propagate wave period throughout the model domain in absence of ambient currents was discussed. As pointed out, the effect of currents on the propagation pattern of wave period needs to be investigated. It is therefore recommended that this effect is assessed numerically as soon as wave-current interaction becomes operational in the frequency prescribed wave drivers in D-Flow FM.

A second aspect of the derived source term in a complex model is the gradient of the group celerity. As Section 3.4 showed, 20% of the growth rate on the growth curve is attributed to the term $A \cdot \nabla \vec{c}_g$. In principle there is no bound on the gradient of the group celerity, and hence the growth rate could take on unphysical high values. In the current implementation the contribution of the gradient in group celerity on the growth rate was bound to 0.5 of the total growth rate. The upper bound for its contribution to the growth rate should be investigated.

Another aspect of the process description which requires more validation cases is the depth and wave height dependence of friction coefficients to account for depth limitations in the growth rates. In the discussed field case the friction coefficients were chosen constant throughout the model domain and throughout all model cases. Soulsby (1997) describes a dependency of the friction coefficient on wave orbital velocity and frequency. This approach should be tested in other field cases.

As the hindcast of the Haringvliet turned out to validate the propagation of offshore wave conditions which were aligned with the wind direction, an additional validation study could provide more confidence in the growth of waves in directions at an angle with boundary conditions. Moreover, as the global model aims to forecast globally on all types of coastal zones, model skill on varying types of foreshores need to be assessed.

Towards operational forecasting

The prospective wave forecaster finds solutions to stationary model problems. The spectrally integrated approach to the stationary problem should be faster than the full spectral description

of the stationary problem. This was, at the green light stage of this thesis, not confirmed yet as the wave drivers were only implemented in the instationary solver for study purposes. Although this implementations is step one towards a faster solver, a recommendation on a second step is also made. The stationary solver for the XBeach wave drivers in D-Flow FM is iterative, and uses a pseudo-time step to move from one iteration to the next. As such, the semi-discretized model problem (the stationary wave action balance) is described similarly to the fully discretized problem (non stationary wave action balance). This means that the two-step approach to the time-integration step (Section 5.2) is also present at each iteration of the stationary solver. In one iteration step two systems of equations are solved. With the introduction of a second evolution relation as proposed in this thesis, a third system of equations is introduced in one iteration step. Incorporating the three systems of equations in one larger system reduces the calls to the solver within one iteration step from three to one. Although solutions to larger systems require more computational time, the convergence behavior could potentially increase as non-linear behavior of the source terms around the breaker zone could be captured better.

Bibliography

Andorka Gal, J., 1982. Verification set haringvliet - october 14, 1982- october 15, 1982 , rep-95.112x. Ministry of Transport, Public Works and Water Management, Den Haag.

Baldock, T., Holmes, P., Bunker, S., Van Weert, P., 1998. Cross-shore hydrodynamics within an unstaturated surf zone. Coastal Engineering 34, 173–196.

Benoit, M., Marcos, F., Becq, F., 1996. Development of a third generation shallow-water wave model with unstructured spatial meshing. Coastal Engineering 25, 465–478.

Booij, N., Ris, R. C., Holthuijsen, L., 1999. A third-generation wave model for coastal regions, 1. model description and validation. Journal of Geophysical Research 104 (C4), 7649–7666.

Bouws, E., 1986. Provisional results of a wind wave experiment in a shallow lake (lake marken, the netherlands). KNMI Afdeling Oceanografisch Onderzoek, Memo 00-86-21.

Bretherton, F., Garret, C., 1969. Wave trains in inhomogeneous moving media. Vol. 302. pp. 529–554.

Bretschneider, C., 1952. The generation and decay of wind waves in deep water. Trans. Am. Geophysical Union 33, 381–389.

Bretschneider, C., 1978. Revised wave forecasting relationships. In: Proceedings of 6th International Conference on Coastal Engineering. FL. ASCE, New York, pp. 30–67.

Breugem, W., Holthuijsen, L., 2007. Generalized shallow water wave growth from lake george. Journal of Waterway, Port, Coastal and Ocean Engineering 133 (3), 173–182.

Deltares, December 2016. Technical Reference D-flow Flexible Mesh. Deltares.

Dietrich, J., Dawson, C., Proft, J., Howard, M., Wells, G., Fleming, J., Lander, H., 2013. Real-time forecasting and visualization of hurricane waves and storm surge using swan+ adcirc and figuregen. In: Computational challenges in the geosciences. Springer, New York, pp. 49–70.

Dietrich, J., Zijlema, M., Westerink, J., Holthuijsen, L., Dawson, C., Luettich Jr, R., Jensen, R., Smith, J., Stelling, G., Stone, G., 2011. Modeling hurricane wave and storm surge using integrally-coupled, scalable computations. Coastal Engineering 58, 45–65.

Dingemans, M., 1983. Verification of numerical wave propagation models with field measurements; crediz verification harinvliet, rep. W488, Part 1B, Delft Hydraulics, Delft.

Dingemans, M., Radder, A., De Vriend, H., 1987. Computation of the driving forces of wave-induced currents. Coastal Engineering 11, 539–563.

Donelan, M., 1982. The dependence of the aerodynamic drag coefficient on wave parameters. In: Proc. First Int. Conf. on Meteorology and Air-Sea Interaction of the Coastal Zone. Amer. Meteor. Soc., pp. 381–397.

Donelan, M., Hamilton, J., Hui, W., 1985. Directional spectra of wind-generated waves. Phil. Trans. R. Soc. Lond. A315, 509–562.

Eldeberky, Y., 1996. Spectral modeling of wave breaking: Application to boussinesq equations. Journal of Geophysical Research: Oceans 101 (C1), 2156–2202.

Ewans, K., 1998. Observations of the directional spectrum of fetch-limited waves. Journal of Phsyical Oceanography 28 (3), 495–512.

Günther, H., 1981. A parametric surface wave model and the statistics of the prediction parameters. Phd thesis, Hamburger Geophysikalische Einzelschriften.

Gunther, H., Rosenthal, W., 1979. A hybrid parametrical wave prediction model. Journal of Geophysical Research 84 (C9), 5727–5738.

Hasselmann, K., Barnett, T., Bouws, E., Carlson, H., Cartwright, D., Enke, K., Eqing, J., Gienapp, H., Hasselmann, D., Kruseman, P., Meerburg, A., M uller, P., Olbers, D., Richter, K., Sell, W., Walden, H., 1973. Measurements of wind-wave growth and swell decay during the joint north sea wave project (jonswap). Deutschen Hydrografischen Institut A8 (12), 1–95.

Hasselmann, K., Ross, D., M uller, P., Sell, W., 1976. A parametric wave prediction model. Journal of Physical Oceanography 6, 200–228.

Hasselmann, S., Hasselman, K., Allender, J., Barnett, T., 1985. Computations and parameterizations of the linear energy transfer in a gravity wave spectrum, ii, parameterizations of the nonlinear transfer for application in wave models. Journal of Physical Oceanography 15, 1378–1391.

Hersbach, H., Janssen, P., 1998. Improvement of the short-fetch behavior in the wave ocean model (wam). Journal of Atmospheric and Oceanic Technology 16, 884–892.

Holthuijsen, L., Booij, N., Herbers, T., 1989. A prediction model for stationary short-crested waves in shallow water with ambient currents. Coastal Engineering 13, 23–54.

Holthuisen, L. H., 2007. Waves in oceanic and coastal waters. Cambridge University Press.

Janssen, P., 1989. Wave-induced stress and the drag of air flow over sea waves. Journal of Physical Oceanography 19, 745–754.

Janssen, P., 1991. Quasi-linear theory of wind-wave generation applied to wave forecasting. Journal of Physical Oceanography 21, 1631–1642.

Kahma, K., 1981. A study of the growth of the wave spectrum with fetch. Journal of Physical Oceanography 11, 1503–1515.

Kahma, K., Calkoen, C., December 1992. Reconciling discrepancies in the observed growth of wind-generated waves. Journal of Physical Oceanography 22, 1389–1405.

Kitaigorodskii, S., 1962. Applications of the theory of similarity to the analysis of wind-generated wave motion as a stochastic process. Izv. Geophys. Ser. Acad. Sci. USSR 1, 105–117.

Kitaigorodskii, S., Krasitskii, V., Zaslavskii, M., 1975. On phillips' theory of equilibrium range in the spectra of wind-generated gravity waves. Journal of Physical Oceanography 5, 410–420.

Longuet-Higgins, M., Stewart, R., 1964. Radiation stresses in water waves; a physical discussion with applications. Deep-Sea Research 11, 529–562.

Mase, H., 2001. Multi-directional random wave transformation model based on energy balance equation. Coastal Engineering Journal 43 (04), 317–337.

Mastenbroek, C., Burgers, G., Janssen, P., 1992. The dynamical coupling of a wave model and a storm surge model through the atmospheric boundary layer. Journal of Physical Oceanography 23, 1856–1866.

McInnes, J., Hoeke, R., Walsh, K., J.G., O., Hubbert, G., 2016. Application of a sysnthetic cyclone method for assessment of tropical cyclone storm tides in samoa. Natural Hazards 80 (1), 425–444.

Miles, J., 1957. On the generation of surface waves by shear flows. Journal of Fluid Mechanics 3, 185–204.

O'Grady, J., McInnes, K., Hoeke, R., 2015. Forecasting maximum wave setup hazards around australia. In: Forecasting wave setup around Australia. Coasts and Ports Conference 2015.

Phillips, O., 1957. On the generation of waves by turbulent wind. Journal of Fluid Mechanics 2, 417–455.

Pierson, W., Moskowitz, L., 1964. A proposed spectral form for fully developed wind seas based on the similarity theory of s.a. kitaigorodskii. Journal of Geophysical Research 69, 5181–5190.

Pierson, W. J., Tuttell, J., Wooley, J., 1964. The theory of the refraction of a short crested gaussian sea surface with application to the northern new jersey coast. Journal of Geophysical Research 69, 5181–5190.

Reyns, J., Becker, J., Merrifield, M., Roelvink, J., 2016. Modeling hydrodynamics on the wave group scale in topographically complex reef environments. In: American Geophysical Union, Ocean Sciences Meeting 2016, abstract #EC23A-06.

Roelvink, D., A., R., van, D. A., Van Thiel de Vries, J., Lescinski, J., McCall, R., 2016. XBeach model description and manual. Unesco IHE Institute for water education, Deltares, Delft University of Technology.

Roelvink, D., Reniers, A., 2011. A guide to modeling coastal morphology. Vol. 12 of Advances in Coastal and Ocean Engineering. World Scientific.

Roelvink, D. J. A., Reiniers, A., Van Dongeren, A., Van Thiel De Vries, J., McCall, R., Lescinski, J., 2009. Modelling storm impacts on beaches, dunes and barrier islands. Coastal Engineering 56, 1133–1152.

Roelvink, J. A., Stive, M., 1989. Bar-generating cross-shore flow mechanisms on a beach. Journal of Geophysical Research: Oceans 94 (C4), 4785–4800.

Rottier, J., Vincent, C., 1982. Fetch limited wave growth observed during arsloe. In: OCEANS82. IEEE, pp. 914–919.

Snyder, R., Dobson, F., Elliot, J., Long, R., 1981. Array measurements of atmospheric pressure fluctuations above surface gravity waves. Journal of Fluid Mechanics 102, 1–59.

Soulsby, R., 1997. Dynamics of Marine Sands. Thomas Telford, London.

Sverdrup, H., Munk, W., 1946. Empirical and theoretical relations between wind, sea and swell. Trans. Am. Geophysical Union 27, 823–827.

Taylor, P., Yelland, M., 2000. The dependence of sea surface roughness on the height and steepness of the waves. Journal of Physical Oceanography 31, 572–590.

Toba, Y., 1972. Local balance in the air-sea boundary processes, i. on the growth process of wind waves. Journal of Oceanographical Society Japan 28 (3), 109–120.

Tolman, H., 1991. A third-generation model for wind waves on slowly varying, unsteady, and inhomogeneous depths and currents. Journal of Physical Oceanography 21, 782–797.

van der Westhuysen, A., Anselmi, C., Calzada, R., Feyen, J., Gonzalez, J., Mercado, A., Westerink, J., 2015. A wave, surge and inundation modeling testbed for puerto rico and the us virgin islands: Year 1 progress. In: 95th AMS Annual Meeting, Phoenix, AZ. pp. 4–8.

van der Westhuysen, A., Van Dongen, A., Groeneweg, J., Van Vledder, G. P., Peters, H., Gautier, C., Van Nieuwkoop, J., 2012. Improvements in spectral wave modeling in tidal inlet seas. Journal of Geophysical Research 117, 1–23.

Van Dongeren, A., Reiniers, A., Battjes, J., Svendsen, I., 2003. Numerical modeling of infragravity wave response during delilah. Journal of Geophysical Research 108 (C9), 4—1–4—19.

Verlaan, M., Zijderveld, A., De Vries, H., Kroos, J., 2005. Operational storm surge forecasting in the netherlands: developments in the last decade. Phil. Trans. Roy. Soc. of London A: Mathematical, Physical and Engineering Sciences 363 (1831), 1441–1453.

Verlaan, M. S., De Kleermaeker, S., Buckman, L., 2015. Glossis: Global storm surge forecasting and information system. In: Australia, E., IPENZ (Eds.), Australasian Coasts & Ports Conference 2015: 22nd Australasian Coastal and Ocean Engineering Conference and the 15th Australasian Port and Harbour Conference.

WAMDI Group, 1988. The wam model - a third generation ocean wave prediction model. Journal of Physical Oceanography 18, 1775–1810.

Yelland, M., Taylor, P., 1996. Wind stress measurements from the open ocean. Journal of Physical Oceanography 26, 541–558.

Young, I., Babanin, A., 2006. The form of the asymptotic depth-limited wind wave frequency spectrum. Journal of Geophysical Research 111, C06031.

Young, I., Verhagen, L., 1996. The growth of fetch-limited waves in water of finite depth. part 1: Total energy and peak frequency. Coastal Engineering 29 (1-2), 47–78.

8. List of Symbols

Roman alphabet

Symbol	Description	Unit
a	Wave amplitude	[m]
A	Wave action density	[J s m^{-2}]
c	phase celerity	[m s^{-1}]
c_g	group celerity	[m s^{-1}]
C	Wave steepness	[-]
C_T	Bottom friction coefficient	[-]
d	Water depth	[m]
D_A	Sink terms in action balance	[W m^{-2}]
D_{br}	Dissipation by depth induced breaking	[W m^{-2}]
D_E	Sink terms in energy balance	[W m^{-2}]
D_f	Dissipation by bottom friction	[W m^{-2}]
ee	Directional energy density	[J m^{-2}rad^{-1}]
E	Energy density	[J m^{-2}]
f	frequency	[Hz]
f_w	Bottom friction coefficient	[-]
F	Fetch	[m]
F_{eq}	Equivalent fetch	[m]
g	Gravitational acceleration	[m s^2]
H	Wave height	[m]
H_{RMS}	Root mean square wave height	[m]
H_s	Significant wave height	[m]
k	Wave number	[m^{-1}]
L	Wave length	[m]
m	Relaxation parameter	[-]
m_i	i-th moment of the wave action spectrum	[varies]
n	Ratio group- and phase celerity	[-]
$\mathcal{Q}$	Dummy for conservative quantities	[varies]
S_A	Source term in action balance	[W m^{-2}]
t	Time	[s]
T_p	wave peak period	[s]
T_{rep}	Representative wave period	[s]
$T_{Mi,j}$	Spectral mean period based on M_i and M_j	[s]
u	Flow velocity	[m s^{-1}]
u_{10}	Wind speed 10 meters above water level	[m s^{-1}]
u^*	Friction velocity	[m s^{-1}]

Greek alphabet

Symbol	Description	Unit
ϵ	Relative error	[-]
ρ	(Water) density	[kg m^{-3}]
σ	relative or intrinsic frequency	[Hz]
ω	absolute frequency	[Hz]
Ω	spectral mean frequency	[Hz]

Sub- superscript

Sub- Superscript	Interpretation
$\widetilde{\mathcal{Q}}$	Dimensionless variable
$\mathcal{Q}_{\infty}$	Fully developed wave characteristic
$\vec{\mathcal{Q}}$	multidimensional variable
$\overline{\mathcal{Q}}$	averaged variable

A. Period evolution under bottom friction

Booij et al. (1999) derived a coupling between dissipation of peak wave frequency and bulk wave energy. Because this approach is not well known, its derivation is repeated below while rewritten to a coupling between representative wave period and energy. In establishing a general relation between dissipation of E and T_{rep}, we assume conservation of the shape of the high frequency tail of the spectrum and a universal shape of the spectrum in general. The assumed spectral shape is given by:

$$E(k) = \alpha k^{-n} \tag{A.1}$$

With n a free parameter defined by balance arguments, assigned a value below. From here, it is assumed that all energy is present in the part of the spectrum with wave numbers greater than k_p:

$$E = \alpha \int_{k_p}^{\infty} k^{-n} dk = \frac{\alpha}{n} k_p^{-n+1} \tag{A.2}$$

Based on wave steepness, the smallest wave numbers can carry higher waves which will experience the influence of bottom friction more severely. Through that reasoning, it is assumed that all dissipation then takes place in the low-wave number side of the spectrum such that the wave number with maximum energy (k_p) moves towards greater values through this process.

$$\left(\frac{\mathrm{d}E}{\mathrm{d}t}\right)_{bottom} = \frac{E}{k_p}(1-n)\left(\frac{\mathrm{d}k_p}{\mathrm{d}t}\right)_{bottom} \tag{A.3}$$

Assuming linear wave theory, the wave number and the wave period are related to each other through the dispersion relationship:

$$\left(\frac{\mathrm{d}k_p}{\mathrm{d}t}\right) = \left(\frac{\partial k_p}{\partial \omega}\right)\left(\frac{\partial \omega}{\partial T}\right)\left(\frac{\partial T}{\partial t}\right) = -\frac{1}{c_g}\frac{2\pi}{T^2}\left(\frac{\partial T}{\partial t}\right) \tag{A.4}$$

Rewriting and substituting gives:

$$\left(\frac{\partial T}{\partial t}\right) = -\frac{T^2}{2\pi} c_g k_p \frac{1}{(1-n)}\frac{1}{E}\left(\frac{\partial E}{\partial t}\right) = -\frac{T^2}{2\pi} c_g k_p \frac{1}{(1-n)}\frac{1}{E}\left(\frac{\partial E}{\partial t}\right) \tag{A.5}$$

Booij suggests $n = 3$ (based on scaling arguments in Kitaigorodskii et al. (1975)). This leads then towards:

$$\left(\frac{\partial T}{\partial t}\right) = \frac{T^2}{4\pi} c_g k_p \frac{1}{E}\left(\frac{\partial E}{\partial t}\right) \tag{A.6}$$

This evolution mechanism forces the wave steepness $\frac{H_s}{L_p}$ towards a deterministic ratio, given the amount of wave energy.

B. Calibration of friction coefficients

This chapter describes the calibration of friction coefficients f_w and C_T in obtaining a balance between wind input S_{in} and bottom friction $\{D_f, D_T\}$. Three depths d=$\{3,6,12\}$ and four different wave speeds $u_{10} = \{8, 12, 16, 20\}$ are assessed. For each of the twelve cases, f_w was varied ranging 0.02-0.07 and C_T was varied ranging 0.9-1.4. The differences between the literature described fully developed conditions (Equations (2.7) and (2.8)) and the computed upper bounds were calculated. These differences were then normalized by the literature prescribed values:

$$\epsilon_E = \frac{\sqrt{(E_\infty^{comp.} - E_\infty)^2}}{E_\infty} \tag{B.1}$$

$$\epsilon_T = \frac{\sqrt{(T_\infty^{comp.} - T_\infty)^2}}{T_\infty} \tag{B.2}$$

Contour plots of these normalized differences are given in Figure B.1. In case only one of the growth curves for energy or period needs to match, both C_T and f_w could be calibrated with the other parameter fixed. If both parameters are varied, the figure suggests a relation between f_w and C_T to describe the minimum error. For the wave energy, C_T depends positively on f_w for miminum differences, while the dependence is negative for the reproduction of the wave period upper bound. The growth curves for both wave energy and period should however be correctly reproduced. Therefore, there is only one unique set of f_w, C_T that describes the minimum error.

The following can be concluded for dependence of f_w and C_T on water depth and wind speed:

depth dependence

In the range of water depths from 3-18 m, f_w ranges 0.02-0.07 and C_T ranges 0.9-1.3. In linear approximation the friction coefficient f_w increases by 0.08 for an increase of water depth of 1 meter. C_T on the other hand decreases for increasing water depth.

wind speed dependence

In the range of wind speeds from 8-20 m/s, f_w equally ranges 0.02-0.07 and C_T ranges 1-1.2. On the investigated domain, The required f_w halves when the wind speed doubles. C_T decreases slightly for increasing wind speed.

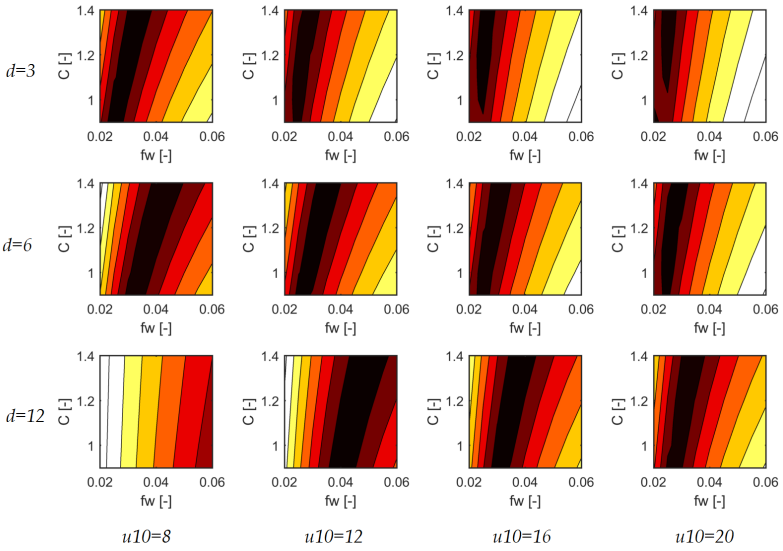

(a) wave energy

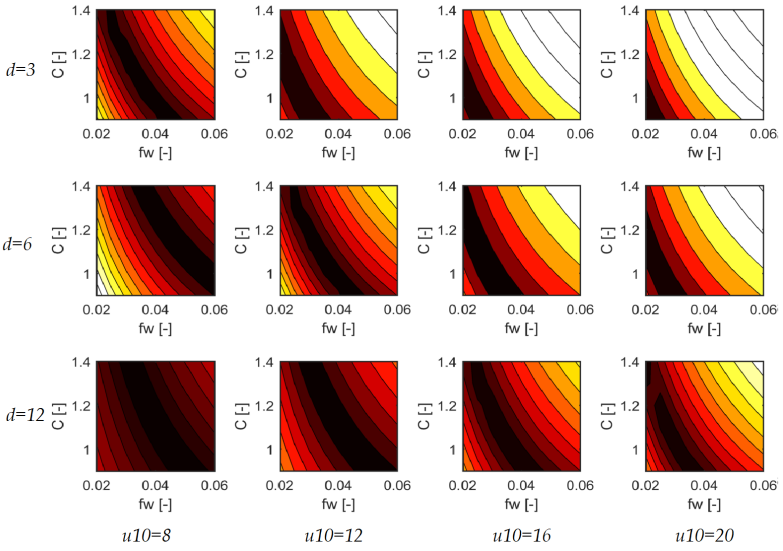

(b) wave period

Figure B.1: *For three water depths and 4 wind speeds the effect of the calibration parameters f_w and C_T was investigated. The contourplots show the normalized difference between the computed upper bound on wave energy (top) and wave period (bottom). Minima are marked dark and lighter shades indicate a greater normalized difference.*

C. Additional figures Haringvliet assessment

Model output for the relevant wave characteristics in storm case 002 has been plotted in Figure C.1.

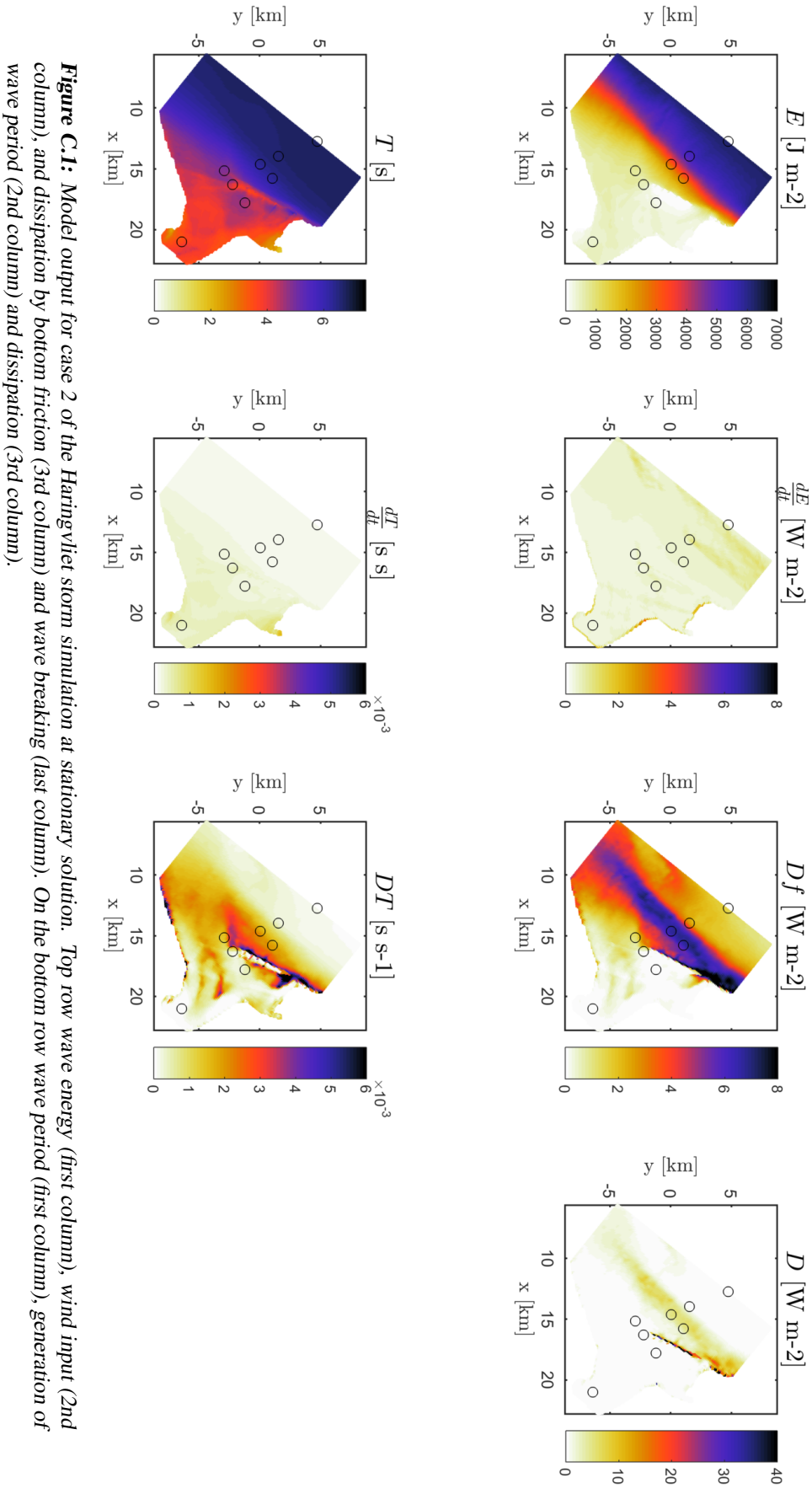

Figure C.1: *Model output for case 2 of the Haringvliet storm simulation at stationary solution. Top row wave energy (first column), wind input (2nd column), and dissipation by bottom friction (3rd column) and wave breaking (last column). On the bottom row wave period (first column), generation of wave period (2nd column) and dissipation (3rd column).*